2009

A Model of the Production of Spontaneous Otoacoustic Emissions in the Tokay Gecko

Michael Gelfand

A MODEL OF THE PRODUCTION OF SPONTANEOUS OTOACOUSTIC EMISSIONS IN THE TOKAY GECKO

A Thesis Presented to the Faculty of

The Rockefeller University

In Partial Fulfillment of the Requirements for

the Degree of Doctor of Philosophy

by

Michael Gelfand

April, 2009

ABSTRACT

The role of the ear is to detect sound. Many ears, however, can also generate sounds and transmit them into the environment. These sounds, known as spontaneous otoacoustic emissions, are the most striking proof of the existence of an active process within the ear. This active process originates in hair cells, the sensory receptors of the inner ear; by augmenting the energy contained in sound, it improves both the sensitivity and the frequency selectivity of hearing. Under certain conditions, the active process generates spontaneous oscillations, which then produce spontaneous emissions. Little is known about the process by which the spontaneous oscillations of a collection of hair cells within the ear are transformed into a particular sound that can be measured externally. Here, we suggest that interactions between tonotopically arranged hair cells play a critical role in the formation of spontaneous otoacoustic emissions.

We have created a model based on the basilar papilla of the tokay gecko, a species notable both for the unusual anatomy of its inner ear and for the prominence of its spontaneous emissions. In this model, the papilla is represented by a tonotopic array of nonlinear van der Pol oscillators, with connections along the array mediated by either viscous or elastic elements. We find that a model incorporating elastic interactions, but not one incorporating viscous interactions, reproduces the appearance of spontaneous emissions. The

model also suggests a prominent role for disorder along the length of the papilla. Finally, the model explains what may be the most distinctive feature of spontaneous emissions: the repulsion of spectral peaks within the emission by pure-tone external stimuli.

To test our model, we also recorded spontaneous otoacoustic emissions from the tokay gecko. Previous recordings of emissions have primarily focused on the behavior of single peaks within the emission spectrum. We chose instead to focus on the relationships between multiple emission peaks. Upon applying single-frequency tones at a range of amplitudes and frequencies into the ears of geckos we have observed novel behaviors previously predicted by our model. We conclude that interactions along the basilar papilla, mediated by elastic elements, play an important role in the formation of spontaneous otoacoustic emissions.

To the many geckos who gave their lives in support of this project. May their sacrifice not be in vain.

ACKNOWLEDGMENTS

Over the last four years, I've had the pleasure of interacting with nearly sixty different members of the Hudspeth Lab, far too many to name here individually. Their various expertises were alternately intimidating and inspiring. Many of my labmates played essential roles in keeping a potentially abstract project grounded in a realer world, albeit one made up of lateral lines, ribbons, bundles, and traveling waves. Their friendship, too, has made an underground lair into a surprisingly pleasant environment. A few lab members, past and present, merit special note. Loïc Le Goff guided me through the early years, dark and fishy. Eugenia Chiappe, my predecessor with the geckos, provided some critical assistance towards working with and understanding those lovable, loathsome creatures. Thomas Risler, Daniel Andor, and Omar Ahmad, each of whose skills with physics dwarfed my own, helped to shape my approach to this project. Cornelia Hagemann, during her brief time in lab, contributed the actual data seen in Figure 1A and made her time in lab far more entertaining. Finally, Brian Fabella, without any doubt the glue holding the downstairs lab together, provided expertise in both gecko management and LabView programming. The former required a physical bravery that took me over a year to acquire, and the second a mental clarity that first helped give focus to the design of my experiments, and then allowed them to run smoothly. Either of these contributions, alone, would have deserved more gratitude than I can express here.

Jim Hudspeth has proved a constant inspiration during my time in lab. The clarity and creativity of his thought are, of course, unparalleled. Conversations with Jim rarely failed to yield a useful insight. His suggestions elicited responses ranging from "why didn't I think of that?" to "I would never have thought of that!" They were always more than welcome, and provided both the ideas underlying this project and the engine driving

it forward. His actions as a mentor, too, were also friendly, supportive, and exactly what was needed, both when research was progressing smoothly and when, on occasion, it was not. I would consider myself fortunate to have such a mentor ever again.

Oreste Piro provided key contributions both at the very beginning of this project, and later on as our model matured. His personal openness and physical insight, and his welcoming me into his lab at IFISC during the summer of 2007, led to the most productive and enjoyable months I have had in graduate school.

The members of my thesis committee, Olaf Andersen and Albert Libchaber, provided essential scientific guidance during the progress of this project. I of course also thank them for taking the time to read this document, and for their comments on it. Olaf has also provided personal guidance over the years, and his unyielding support has been greatly appreciated. Marcelo Magnasco, the final member of the committee, merits special note for his hospitality, his generosity, his personality, and of course his intellect, a physical intuition that is often a marvel to see.

On a personal note, I'd like to thanks my friends, especially those whose own experiences in grad school have given them an appreciation for my own. I'd like to thank Julia, Mom, and Dad, who've always been there for me. Finally, Aruni, a damn fine cook and the single best person I have ever known.

TABLE OF CONTENTS

LIST OF FIGURES

LIST OF TABLES

CHAPTER 1

Introduction

Hair cells and the active process

The peripheral auditory system transforms pressure waves that reach the ear into nervous impulses sent towards auditory nuclei in the brain. It is able to reliably accomplish this task for sounds covering six orders of magnitude in intensity and three orders of magnitude in frequency. It is additionally able to discern, with microsecond-scale time resolution, the multiple frequencies that compose everyday sounds. Critical to accomplishing these feats are the organs of the inner ear, which are responsible for converting the pressure waves conveyed by the structures of the outer and middle ears into synaptic release that trigger firing in downstream neurons.

Hair cells are the elements of the inner ear that accomplish the key change of mechanical energy into chemical and electrical signals. Their operation is complex. Pressure gradients that develop within the cochlea apply mechanical forces to the apical surfaces of hair cells. Above the apical surface of each hair cell sits a hair bundle, a closely interlinked geometric arrangement of elongated actin-filled projections known as stereocilia. Forces acting on the tops of these hair bundles cause the stereocilia to rotate individually about their basal insertions in the body of the hair cell; this rotation then introduces a shear

between the tips of adjacent stereocilia. The shearing motion, by introducing tension into the tip links that connect stereocilia, opens transduction channels connected to the tip links that lie in the plasma membrane of the stereocilia. The resultant flow of cations down an electrochemical gradient depolarizes the hair cell and culminates in the release of glutamate into the synaptic cleft between the base of the hair cell and the neurons of the VIIIth nerve that innervate it.

Hair cells are able to detect signals containing energy comparable to that of thermal noise (De Vries, 1948). To accomplish this, while also overcoming the damping effect of movement through a fluid, they require an active process to add energy to that of the incoming pressure waves. This active process has been shown to amplify weak signals in a frequency-specific manner. In addition, it introduces a compressive nonlinearity into the cochlear response function; six orders of magnitude of sound pressure are represented by only two orders of magnitude of basilar membrane response (Ruggero et al., 1997). Similar patterns are seen in auditory nerve firing rates and in perceived sound levels (Martin and Hudspeth, 2001). This phenomenon implies that as signals become fainter, the active process inputs more energy into the system, in effect compensating for the weaker stimulus. Perhaps the most striking demonstration of the active process is the existence of spontaneous otoacoustic emissions (SOAEs), sounds created within the inner ear and emitted in the absence of external stimuli.

Spontaneous otoacoustic emissions

In a reversed form of normal mechanosensory transduction, the active process is able to produce pressure changes in cochlear fluid. These pressure changes are then translated in reverse, with vibrations at the oval window between the inner and middle ears leading to movement of the ossicles. The vibrations cause the tympanic membrane to function as a speaker, producing sounds that can be detected externally. In extreme cases these emissions are of sufficient magnitude to be heard by an unaided ear; more typically, they can be detected using a sensitive microphone. SOAEs usually display a constant frequency spectrum for a given ear over a period of hours (Probst et al., 1991). Because they can be studied over extended time periods in animals with fully intact auditory apparatuses, SOAEs can provide useful insights into the mechanics of the inner ear. In fact, SOAEs are often complex, carrying a great deal of information about the operations of the inner ear: the frequency spectrum of externally-measured emissions most often consists of a variable number of peaks superimposed on an elevated baseline (Manley et al., 1996; Martin et al., 1990) (Figure 1).

There is extensive evidence supporting the cochlear origin of SOAEs. Processes known to damage the cochlea are consistently found to also inhibit the production of SOAEs. For example, exposure to excessively loud noise, which limits hearing acuity by damaging the inner ear both structurally and

Figure 1. Spontaneous otoacoustic emissions. A. The power spectrum recorded from the ear of a tokay gecko portrays the typical features of the spontaneous otoacoustic emissions from this species, including a broad hump of power extending from less than 1 kHz to more than 4 kHz and a series of superimposed peaks. The frequency spacing between 13 successive peaks averages 240 ± 50 Hz. In addition, the spectrum displays several features of internal organization: a nearly constant interval of 281 ± 6 Hz separates three pairs of peaks at both the low- and high-frequency ends of the spectrum, and the peaks at 3560 Hz and 4120 Hz are the second harmonics of those at 1780 Hz and 2060 Hz. B. A second spectrum shows the variability of emissions between geckos. In this instance, the mean interval between 14 successive peaks is 270 ± 70 Hz. Again, local regions show even greater regularity: the spacings between the four peaks to the left of the larger central peaks are 229 ± 8 Hz, whereas those to the right are separated by 277 ± 3 Hz. Cornelia Hagemann contributed to the collection of data presented in this figure.

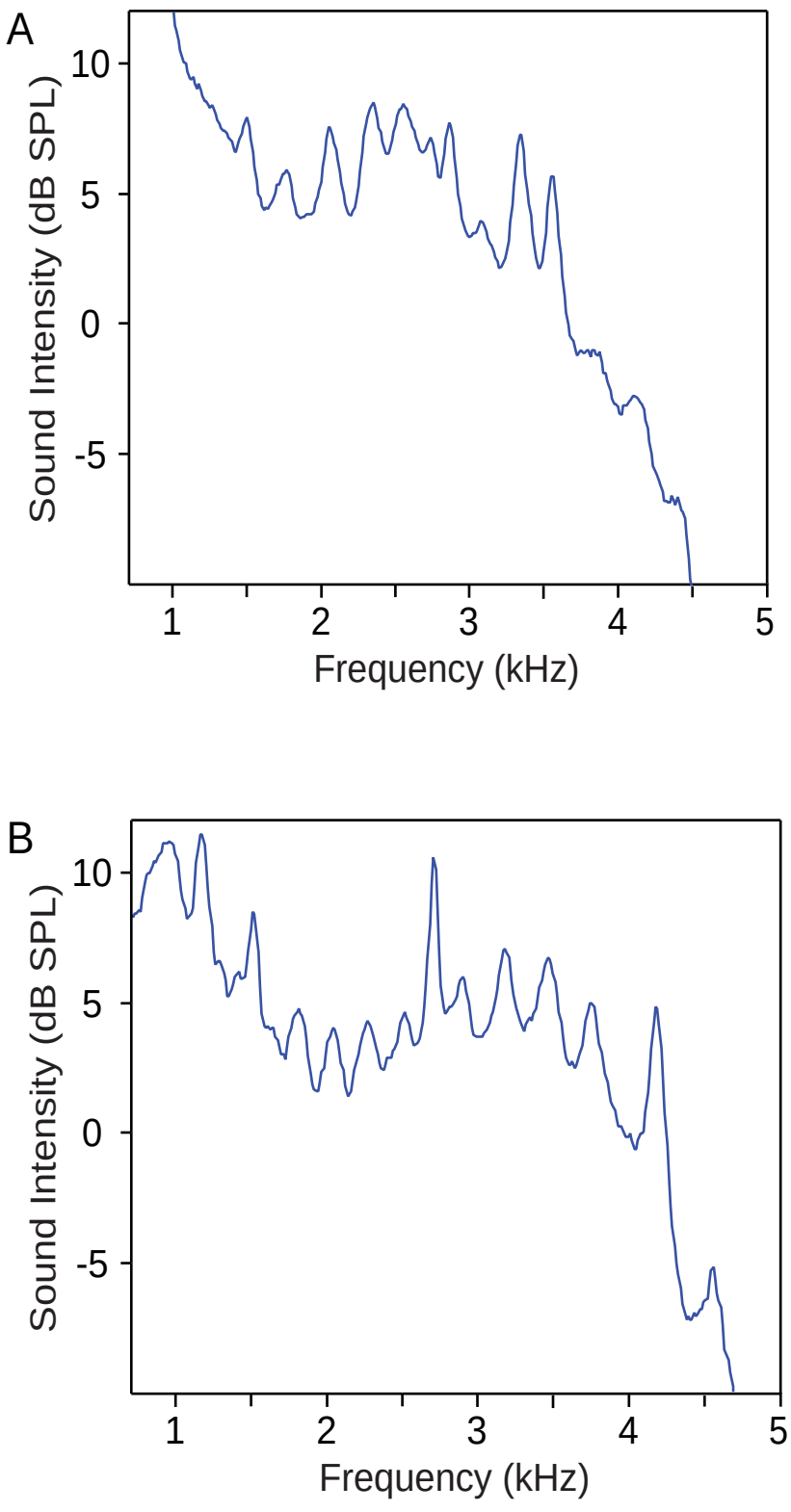
A
Sound Intensity (dB SPL)
10
5
0
-5
1
2
3
4
5
Frequency (kHz)
B
Sound Intensity (dB SPL)
10
5
0
-5
1
2
3
4
5
Frequency (kHz)

Figure 1

metabolically, also reduces the prevalence and amplitude of SOAEs (Veuillet et al., 2001). Brief exposure to loud noises temporarily reduces the amplitude of SOAEs, whereas longer exposures are more often permanently damaging, and therefore eliminate SOAEs and decrease the production of other types of OAEs. When the noises are narrow-band, this damage is mostly limited to nearby frequencies. Similarly, the production of SOAEs in humans positively correlates with hearing acuity. This link applies to the progressive hearing impairment that results from a lifetime of cumulative exposure to damaging sounds (Rebillard et al., 1987). In a final correlation, the use of ototoxic drugs can both limit hearing and in many cases reduce SOAEs (Stewart and Hudspeth, 2000). Aminoglycosides, which reversibly block the hair bundle's transduction channels (Ohmori, 1985; Kroese et al., 1989), and salicylates, which temporarily damage hearing through an unknown mechanism (Martin et al., 1988), provide clear examples of this link between cochlear function and SOAEs. Additional evidence for the cochlear origin of SOAEs is found in the connection between their production and VIIIth nerve tuning curves. The suppression of SOAEs by external tones varies with the tones' frequency and intensity in a manner that is strikingly similar to single-neuron responses to tonal stimuli (Köppl and Manley, 1994).

Otoacoustic emissions are unlikely to play a role in the physiological processes of the inner ear. Instead, evidence suggests that they are an epiphenomenon arising from an active oscillator tuned near a Hopf bifurcation,

which exhibits characteristics that *are* critical to the proper functioning of the ear. A system is said to contain a Hopf bifurcation when variation of a parameter causes a transition from quiescence to spontaneous oscillations. This transition occurs at a critical value of this parameter, known as the control parameter. When this parameter lies on one side of the critical value, the system contains a stable fixed point, and is therefore quiescent. A system initially located at the fixed point remains there, and any small deviation away from this point decays to zero. When the control parameter lies on the other side of the critical value, however, the fixed point is replaced by a stable limit cycle, a trajectory through phase space along which the system continuously oscillates with a frequency ω_0. Small deviations away from the limit cycle now decay back to the cycle rather than to a fixed point.

An active oscillator tuned near a Hopf bifurcation exhibits behaviors that are needed for proper auditory function. When the control parameter of a system containing a Hopf bifurcation is tuned near the critical value, its response to sinusoidal stimuli of amplitude f is proportional either to $f^{1/3}$, for $\omega=\omega_0$, or to f, for ω sufficiently far from ω_0, with a gradual transition between the two regimes (Camalet et al., 2000). Such a system evidently provides frequency selectivity, while the amplification and compressive nonlinearity that the auditory system additionally requires emerge from the sublinear response to sinusoidal stimuli with frequencies near ω_0.

When the critical parameter is tuned slightly away from the critical value on the active side, a system containing a Hopf bifurcation oscillates spontaneously at its characteristic frequency; such oscillations are the source of SOAEs. While SOAEs seem not to have any primary purpose in auditory physiology, they are tightly linked to the proper function of the cochlear amplifier, and can additionally be measured noninvasively in human and animal subjects. Thus, otoacoustic emissions have proven useful as a window into the functioning of an organ that is often both too small and too sensitive to study under physiological conditions. Clinically, otoacoustic emissions provide an easy test of hearing function and the most direct means available to examine dysfunctions of the cochlea, where most hearing defects originate (Probst et al., 1991).

SOAEs are not the only type of otoacoustic emission (OAE). All OAEs are characterized as manifestations of acoustic energy generated in the inner ear and recorded externally. They are divided into two classes: SOAEs, and evoked OAEs (EOAEs), whose production requires prior application of an external stimulus. Although these stimuli may themselves contain acoustic energy, EOAEs are not mere 'echoes'; sounds are designated OAEs only if the ear contributes energy to that present in the stimulus.

Simple EOAEs can be produced in response to short stimuli, such as tone bursts or square-wave 'clicks'. In addition, a single-frequency tone introduced into the ear often elicits a response at the same frequency with greater energy than was present in the stimulus (Probst et al., 1991). These

responses, known as stimulus-frequency OAEs, are especially difficult to distinguish from passive responses such as echoes. Finally, simultaneous introduction of two different-frequency (f_1 and f_2) tones can produce OAEs at frequencies that are linear combinations of the two stimulus frequencies (such as $2f_1$-f_2); these are known as distortion-product OAEs (Lonsbury-Martin et al., 1990). Although SOAEs and the various types of EOAEs are each produced in response to different stimuli, all are believed to share a common origin in the nonlinear behavior of the active process.

The gecko basilar papilla

Otoacoustic emissions have been described and studied in a wide variety of species, including mammals, birds, and frogs (Köppl, 1995; Bergevin et al., 2008). Emissions have also been extensively studied in lizards, a group in which SOAEs are unusually common and demonstrate systematic variations corresponding to the structure of the inner ear (Köppl, 1995; Manley, 1997).

The primary hearing organ of lizards is known as the basilar papilla. Like other vertebrate hearing organs, the basilar papilla is organized tonotopically: hair cells responsive to low frequencies are found at one end, and those responsive to high frequencies are found at the other (Manley, 2002). It is believed that the basilar papillae of ancestral lizard had hair cells that were uniformly covered by a continuous tectorial membrane and all oriented in the same direction. Electrical tuning allowed hair cells along the papilla to respond to

frequencies up to only 1 kHz (Manley, 2002). Modern lizards have since added micromechanical tuning. This second form of tuning, mediated through variations in the physical properties of hair bundles, allows sensitivity to frequencies up to at least 7 kHz (Manley, 2002). For example, hair cells that respond to lower frequencies have taller bundles with fewer stereocilia per bundle, resulting in a lower mechanical stiffness (Authier and Manley, 1995). These micromechanical effects are traditionally distinguished from the global macromechanical properties of the basilar membrane, which provide the first level of tonotopic organization of the inner ear (Probst et al., 2006).

Macromechanical tuning evidently introduces interdependence between the activities of hair cells that is not present with only electrical tuning. While the effect is subtler, micromechanical tuning, which unlike macromechanical tuning is found in modern lizards, also magnifies the significance of the inevitable mechanical interactions between hair cells. These limit the ability of mechanically-tuned hair cells to operate independently, decreasing the information content of auditory responses. Perhaps to compensate for this effect, the lengths of basilar papillae are much greater in species employing mechanical tuning, with greater distances between hair cells tuned to different frequencies. In the gecko, for example, the basilar papilla is 2 mm in length, versus as little as 100 μm in some other lizards (Miller, 1973; Manley, 2002). This increased spacing may partially restore the independence of hair cell responses.

Another approach to decreasing the coupling between adjacent hair cells, used in several other lizard families, is the removal of the continuous tectorial membrane that contributes significantly to the coupling (Manley, 2002). This latter strategy has drawbacks, however, for the tectorial membrane is believed to contribute to both sensitivity and frequency selectivity (Authier and Manley, 1995). The partial replacement of a continuous tectorial membrane by discrete tectorial masses, known as sallets because of their resemblance to an antique helmet of that name, may represent a compromise. Their direct coupling, mediated only by a thin strand connecting their tips, is likely weaker than that introduced by continuous tectorial structures. This weaker coupling, seen in geckos and other species, correlates to the production of SOAEs with a larger number of spectral peaks than are seen in SOAEs from lizards with continuous tectorial membranes (Manley, 2002). This pattern of SOAEs is similar to that seen in several species of lizard lacking any tectorial structures (Manley, 2006), supporting the view of sallets as a more weakly coupled form of tectorial structure. However, the presence of sallets nevertheless assists with tuning and maximizing sensitivity to weak stimuli (Manley, 2002). The significance of the variation seen in tectorial structures, and the role of these structures in coupling along the basilar papilla, remains an open question.

The basilar papilla of geckos is approximately 2 mm long and between 50 and 130 μm in width. (Miller, 1973). The approximately 2,000 hair cells it comprises are divided into three regions. One, located at the basal end of the

papilla, is covered by a loose tectorial meshwork and is involved in sensory transduction at frequencies below 1 kHz. Hair cells in this first region are unidirectionally oriented. The other two regions are arranged in parallel along the apical two-thirds of the papilla, and together are responsible for detection of sounds at frequencies between 1 kHz and 7 kHz. Hair cells in these regions are arranged tonotopically, with response frequencies increasing exponentially toward the apex of the papilla. The location of high-frequency hair cells at the papilla's apex is reversed from the pattern found in nearly every other species, including most lizards as well as mammals (Manley et al., 1999). This unusual orientation evolved from the ancestral lizard papilla, in which high-frequency regions relying on micromechanical tuning, were initially added to *both* ends of a low-frequency, electrically-tuned central region. In many lizard species, the loss of the apical high-frequency region resulted in the standard orientation; unusually, the basal region was lost in geckos, resulting in a characteristic, tonotopically-reversed basilar papilla (Manley, 2002).

The two apical, high-frequency regions in geckos are structurally distinguished by both the nature of the tectorial structures overlying the hair cells as well as the innervation of those cells (Figure 2). Afferent innervation enters the papilla from a direction that is consequently known as neural, while the opposite direction is known as abneural. A continuous tectorial membrane covers hair cells on the neural side of the papilla; this membrane is connected through a thin sheet of tectorial material to the overhanging neural limbus, part of the

cartilaginous ring which surrounds and supports the basilar papilla. This tectorial membrane is also continuous with the tectorial meshwork covering the basal region. Hair cells on the abneural half of the apical region, on the other hand, are covered by a series of approximately 170 discrete tectorial sallets. Additionally, hair cells in the neural half of the papilla receive no innervation while those on the abneural half have afferent innervation (Chiappe et al., 2007). It has therefore been suggested that the tectorial and salletal hair cells, by analogy to the outer and inner hair cells of mammalian cochleae, are responsible for motor and sensory function, respectively (Chiappe et al., 2007).

Sallets are separated from each other by approximately 5 μm. Each covers an average of 5-6 hair cells, which are arranged in a row perpendicular to the long axis of the papilla (Miller, 1973). Unlike the continuous tectorial membrane, the sallets are not connected to the neural limbus or any other supporting structure; other than the hair bundles on which they sit, their only attachment is to their neighbors through a thin strand connecting their apices along the length of the papilla.

Hair cells within both the salletal and tectorial areas are divided into two groups by planes of mirror symmetry running lengthwise along the papilla (Miller, 1973). That is, of the hair cells under a single sallet, or under a comparable region of tectorial membrane, half are arranged with their axes of excitability facing in the neural direction, while the other half are excitable in the opposing,

Figure 2. The gecko basilar papilla. A. A schematic view portrays one-tenth of the apical portion of the cochlea's sensory structure, the basilar papilla. The papilla rests upon the basilar membrane, a sheet of connective tissue suspended from the limbic cartilages and separating the scala media from the scala tympani. Acoustic stimulation creates a pressure difference between these liquid-filled compartments, thus setting the basilar papilla into up-and-down oscillation accompanied by side-to-side rocking. Above the papilla lie a continuous tectorial membrane and an array of about 170 sallets, 17 of which are depicted here, joined by a fine filament at their tops. B. A cross-section through the basilar papilla reveals one transverse row of hair cells. On the neural side of the papilla, the hair bundles of the six tectorial hair cells insert into the continuous tectorial membrane, which hangs by the tectorial curtain from the limbic lip. On the opposite, abneural side of the papilla, the hair bundles of the six salletal hair cells contact a sallet, a discrete tectorial structure about 20 mm in height. The remainder of the basilar papilla consists of supporting cells (yellow) atop a stiff, cartilaginous stylus that extends the entire length of the papilla (A. Le Boeuf and A.J. Hudspeth, unpublished observations).

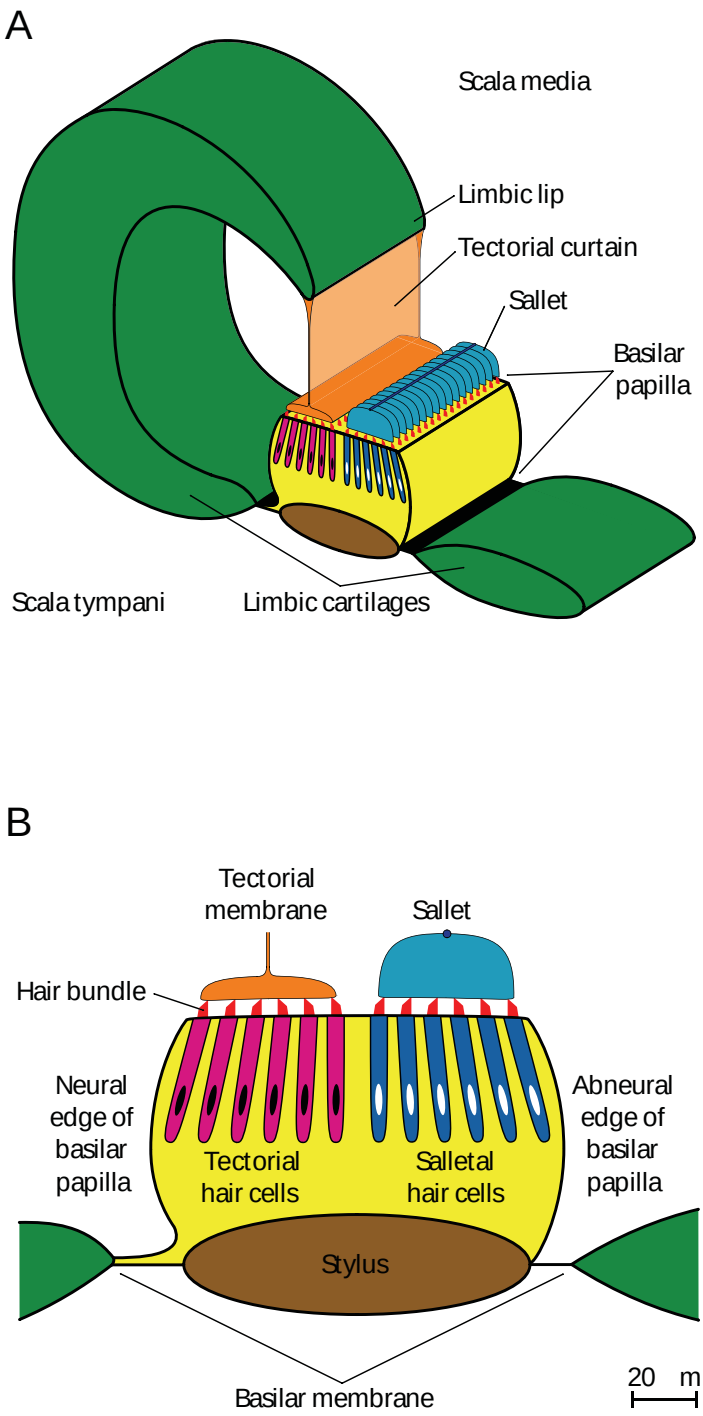
A
Scala media
Limbic lip
Tectorial curtain
Sallet
Basilar papilla
Scala tympani
Limbic cartilages
B
Tectorial membrane
Sallet
Hair bundle
Neural edge of basilar papilla
Tectorial hair cells
Salletal hair cells
Abneural edge of basilar papilla
Stylus
Basilar membrane
20 m

Figure 2

abneural direction. These two groups then face each other at the midline of the sallet or of the tectorial membrane.

SOAEs in geckos

Previous studies of SOAEs in the tokay gecko have described their typical properties (Manley et al., 1996). In gecko ears that produce SOAEs, an average 12 emission peaks are found. A peak is identified as being part of an SOAE depending on its height, sensitivity to temperature changes, and suppressibility by external tones. These peaks fall at frequencies between 0.95 kHz and 4.55 kHz, and reach maximal sound pressures that can be as high as 10 dB SPL or as low as -6 dB SPL. They are superimposed on a diffuse, elevated baseline, which is also suppressible by external tones.

As in other species (van Dijk et al., 1989; Manley and Köppl, 1994), the frequency of gecko SOAE peaks increases with warming and decreases with cooling (Manley et al., 1996). The magnitude of frequency shift is proportional to the room-temperature frequency of a given peak. Above 35°C, further increases in temperature depress and then eliminate emissions. At times, a rise in temperature also leads to a reversible splitting of single peaks into pairs.

A characteristic of SOAEs across species is the suppressibility of peaks by tones of nearby frequencies, with the intensity of tone required to suppress a peak usually increasing with the tone's distance from the peak's central frequency (Manley et al., 1996). In certain cases, tones can instead *increase* the

size of an SOAE peak; this generally occurs for low intensity applied tones with frequencies slightly above those of the SOAE peaks.

External tones can also shift the frequencies of SOAE peaks, most commonly 'pushing' the peak away from the tone (Manley et al., 1996; Köppl and Manley, 1994). This effect depends on the intensity of the applied tone, and is stronger for tones nearer in frequency to the peak. This behavior is asymmetric for tones of a frequency higher or lower than a peak. For tones at frequencies above the SOAE peak, only 'pushing' is seen, while for tones at lower frequencies, 'pulling' can occasionally be seen in addition to 'pushing'. The frequency shift is also smaller, on average, for tones below a peak than for those above.

Modeling otoacoustic emissions

Numerous models of SOAEs have previously been developed. These models share many elements. These commonly include a tonotopic frequency distribution, which has been observed in the hearing organs of many species (Lewis et al., 1985). The statistical properties of SOAEs indicate that these signals originate from self-sustained oscillators in the cochlea (Bialek and Wit, 1984). Thus, such an oscillatory element is also a common ingredient of these models. However, the models differ widely in their details. In particular, some consider emissions as the product of global features of the cochlea, while others focus on individual oscillators as the source of emissions.

Some models suggest that certain classes of emissions, most notably stimulus-frequency OAEs, are best described as arising from the linear 'reflection' of stimulus waves, rather than from nonlinear distortion by an active process located within the hair cell (Zweig and Shera, 1995; Shera and Guinan, 1999). Such reflections are generated throughout the length of the cochlea, and their summation is recorded as the OAE. The properties of emissions thus depend on the summation of responses from different locations, and accordingly on the global features of the cochlea rather than the properties of a small number of dominant oscillators. This interpretation hinges on the finding that the complex ratio of emitted tones to stimulus tones (the 'reflectance') has a phase that varies linearly and rapidly with frequency, but an amplitude that remains approximately constant over narrow ranges. Models based on nonlinear distortion struggle to explain this rapid variation of phase. Models in which the critical element is reflection, in contrast, easily explain it as arising from the combination of a varying stimulus frequency with a delay of constant time in the process of reflection. These models can additionally explain spontaneous otoacoustic emissions by supposing that the reflection described above is accompanied by a re-reflection off the ossicles of the middle ear, and that the paired reflections have a combined amplitude greater than unity for a particular frequency (Shera, 2003). The inner ear then acts to coherently amplify fluctuations at specific frequencies, leading to the recorded peaks of SOAEs.

While a reflection-based approach has advantages in modeling some aspects of emissions, the more popular approach considers nonlinear oscillators to be fundamental, and thus begins with the construction of elements representing individual oscillators. Although the detailed biophysics of oscillations have been described in competing models (Nadrowski et al., 2004; Dallos et al., 2006), models describing emissions usually seek to recapture the essential elements of emissions using simpler, more generic nonlinear oscillators.

The van der Pol oscillator is a nonlinear oscillator which originated in the study of electrical circuits (Van der Pol and van der Mark, 1927), and has since found applications not just in physics but in biological systems as well, perhaps most famously in the FitzHugh-Nagumo model of action potentials (FitzHugh, 1961; Nagumo et al., 1962). The van der Pol oscillator behaves according to the equation

$$\ddot{x} + \mu(x^2 - 1)\dot{x} + x = 0, \qquad \textbf{[1.1]}$$

in which x is often interpreted as representing the oscillator's position. The van der Pol oscillator resembles a harmonic oscillator with an additional element of nonlinear damping, whose magnitude is controlled by the parameter μ. When μ equals zero, the system reduces to an undamped harmonic oscillator. For positive μ, however, the system includes both a linear, negative damping and a positive damping that depends on x^2. When x is small the negative damping dominates, and the amplitude of oscillations grows. When x is large, on the other

hand, the nonlinear positive damping takes over, and oscillations decay. In both cases, a stable limit cycle with $|x|^2 \sim 1$ is asymptotically approached. For small, positive values of μ, the system is weakly nonlinear, and behaves very similarly to a harmonic oscillator. For larger values of μ, the system becomes more strongly nonlinear, and acts as a relaxation oscillator, with periods of gradual evolution alternating with sudden jumps.

The van der Pol oscillator has often been used in modeling otoacoustic emissions emerging from the ear's active element. The suppression of SOAEs by a stimulus tone, as well as the recovery from that suppression, can be described in terms of a van der Pol oscillator (Talmadge et al., 1990). A model of a similar interaction in the presence of noise describes the synchronization of an SOAE to a cubic distortion product in human subjects (Van Dijk and Wit, 1990a). When the noise in this experimental system is of sufficient strength, the oscillator undergoes sporadic 2π phase slips, consistent with the forcing of a nonlinear oscillator. A similar model predicts the changes in the synchronization of SOAEs by pure tones with aspirin administration (Long *et al.*, 1991). On the other hand, the fluctuations of the amplitudes and periods of SOAEs are not consistent with a model of a single Van der Pol oscillator driven by white noise (Van Dijk and Wit, 1990b).

While studies of the behavior of single oscillators succeed in explaining some properties of spontaneous otoacoustic emissions, interactions between oscillators have also been shown to play a role in the behavior of emissions. For

example, a model of two asymmetrically-coupled van der Pol oscillators helps explain the response of human SOAEs to externally applied stimuli (Murphy *et al.*, 1995; Murphy *et al.*, 1996). In this model, a lower-frequency 'primary' oscillator is unidirectionally coupled to the displacement of a higher-frequency 'secondary' oscillator. The response of the primary oscillator to a sinusoidal forcing then combines a direct effect with an indirect effect mediated by the independent effect of the forcing on the secondary oscillator. The resulting behavior resembles the response of a 'primary' human SOAE to an externally applied suppressing tone.

Interactions among multiple oscillators in systems representing the entire cochlea have also been incorporated into models. The entrainment of weak oscillators by anomalously strong oscillators explains the observed minumum value for the frequency interval between SOAEs in the human cochlea (Van Hengel *et al.*, 1996). This entrainment is least effective at a distance determined by the standing waves generated upon reflection of SOAEs back into the cochlea by the stapes; this distance determines the minimum spacing between adjacent emissions. The response of the basilar membrane to sinusoidal stimulation is consistent with a chain of Hopf oscillators, and depends on the form of coupling between oscillators (Kern and Stroop, 2003). Finally, a model based on a similar oscillator explains many features of the spontaneous otoacoustic emissions in another lizard, the Australian bobtail skink (Vilfan and Duke, 2008). This last

model shares many features with the model developed here; more detailed comparisons of the two are presented below.

The above examples suggest the importance of interactions between oscillators in the formation of SOAEs. Additionally, it has been shown that the power produced by individual hair cells is much smaller than that carried by SOAEs (Manley and Gallo, 1997), further supporting the importance of coordination of the outputs of individual hair. Based on the observation that the pattern of SOAEs produced by a lizard species relates to anatomical characteristics of the basilar papilla, and in particular to those concerning the tectorial structures that overlie hair cells (Manley, 1997), we supposed that connections between individual hair cells, mediated by those tectorial structures, are responsible for shaping the pattern of emissions in the ear of the tokay gecko. To test this hypothesis, we developed models of the gecko basilar papilla that focus on different potential modes of interaction between hair cells, and compared those models to recordings of geckos SOAEs.

CHAPTER 2

Materials and methods

Recording of spontaneous otoacoustic emissions

We used published techniques (Stewart and Hudspeth, 2000) to record spontaneous otoacoustic emissions from the ears of mature tokay geckos (*Gekko gecko*). In brief, we placed an animal sedated with 25 $mg \cdot kg^{-1}$ pentobarbital sodium (Nembutal, Ovation Pharmaceuticals, Inc., Deerfield, IL) in a folded heating pad maintained at 25 °C and located in a darkened, double-walled acoustic-isolation chamber. Under these conditions, the animal maintained normal respiration but remained dormant for several hours. We inserted a microphone snugly into an acoustic adapter with an opening 5 mm in internal diameter and then sealed the adapter carefully around the animal's tympanum with silicone vacuum grease. The power spectrum of recording showed a broad peak with a frequency near 1 kHz when the seal between the microphone adapter and the skin of the gecko formed improperly. When this peak was present in an initial recording, the adapter was readjusted to achieve a more complete seal until the peak was no longer observed. Polarized to 200 V, the calibrated, low-noise microphone (4179, Brüel & Kjær, Nærum, Denmark) had a nominal sensitivity of 100 $mV \cdot Pa^{-1}$.

Sound-pressure signals were measured with a preamplifier with a gain of 10x (2660, Brüel & Kjær) and an A-weighted amplifier operated at a gain of 1000x (2609, Brüel & Kjær) and digitized at 20-ms intervals in overlapping, 200-ms segments for a total period of either 5 s (experiments with many consecutive recordings) or 30-120 s (experiments with single or few recordings). After tapering each record with a Hann window and subjecting it to fast Fourier transformation, we computed power spectra and averaged them across the ensemble of records. The power spectra displayed in Figure 1 were processed to remove background noise. Each spectrum represents the difference between that recorded from a living gecko and a control spectrum obtained after the animal's death.

For pure-tone stimulation, sounds were produces by an Etymotic ER-2 speaker driven by an ED1 Electrostatic Speaker Driver with a gain of -27 dB. The speaker was attached to the same adapter used to connect the microphone to the gecko. Stimuli at a particular amplitude and frequency were most commonly generated for a single recording, lasting 5 s as described above. Stimuli were presented in an order that was randomized by whichever of frequency or amplitude served as the dependent variable in an experiment. When both were varied in recordings from a single gecko ear, all frequencies at a single amplitude were presented consecutively, again in a random order.

Modeling studies

We simulated the behavior of various models with Matlab (versions 7.1 and 7.6; The MathWorks, Inc., Natick, MA), using the function **ode45** for the solution of stiff ordinary differential equations. Each oscillator was initialized by assigning it a random phase in a cycle of unperturbed oscillation at its natural frequency. After discarding the results from an initial period of equilibration, we summed the simulated values of the hair-bundle displacement across the ensemble of oscillators. These data were divided into a variable number of time segments, each of which was tapered with a Hann window and subjected to fast Fourier transformation. We then computed power spectra and averaged them across the data segments.

CHAPTER 3

Development of a model of spontaneous otoacoustic emissions based on the gecko basilar papilla

Modeling individual oscillators

Our approach to generating a model of the gecko's spontaneous otoacoustic emissions included describing both individual oscillators and their interactions along the basilar papilla. Although detailed quantitative descriptions exist for hair-bundle oscillations in the bullfrog's sacculus (Bozovic and Hudspeth, 2003; Martin et al., 2003; Nadrowski et al., 2004), these equations cannot be applied directly to the gecko. Emissions in the gecko occur at frequencies two orders of magnitude higher than those observed in the frog. In addition, the structures of the receptor organs differ dramatically between the two species. The bullfrog sacculus is a nearly circular area of hair bundles covered by a continuous otolithic membrane (Corey and Hudspeth, 1983), while the gecko basilar papilla is linear and covered by both a continuous tectorial membrane and discrete sallets, and contains small groups of tightly connected, bidirectionally-oriented hair bundles. Since existing bundle models are not appropriate for the gecko, and since we wished to investigate the essential ingredients necessary to reproduce the observed emission spectra, we adopted a more qualitative strategy. To this end, we made two assumptions about the features that shape

spontaneous emissions. First, we assumed that the relevant oscillating unit consists not of a single hair cell but of a transverse row of hair cells operating at a single frequency (Köppl and Authier, 1995; Authier and Manley, 1995). Second, we posited that the qualities of spontaneous otoacoustic emissions depend primarily on interactions along the receptor organ rather than on the detailed biophysics of individual oscillations. Following these assumptions, we chose a generic description of the individual oscillators.

In our model, each of *N* units denoted by the index *n* was represented as a van der Pol oscillator characterized by the equations

$$\dot{x}_n = \mu_n \left(y_n - \frac{x_n^3}{3} + \alpha_n x_n \right), \qquad \textbf{[3.1]}$$

$$\dot{y}_n = \left[\frac{-(2\pi f_n)^2}{\mu_n} \right] x_n . \qquad \textbf{[3.2]}$$

Here *x* represents hair-bundle position; the variable *y* has no simple physical interpretation, but encompasses the adaptation process and other features of the hair bundle's internal dynamics (Nadrowski *et al.*, 2004). This formulation incorporates the assumption, elaborated below, that the bundle's inertia can be neglected in the description of its dynamics. The elastic force that influences the hair bundle's position includes a cubic term that accords with the structure of the models for the bullfrog's hair bundle (Hudspeth *et al.*, 2000). The parameters α, *f*, and μ determine respectively the amplitude, characteristic frequency, and nonlinearity of an individual unit's unforced oscillation.

We performed simulations of a one-dimensional array of oscillators each behaving according to these equations. The number of oscillators was ordinarily $N=110$. The value of the parameter α was initially set to 1. The value of $2\pi f_n$ varied exponentially along the chain from 1 to 2.97; the characteristic frequencies of successive oscillators thus differed by about 1%. Given the arbitrary timescale of the simulations, these frequencies are here represented as falling between 1 kHz and 2.97 kHz to facilitate comparison with experimental data. Time intervals are presented in the corresponding units, generally in the millisecond range. The parameter μ also varied exponentially so that the ratio $2\pi f/\mu$ remained constant at 5. Every unit thus differed from a harmonic oscillator by an equivalent amount. This rendered each of the oscillations nearly sinusoidal; the unperturbed oscillations of the various units differed only in timescale. The parameter values employed in the specific simulations displayed below are listed in Table 1.

Introduction of viscous coupling

In addition to the equations governing the behavior of individual oscillators, the second component of our model was the coupling between adjacent oscillators. The number of possible forces mediating this coupling is, in principle, infinite. However, most of these possibilities would be difficult or impossible to implement in a physical system, and therefore were not examined. We chose instead to examine two potential couplings that seemed most likely to reflect

physical elements in the gecko basilar papilla: viscous forces, as conveyed through short-range hydrodynamic interactions, and elastic forces, probably conveyed through the structures of the papilla itself.

In the gecko's cochlea, viscous coupling between oscillators could arise from the mechanical activity of salletal hair cells. Because adjacent sallets are slabs of tectorial material separated by only a few micrometers, it is plausible that adjacent sallets interact hydrodynamically. Emissions are known to emerge from lizard species with only salletal hair cells (Köppl and Manley, 2003; Köppl, 1998; Köppl and Manley, 1994; Manley *et al.*, 2001), so those cells are potentially capable of sustaining spontaneous oscillations. Indeed, species lacking any tectorial structures whatsoever along segments of the basilar papilla are nevertheless able to produce SOAEs, which are believed to originate form those segments (Manley, 2006). We therefore initially examined a model in which hair bundles are coupled by viscous drag.

Drag forces operating on an object moving through a medium take the form $F = \beta V$, where V is the velocity of the object and β, the drag coefficient, depends on the object's shape as well as the viscosity of the medium. For two adjacent objects moving through same medium, the force instead depends on the velocity difference ΔV between the two objects, while β depends on the relative orientations of the objects as well as the distance between them. In the case of salletal units, which move perpendicular to the long axis of the papilla by a distance much smaller than their width, the factors constituting β are assumed to

Table 1. Parameter values for simulations

Figure	*N*	α_n	β	γ	δ	*F*	Noise
3A, 3B	110	1	0.2	0	0	0	–
4A, 4B	110	1	0	1	0	0	–
5	110	*n*/18 for *n*=1-18 1 for *n*=19-92 (111-*n*)/18 for *n*=93-110	0.0-0.3	1	0	0	–
6	110	*n*/18 for *n*=1-18 1 for *n*=19-92 (111-*n*)/18 for *n*=93-110	0.2	0.025	0	0	–
7A	110	*n*/18 for *n*=1-18 1 for *n*=19-92 (111-*n*)/18 for *n*=93-110	0.0-0.3	0.025	0	0	–
7B	110	*n*/18 for *n*=1-18 1 for *n*=19-92 (111-*n*)/18 for *n*=93-110	0.2	0-1	0	0	–
8, 10A	110	*n*/18 for *n*=1-18 1 for *n*=19-92 (111-*n*)/18 for *n*=93-110	0	1	0	0	–
9A	110	*n*(111-*n*)/3025	0	0.5	0	0	–
9B	210	1	0	1	0	0	–
10B	110	*n*/18 for *n*=1-18 1 for *n*=19-92 (111-*n*)/18 for *n*=93-110	0	0-2	0	0	–
11A	110	*n*/18 for *n*=1-18 1 for *n*=19-63,65-92 .84-1.16 for n=64 (111-*n*)/18 for *n*=93-110	0	1	0	0	–
11A	110	*n*/18 for *n*=1-18 1 for *n*=19-67,69-92 .84-1.16 for n=68 (111-*n*)/18 for *n*=93-110	0	1	0	0	–
12A	110	*n*/18 for *n*=1-18 1±0.03 for *n*=19-92 (111-*n*)/18 for *n*=93-110	0	1	0	0	–
12B	110	*n*/18 for *n*=1-18 1 for *n*=19-92 (111-*n*)/18 for *n*=93-110	0	1	0	0	+

12C	110	*n*/18 for *n*=1-18 1±0.03 for *n*=19-92 (111-*n*)/18 for *n*=93-110	0	1	0	0	+
13A, 13B	110	*n*/18 for *n*=1-18 1 for *n*=19-92 (111-*n*)/18 for *n*=93-110	0	1	0.2	1.8	–
14A	110	*n*/18 for *n*=1-18 1 for *n*=19-92 (111-*n*)/18 for *n*=93-110	0	1	0-1	1.8	–
14B	110	*n*/18 for *n*=1-18 1 for *n*=19-92 (111-*n*)/18 for *n*=93-110	0	1	0.2	0.6-3.6	–
15	110	*n*/18 for *n*=1-18 1±0.03 for *n*=19-92 (111-*n*)/18 for *n*=93-110	0	1	0.025	0.8-3.2	–
16	110	*n*/18 for *n*=1-18 1±0.10 for *n*=19-92 (111-*n*)/18 for *n*=93-110	0	1	0.025	0.8-3.2	–
17	110	*n*/18 for *n*=1-18 1±0.10 for *n*=19-92 (111-*n*)/18 for *n*=93-110	0	1	0.2	0.8-3.2	–
18	110	*n*/18 for *n*=1-18 1±0.10 for *n*=19-92 (111-*n*)/18 for *n*=93-110	0	1	0.0-0.7	1.8	–

In each simulation, the frequency $2\pi f_n$ for the n^{th} oscillator assumes the value $3^{(n-1)/110}$ and the ratio $(2\pi f_n)/\mu_n$ remains constant at 5. In the dimensionless model, N and β have no units; the units of the remaining parameters are: α_n, distance squared; γ, inverse time; δ, distance per time; f_n and F, inverse time; and μ_n, inverse distance squared times inverse time.

remain very nearly constant. We thus modeled the interactions between adjacent oscillators by modifying Equation 3.1 with a term proportional to the Laplacian of velocity:

$$\dot{x}_n = \mu_n\left(y_n - \frac{x_n^{\,3}}{3} + \alpha_n x_n \right) + \beta\left(\dot{x}_{n-1} - 2\dot{x}_n + \dot{x}_{n+1}\right). \qquad \textbf{[3.3]}$$

This additional term represents the expected effect of viscous coupling, in which the dominant force of interaction is the drag that results from the differencebetween a particular oscillator's velocity and those of the two adjacent oscillators. An exception is found at the ends of the array, where each outermost oscillator experiences a drag on its lateral side depending only on the velocity of that oscillator. As will be described below, the system lacks inertia. The drag consequently contributes not to the oscillator's acceleration, but instead to its velocity.

In the set of equations represented by Equation 3.3 the velocity of each object is described as a function of both itself and the velocities of the neighboring oscillators. Numerical solutions to these equations can therefore not be directly calculated. Instead, these equations must first be rewritten as

$$\mathbf{B}\dot{\mathbf{X}} = \mathbf{G}, \qquad [3.4]$$

in which

$$\mathbf{B} = \begin{bmatrix} 1+2\beta & -\beta & 0 & 0 & \dots & 0 & 0 \\ -\beta & 1+2\beta & -\beta & 0 & \dots & 0 & 0 \\ 0 & -\beta & 1+2\beta & -\beta & \dots & 0 & 0 \\ 0 & 0 & -\beta & 1+2\beta & \dots & 0 & 0 \\ \vdots & \vdots & \vdots & \vdots & \ddots & \vdots & \vdots \\ 0 & 0 & 0 & 0 & \dots & 1+2\beta & -\beta \\ 0 & 0 & 0 & 0 & \dots & -\beta & 1+2\beta \end{bmatrix}; \qquad [3.5]$$

$$\dot{\mathbf{X}} = \begin{bmatrix} \dot{x}_1 \\ \vdots \\ \dot{x}_N \end{bmatrix}; \qquad [3.6]$$

$$\mathbf{G} = \begin{bmatrix} g_1(x_1, y_1) \\ \vdots \\ g_N(x_N, y_N) \end{bmatrix}, \qquad [3.7]$$

with the individual g_n representing the right side of Equation 3.1. Inversion of **B** in Equation 3.4 then yields a set of equations that can be solved numerically. For positive values of β, every element of the matrix $\mathbf{B}^{-1}$ has a non-zero value. As a result, the behavior of each oscillator depends in principle on the activity not just of its immediate neighbors, but also of the entire ensemble. The system thus experiences an effective global coupling mediated by local interactions.

A viscously-coupled system exhibited several unexpected behaviors (Figure 3A). While the phases of lower-natural-frequency oscillators normally lag those of higher-natural-frequency oscillators within a heterogeneous

Figure 3. The effect of viscous coupling. A. In this spatiotemporal plot of the system's behavior in the presence of viscous coupling, the abscissa represents time. The ordinate displays the behavior of the 110 coupled oscillators, with those of progressively higher natural frequencies situated toward the top. Colors encode the instantaneous values of the hair-bundle displacement *x*, with red representing positive values, blue negative values, and green values near zero. The oscillators display traveling waves moving along the chain in both directions (arrows) and regions of antiphase synchronization (polygon) B. The power spectrum for the same system shows a concentration of power in the frequency range 0.7-2.6 kHz but no well-defined peaks. In this and subsequent figures, the spectral power density is defined relative to that produced by a single, free-running oscillator at its natural frequency. The parameter values for this and further simulations are provided in Table 1.

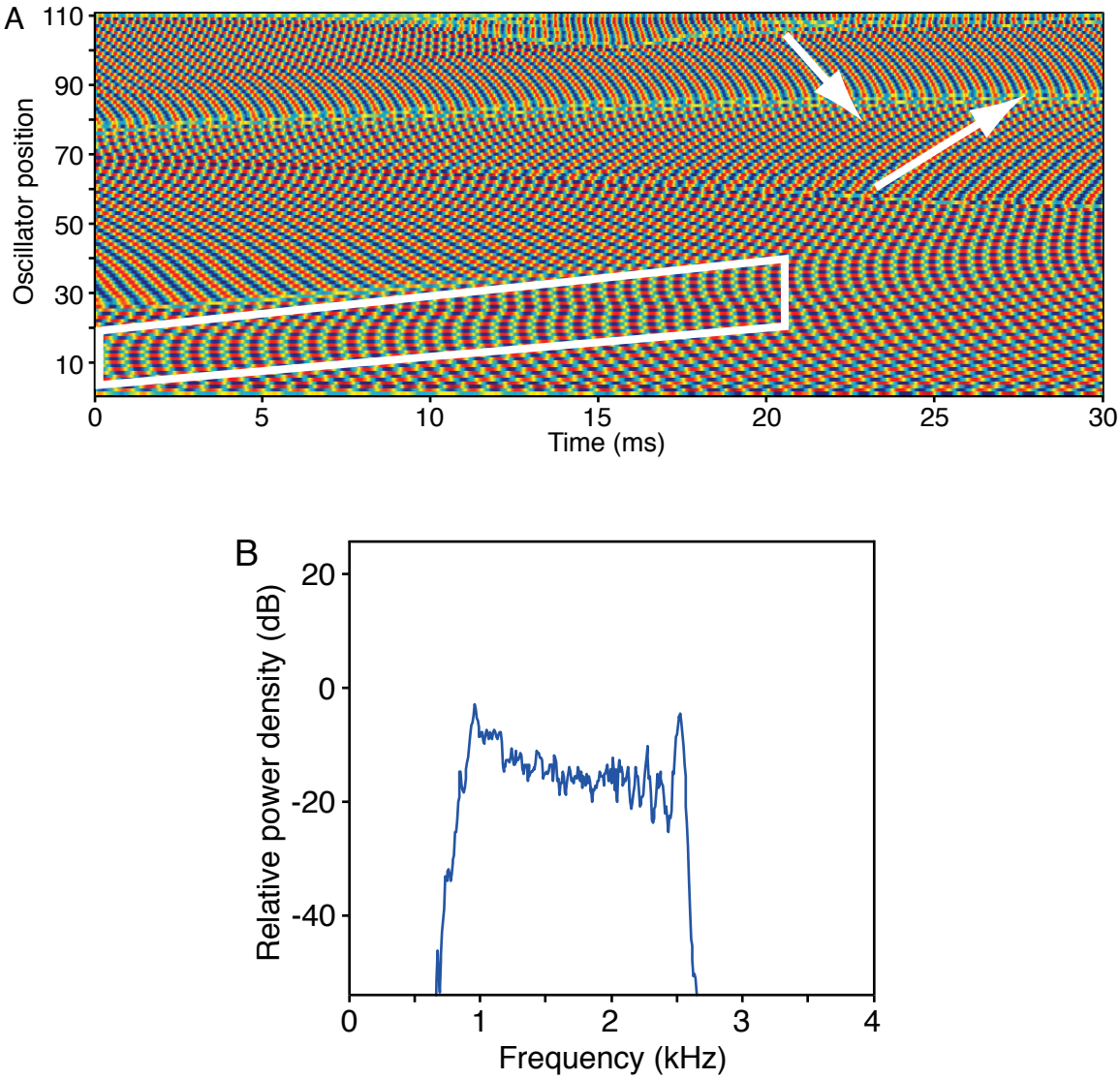
A
110
90
70
50
30
10
Oscillator position
0
5
10
15
20
25
30
Time (ms)
B
20
0
-20
-40
Relative power density (dB)
0
1
2
3
4
Frequency (kHz)

Figure 3

synchronized group, in this system traveling waves advanced in both directions along the array. Thus, lower frequency oscillators often led their higher frequency neighbors in phase. There were also extended periods in which alternating antiphase synchronization encompassed numerous oscillators. Antiphase in this case lay on a continuum between traveling waves in the two opposite directions. Finally, the locations of defects, where phase slippage between adjacent oscillators occurs, migrated cyclically across the array. It is unclear what caused the sequence of defects, which was usually continuous in its motion over time, to drift in one direction or the other. These unusual characteristics were reflected in the power spectrum of the simulated emissions (Figure 3B), which differed substantially from experimentally recorded spectra. Although power was concentrated between 1 and 3 kHz, as expected, within this range the well-defined peaks of experimental spectra were not seen. The sole exception was a peak just below 3 kHz, which had a maximal power density approximately triple that of the surrounding baseline, an increase of nearly 5 dB.

Introduction of elastic coupling

Elastic forces could also couple adjacent oscillators. In the gecko, the hair bundles of both tectorial and salletal hair cells are linked by structures with the potential to mediate elastic coupling. Tectorial hair cells insert their hair bundles into a continuous tectorial membrane that encompasses the entire length of the

high-frequency region of the basilar papilla; the tectorial membrane applies an elastic restoring force upon deformation (Freeman *et al.,* 2003). In addition, a longitudinal strand joins adjacent sallets along their top edges. In light of these connections, we next investigated the effect of elastic interactions between hair cells.

We modeled the elastic coupling between successive oscillators by augmenting Equation 3.1 with a term proportional to the Laplacian of position, giving

$$\dot{x}_n = \mu\left(y - \frac{x^3}{3} + \alpha x\right) + \gamma\left(x_{n-1} - 2x_n + x_{n+1}\right). \qquad \textbf{[3.8]}$$

Here, the elastic coupling coefficient γ represents the strength of interaction between adjacent oscillators. Except for the first and last, each oscillator thus experiences a force proportional to the difference between its position and those of the adjacent oscillators, of which one has a slightly lower and the other a slightly higher natural frequency. Owing to the chain's linear configuration, the outermost oscillators are again necessarily subject to asymmetrical forces. Each is linked on one side to the single adjacent oscillator and is connected on the other side to a point whose displacement is fixed at zero ($x_0 = x_{N+1} = 0$). This arrangement inevitably resulted in smaller oscillations near the ends of the array.

Elastic coupling, unlike viscous coupling, does not introduce a velocity-dependent term and therefore does not fundamentally alter the nature of the oscillator by introducing a velocity-dependent term. Instead, the new terms,

which depend on the position of oscillators, are similar to those already found in the uncoupled equations. Thus, elastic coupling remains local, with interactions between nonadjacent oscillators occurring only indirectly.

A chain of 110 elastically-coupled oscillators readily formed a series of synchronized groups (Figure 4A). The temporal evolution of these oscillators differed qualitatively from that observed with viscous coupling. Waves of synchronized oscillation traveled from the high-frequency extreme of the chain toward the low-frequency end, consistent with the usual behavior of coupled oscillators, where the phase of high-frequency elements usually leads that of lower-frequency elements coupled to them. Defects in these waves formed when the phase difference between adjacent oscillators within a synchronized group grew unsustainably great. The phase slippage that occurred at these defects was accompanied by a transient loss of amplitude across the oscillators surrounding the defect. Although these defects seemed to appear irregularly during the brief, 30-ms interval represented in the figure, over longer times they occurred preferentially at certain positions along the chain. Oscillators at these positions thus had lower average amplitudes than those at positions where defects occurred less frequently. In addition, oscillators at positions where defects infrequently occurred formed stable synchronized groups, while those at defects alternated affiliations between nearby synchronized groups. As a result, the power spectrum (Figure 4b) contained distinct peaks that correspond to relatively stable groups of synchronized oscillators.

Viscoelastic coupling

Purely elastic coupling proved superior to purely viscous coupling in modeling the production of spontaneous emissions. However, it is unlikely that either purely elastic or purely viscous coupling functions as the sole interaction along the basilar papilla. We accordingly simulated a system in which adjacent oscillators interacted viscoelastically. That is, both β and γ were set to nonzero values.

The addition of slight amounts of viscous coupling to an elastically coupled system led to shifts and rearrangements of synchronized groups, but resulted in slight changes in the system's behavior. The addition of viscous coupling shifted spectral peaks toward higher frequencies relative to purely elastic coupling. Synchronized groups near the chain's ends, and the corresponding spectral peaks, were an exception. Further augmentation of viscous coupling strength destabilized many central groups, resulting in more diffuse spectral peaks; however, the system never became as undifferentiated as that seen with purely viscous coupling. Unexpectedly, for γ fixed at 1, certain viscous coupling strengths led to stably synchronized groups at particular locations along the array; the resulting spectral peaks were often more closely spaced in frequency than those seen in the absence of viscous coupling, contrary to what was expected from a greater total amount of coupling (Figure 5).

Figure 4. The effect of elastic coupling. A. A spatiotemporal plot portrays traveling waves progressing systematically from the high-frequency end of the chain toward the low-frequency end (arrow). Although each oscillator spends most of its time as a component of a group oscillating at a common frequency, the waves are interrupted sporadically by defects as individual oscillators shift from group to group. B. In the power spectrum for elastically coupled oscillators, power is concentrated in 15 central peaks.

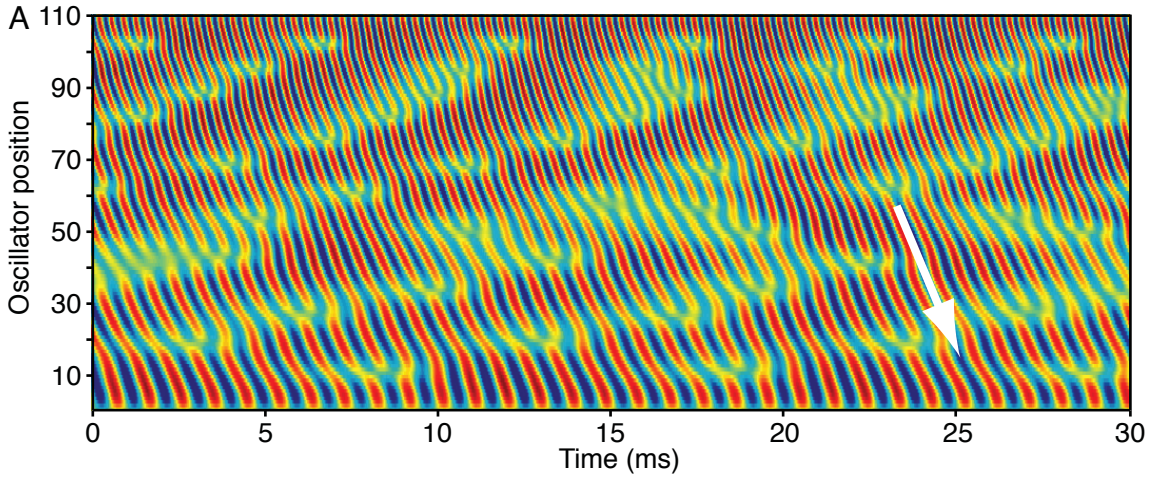
A
110
90
70
50
30
10
Oscillator position
0
5
10
15
20
25
30
Time (ms)

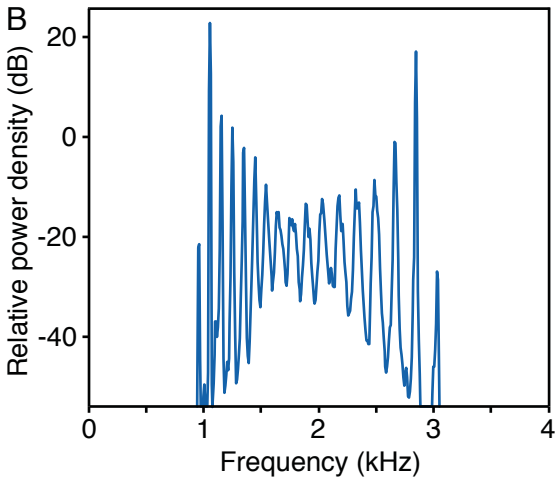
B
20
0
-20
-40
Relative power density (dB)
0
1
2
3
4
Frequency (kHz)

Figure 4

Figure 5: Addition of viscous coupling to elastic Coupling

As the viscous coupling coefficient β increases from the bottom of the figure toward the top, spectral peaks become more diffuse. A brief interlude of well-defined spectral peaks is visible for frequencies above 2 kHz with β near .15.

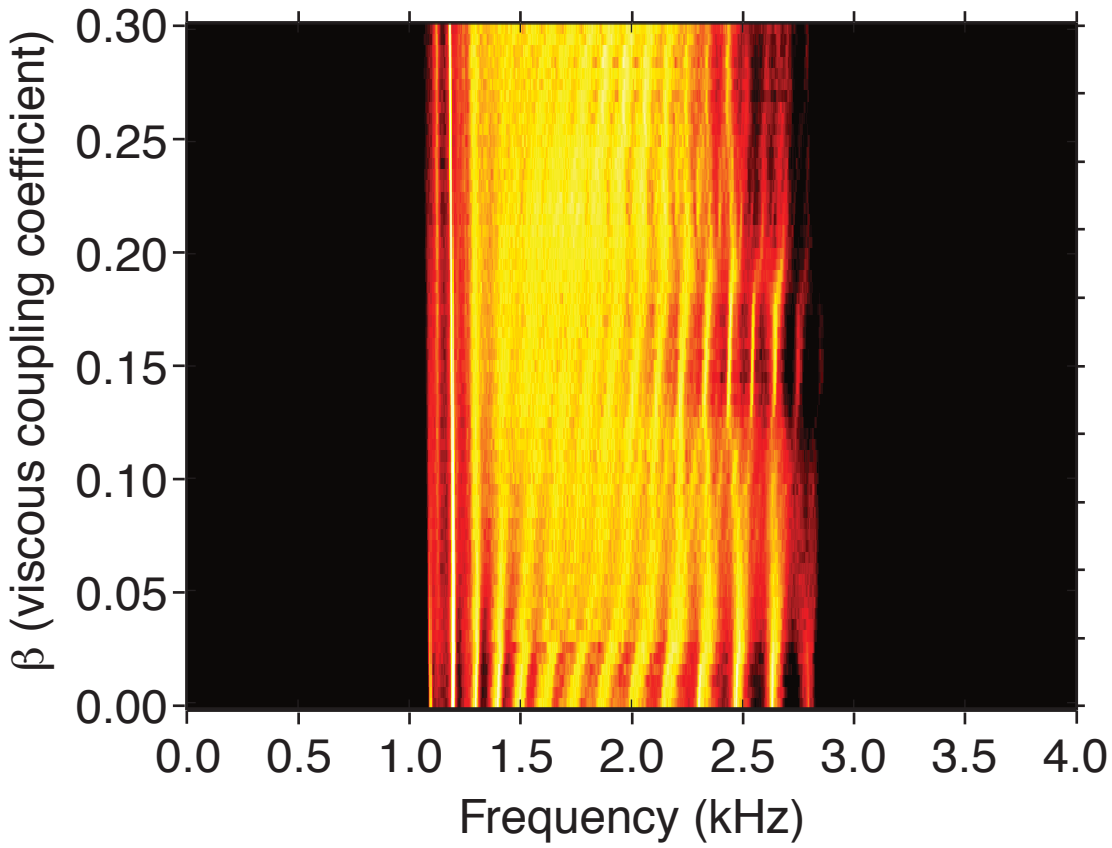
β (viscous coupling coefficient)
0.30
0.25
0.20
0.15
0.10
0.05
0.00
0.0
0.5
1.0
1.5
2.0
2.5
3.0
3.5
4.0
Frequency (kHz)

Figure 5

The introduction of elastic coupling into a viscously-coupled system, in contrast, led to the formation of stably synchronized groups. In fact, the spectral peaks that resulted from such a system were narrower than those seen in purely elastic coupling (Figure 6). The addition of a small increment of elastic coupling to a system with pure viscous coupling led to the formation of a small number of stable groups of synchronized oscillators, which appeared in power spectra as narrow, unevenly-spaced peaks. A minimal value of β was required for this synchronization pattern to occur; above this value, the number and spacing of groups was highly dependent on the amounts of both viscous and elastic coupling. Increases in viscous coupling led to groups diverging as they each rapidly shifted toward the higher frequency end of the tonotopic array; those groups that passed the high-frequency end of the array disappeared (Figure 7A). Thus, increases in viscous coupling increased the spacing between peaks, and decreased their number. Increasing elastic coupling, in contrast, had nearly the opposite effect, underscoring the fundamental differences between these two apparently similar coupling modes. Peaks converged and moved towards lower frequencies, with new peaks appearing at the high frequency end of the array (Figure 7B). Above a certain critical value of γ, the system abruptly transitioned to the behavior seen previously for high values of viscous and elastic coupling.

The significance of boundaries

The elastic interactions above were modeled as being identical along the length of the array. So, too, were the dynamics of individual oscillators, except for changes in timescale. Because of these symmetries, the frequencies of synchronized groups were not specified by the basic elements of the model. Instead, the presence of symmetry-breaking boundaries in the model determined the positions where defects rarely occur, and thus the pattern of spectral peaks. In the simplest case, the ends of the oscillator chain provided these boundaries: synchronized groups localized in position owing to the asymmetrical interactions of the first and last oscillators. The absence of additional units on one side of each of these oscillators allowed them to remain synchronized to their respective neighbors. This stability propagated towards the center of the chain by a distance that depended on the strength of elastic coupling. Thus, dramatic differences were seen between the behavior of groups near the ends of the oscillator array and those at its center, which were more fluid.

Due to this effect, spectral peaks near the margins displayed greater power and less frequency dispersion than those in the chain's middle (Figure 4B). This contrasts with experimentally-recorded emission spectra, in which no such pattern is seen. A model in which α, the amplitude of natural oscillations, was constant and equal to 1 along most of the chain but decreased linearly to 0 over the first and the last 18 oscillators, produced results similar to those obtained experimentally. Such a pattern of variation in α may correspond to

Figure 6: Viscous coupling with a weak elastic component

A combination of strong viscous coupling and weak elastic coupling results in the formation of four synchronized groups with stable frequencies. The five weaker peaks that are visible are distortion products with frequencies corresponding to linear combinations of the four stronger peaks.

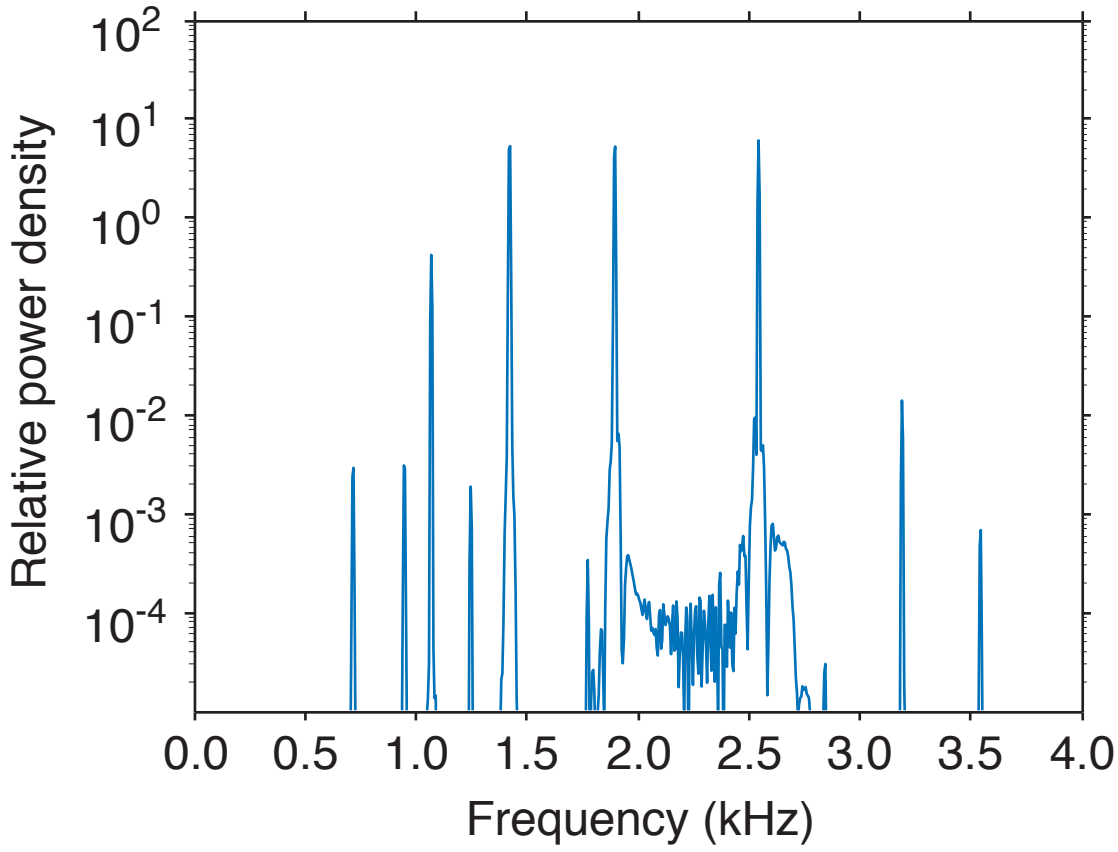
Relative power density
10^{2}
10^{1}
10^{0}
10^{-1}
10^{-2}
10^{-3}
10^{-4}
0.0
0.5
1.0
1.5
2.0
2.5
3.0
3.5
4.0
Frequency (kHz)

Figure 6

Figure 7: Dependence of behavior on changes to elastic and viscous coupling coefficients

A. In the presence of weak elastic coupling, a minimum amount of viscous coupling is required for the formation of synchronized groups. Further increases in β lead these groups to simultaneously shift toward higher frequencies and diverge. B. With strong viscous coupling, increasing in the elastic coupling γ lead synchronized groups to converge and shift toward lower frequencies. For γ sufficiently large, well-defined spectral peaks disappear abruptly.

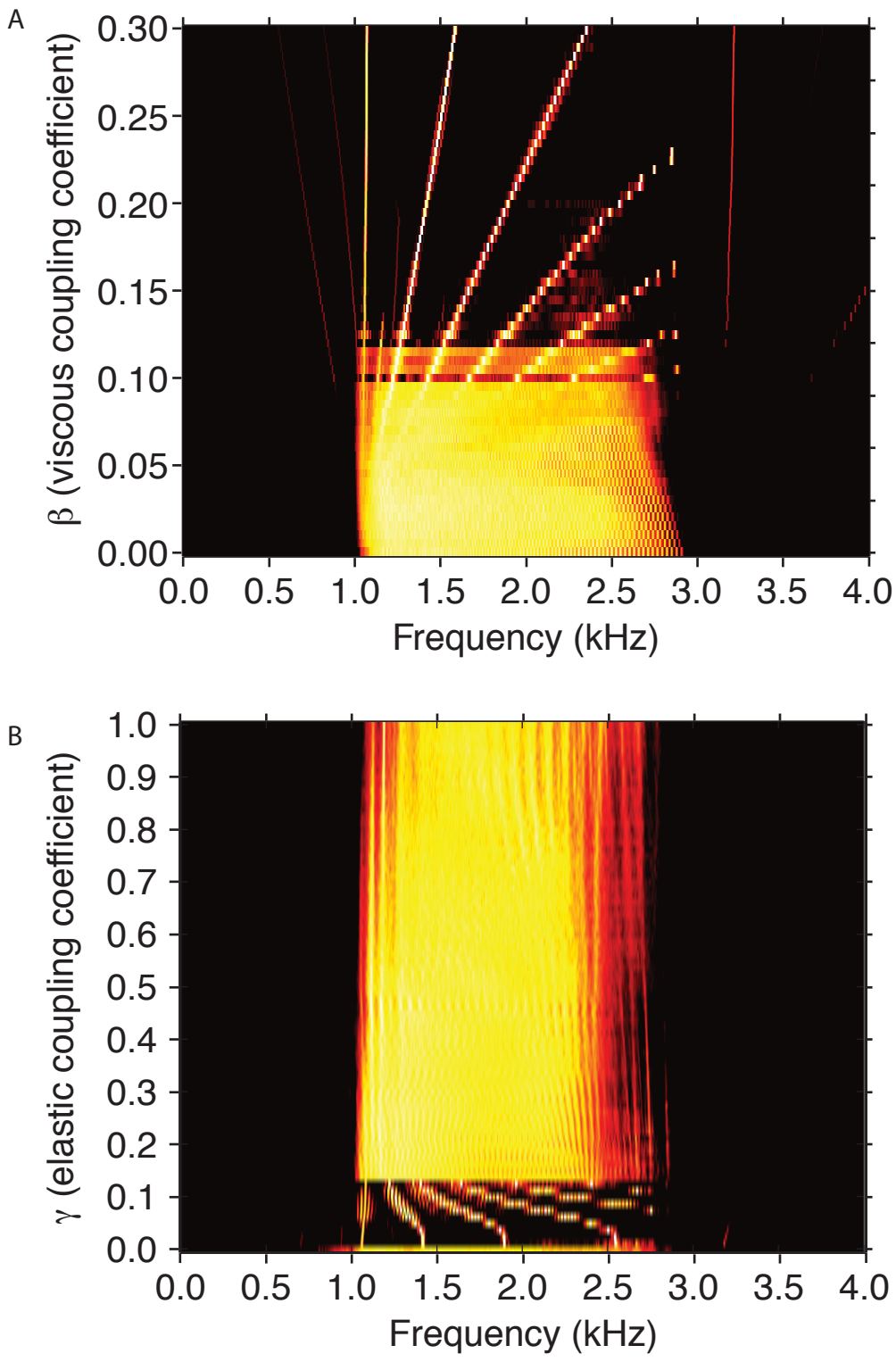
A
β (viscous coupling coefficient)
0.30
0.25
0.20
0.15
0.10
0.05
0.00
0.0
0.5
1.0
1.5
2.0
2.5
3.0
3.5
4.0
Frequency (kHz)
B
γ (elastic coupling coefficient)
1.0
0.9
0.8
0.7
0.6
0.5
0.4
0.3
0.2
0.1
0.0
0.0
0.5
1.0
1.5
2.0
2.5
3.0
3.5
4.0
Frequency (kHz)

Figure 7

previously reported variations along the length of the basilar papilla. Notably, the number of stereocilia in each hair bundle, a possible proxy for motor strength, increases and then decreases from base to apex along the neural, tectorially-covered part of the basilar papilla (Köppl and Authier, 1995). The power spectrum for simulation of a tapered system displayed localized peaks, but was not dominated by those near the extremes (Figure 8). We therefore used this pattern of oscillation amplitudes in most of the remaining simulations.

If boundaries at the ends of the array stabilized the positions of synchronized groups, the absence of any such boundaries should have the opposite effect. Although simulating an infinite chain of oscillators would be necessary to study this condition, the result was approximated by smoothly varying α along a parabola scaled to unity in the center but to zero at both extremes. Even more than the linearly tapered system, such a system lacks sharp boundaries, as no oscillator has a substantially larger amplitude than either of its nearest neighbors. As a result, when such a system was simulated, the positions of synchronized groups were poorly localized and drifted over a wide range. Thus, the power spectrum, which was averaged over timescales greater than that on which this drift occurs, showed reduced distinctions between peaks (Figure 9A). A similar effect was seen with longer chains of oscillators, in which groups near the middle were distant from the symmetry-breaking boundaries; the corresponding peaks were again poorly localized (Figure 9B).

Formation of synchronized groups

In simulations, each oscillator exhibited power at frequencies corresponding to as many as four different groups, emphasizing the fluid nature of these interactions (Figure 10A). The relative proportion of time within the two or three dominant groups varied with the proximity of the oscillator's natural frequency to the mean frequency of the group. The weaker contributions of more distant groups to the power spectrum of a given oscillator were probably transmitted by intermediate oscillators. The power spectra for individual oscillators indicated each oscillated nearly all of the time at the frequency of a synchronized group, rather than at its own natural frequency. This result implies that nearly all oscillators participated in synchronized groups at any instant, and thus that the ceaseless rearrangements of synchronization were associated with insignificant delays. The apparent broad hump of emission in power spectra thus reflected the superposition of the wide bases of multiple emission peaks, rather than continuum emission from numerous unsynchronized oscillators.

The number of synchronized groups was determined primarily by the value of the coupling coefficient γ, which fixes both the number of oscillators within each group and the frequency spacing between groups. As γ increased, the number of groups declined, and they diverged in frequency (Figure 10B). In addition, increasing γ decreased the system's total power due to the phenomenon of amplitude death, in which interactions between nonlinear

Figure 8: Tapering of oscillator amplitudes

A chain in which the amplitude α tapers linearly over the last 18 oscillators at each end yields a power spectrum in which the peaks near the margins are sharper than those near the center. The variation is less pronounced than in (4B), however, and resembles that in experimentally recorded spectra.

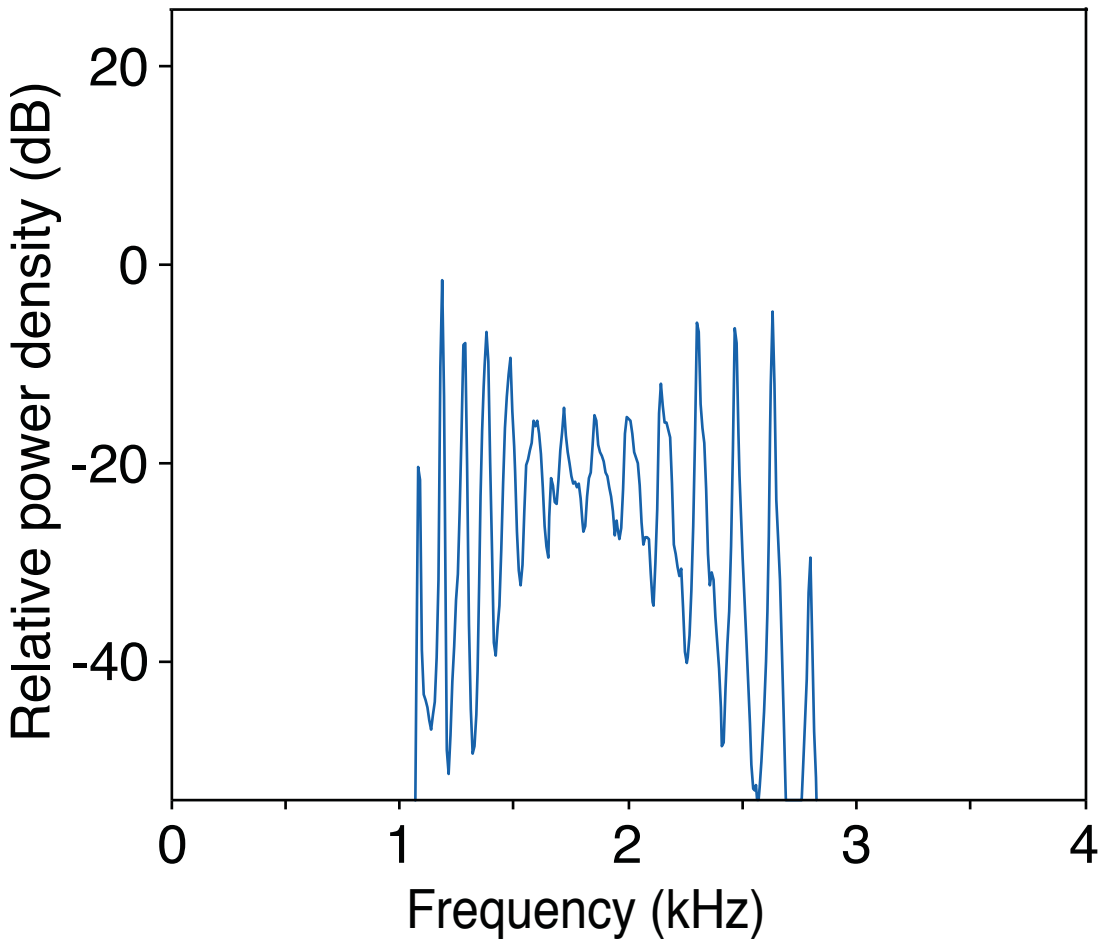

Figure 8

Figure 9. The effect of boundary conditions. A. For a system in which the amplitude of free-running oscillation α varies parabolically across the array, the power spectrum displays poorly defined peaks owing to the absence of sharp boundaries between oscillating groups. B. For a lengthened chain, the power spectrum shows sharp peaks produced by oscillators near the boundaries of the basilar papilla, but a poorly defined structure at the frequencies represented by oscillators in the chain's middle. The frequencies are exponentially distributed over an extended range, from 1 to 8.06, owing to the increased length of the chain.

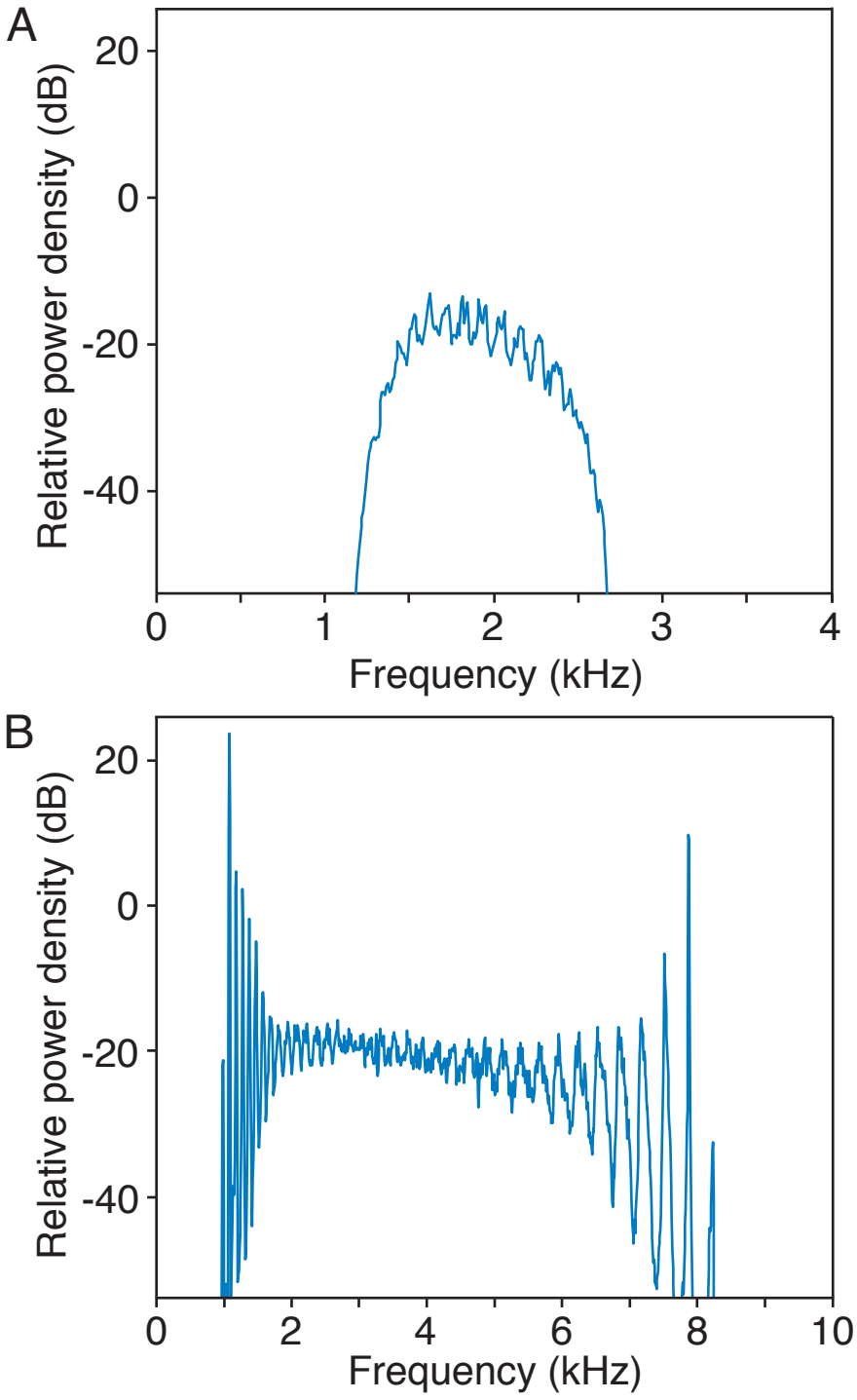
A
20
0
-20
-40
Relative power density (dB)
0
1
2
3
4
Frequency (kHz)
B
20
0
-20
-40
Relative power density (dB)
0
2
4
6
8
10
Frequency (kHz)

Figure 9

Figure 10. The formation of synchronized groups A. Vertically layered power spectra for the 110 individual oscillators indicate that each contributes power to multiple peaks as it shifts its affiliation over time. Colors encode the power-spectral density at each frequency for each oscillator, with brighter areas indicating an increase in density. The inset portrays the power spectrum for the single oscillator indicated by the dashed line. B. Increasing the elastic coupling strength from the bottom power spectrum toward the top causes a progressive reduction in the number of oscillating groups and a sharpening of the group boundaries.

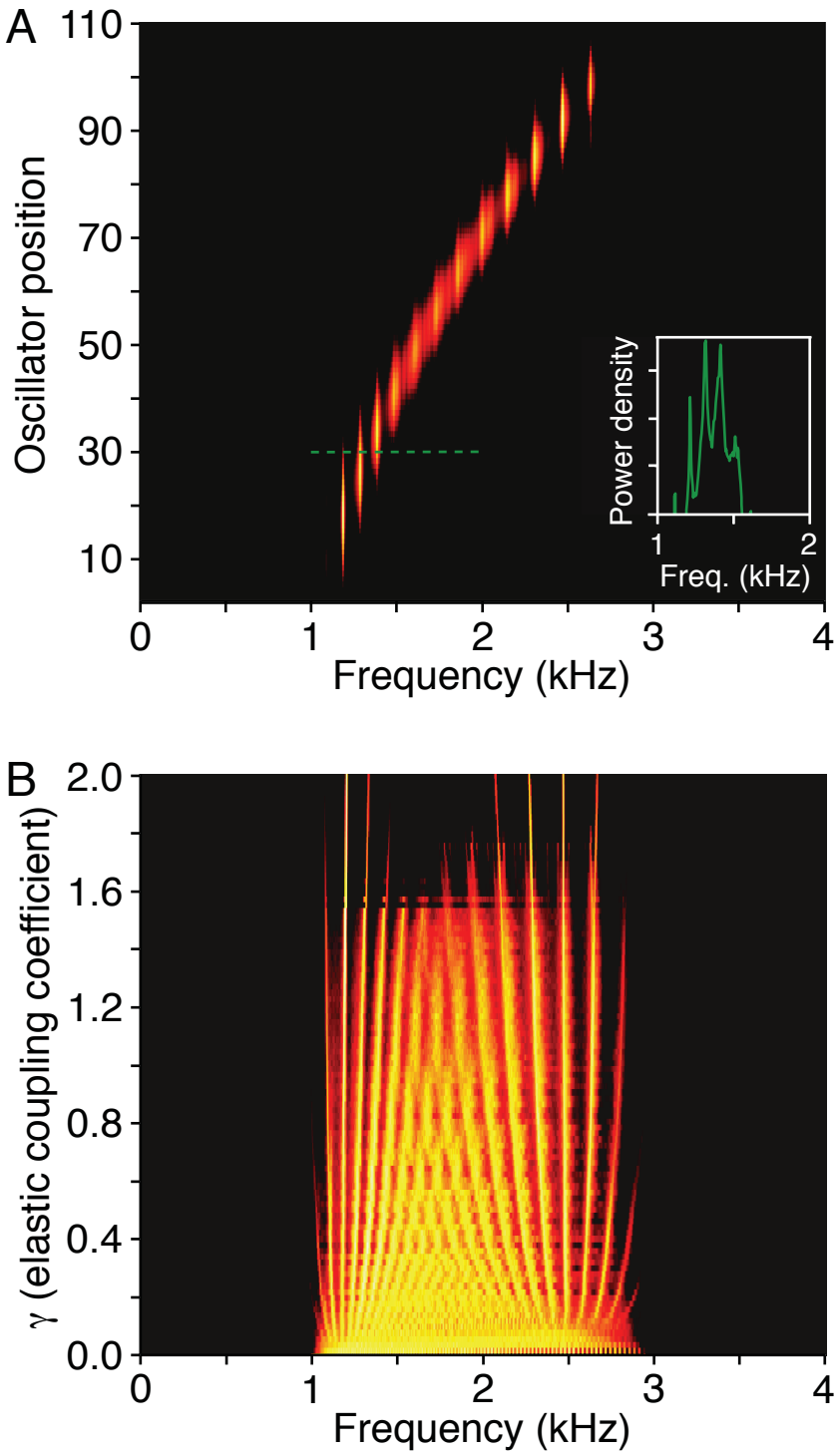
A
110
90
70
50
30
10
Oscillator position
0
1
2
3
4
Frequency (kHz)
Power density
1
2
Freq. (kHz)
B
2.0
1.6
1.2
0.8
0.4
0.0
γ (elastic coupling coefficient)
0
1
2
3
4
Frequency (kHz)

Figure 10

oscillators leads, under appropriate conditions, to the generation of a stable fixed point and the decay of oscillations (Mirollo and Strogatz, 1990). The power decreased rapidly for small values of γ, and more gradually for greater values.

This variation of synchronized groups with γ relates to an Arnold tongue. This concept describes the way in which the frequency interval between an oscillator and a sinusoidal force acting on it determines the amplitude required for the force to entrain the oscillator. However, in this case the force acting on an individual oscillator came from a nearby synchronized group, which itself comprised several synchronized oscillators and thus had significant internal interactions and was susceptible to forces from other nearby groups. These complex interactions resulted in a pattern of affiliations that shifted with γ. Because the synchronization of an oscillator to a particular group led to a positive feedback cycle in which the frequency of the group moved slightly towards that of the newly entrained oscillator, this process occurred through a series of abrupt transitions. In each of these transitions, the locations and frequencies of several groups near the center of the chain suddenly shifted, resulting in one fewer group (for increasing γ). At any instant, the oscillation frequency of a synchronized group lay near the median natural frequency of the oscillators within that group. The distribution of frequencies for oscillating groups consequently resembled that of the individual oscillators. An exponential distribution of oscillator frequencies,

as used in most simulations, led to an approximately exponential distribution of peak frequencies; a linear distribution of oscillator frequencies resulted in a similar distribution of peaks. Deviations from this ideal likely resulted from the stabilizing effects of the ends of the chain on nearby groups, causing those groups to be slightly larger and to have different frequency distributions than would otherwise be expected.

The role of roughness

The model so far developed explains many of the features of experimentally-recorded SOAE spectra; tuning of γ to the proper value allows the formation of the proper number of synchronized groups covering an appropriate range of frequencies. However, some aspects of experimental spectra have not yet been replicated in simulations. First, peaks in simulated spectra were sharper than those recorded from geckos, with less frequency dispersion. Second, gecko emissions show greater variability and less consistent patterning of both peak amplitude and interpeak spacing than simulations, in which peak amplitudes and spacings deviated from uniformity only slightly and in a systematic manner that varied with distance from the end of the array. We thus added additional elements to the model to help explain these discrepancies.

Our results to this point suggest that the emission spectrum is determined by the boundary conditions for the chain of oscillators. However, boundaries capable of breaking the symmetry along the oscillator chain are not limited to the

ends. Any deviation in the properties of an oscillator from those of its neighbors could bias the formation of synchronized groups away from certain positions and towards others. These deviations could be in any of the parameters that determine the behavior of the oscillators, including μ, the nonlinearity of oscillations, or their frequency *f*; variations in the latter change the relative frequency intervals between the oscillator and its two neighbors. A potential boundary could also be introduced by varying γ, the elastic coupling coefficient. We chose to examine variations in the final parameter, α, which determines the amplitude of oscillations and which was previously used to taper the oscillations of units near then ends of the array.

We initially introduced internal boundaries by varying the value of α for a single oscillator near the center of the array. The effect of this change depended on whether that oscillator fell in the middle of an existing group, at the more fluid transition between adjacent groups. When an oscillator in the center of an existing group was strengthened, the existing pattern of synchronized groups was reinforced (Figure 11a). There were no significant shifts in the frequencies of peaks, but peaks corresponding to synchronized groups near the augmented oscillator become markedly sharper and with greater power following as little as a 2% change. When this same oscillator was instead weakened the pattern of synchronization was disrupted; in the resulting power spectrum, the peak containing the weakened oscillator disappeared, as did other nearby peaks, to be replaced by peaks falling near the original spectrum's troughs. This latter effect

required more of a change than that seen in augmentation, but was still able to shift the pattern for decrements of only 10% in a single oscillator. An opposite effect was seen for changes to oscillators whose natural frequency fell between two existing spectral peaks (Figure 11b).

Weakening these oscillators reinforced the existing pattern, while strengthening them overturned it. Again, the former effect required less of a deviation than the latter, but either could be accomplished with no more than a 10% change in one oscillator.

Variation of α for a single oscillator was able to induce changes in the behavior of oscillators along a substantial fraction of the complete array. The behavior of oscillators in experimental systems, of course, is expected to vary at more than a single location. We simulated a system in which roughness, or variation in the value of a parameter, was present along the entire length of the chain of oscillators. The result, consistent with that seen for a single variation, was a combination of shifts of peak frequencies and peak stabilization. An array in which the value of α was not constant across the central group of oscillators, but instead varied randomly by a small percentage, yielded stable groups, and spectral peaks with little frequency dispersion (Figure 12A). This phenomenon occured even when α deviated by as little as 3% from its average value, a level of roughness far smaller than is likely to exist in the biological system under study. Greater levels of roughness localized the groups still more precisely and resulted in spectra with uneven spacing between peaks.

Figure 11: The effect of variation in the strength of a single oscillator

A. Systematic variation of the amplitude α of a single oscillator induces a widespread rearrangement of spectral peaks. The natural frequency of the oscillator, 1.88 kHz (blue dashed line), falls in the middle of a synchronized group that forms in the case of uniform amplitudes (green arrow). B. Systematic variation of the amplitude α of a single oscillator induces a widespread rearrangement of spectral peaks. The natural frequency of the oscillator, 1.95 kHz (blue dashed line), falls between two synchronized groups that form in the case of uniform amplitudes (green arrow).

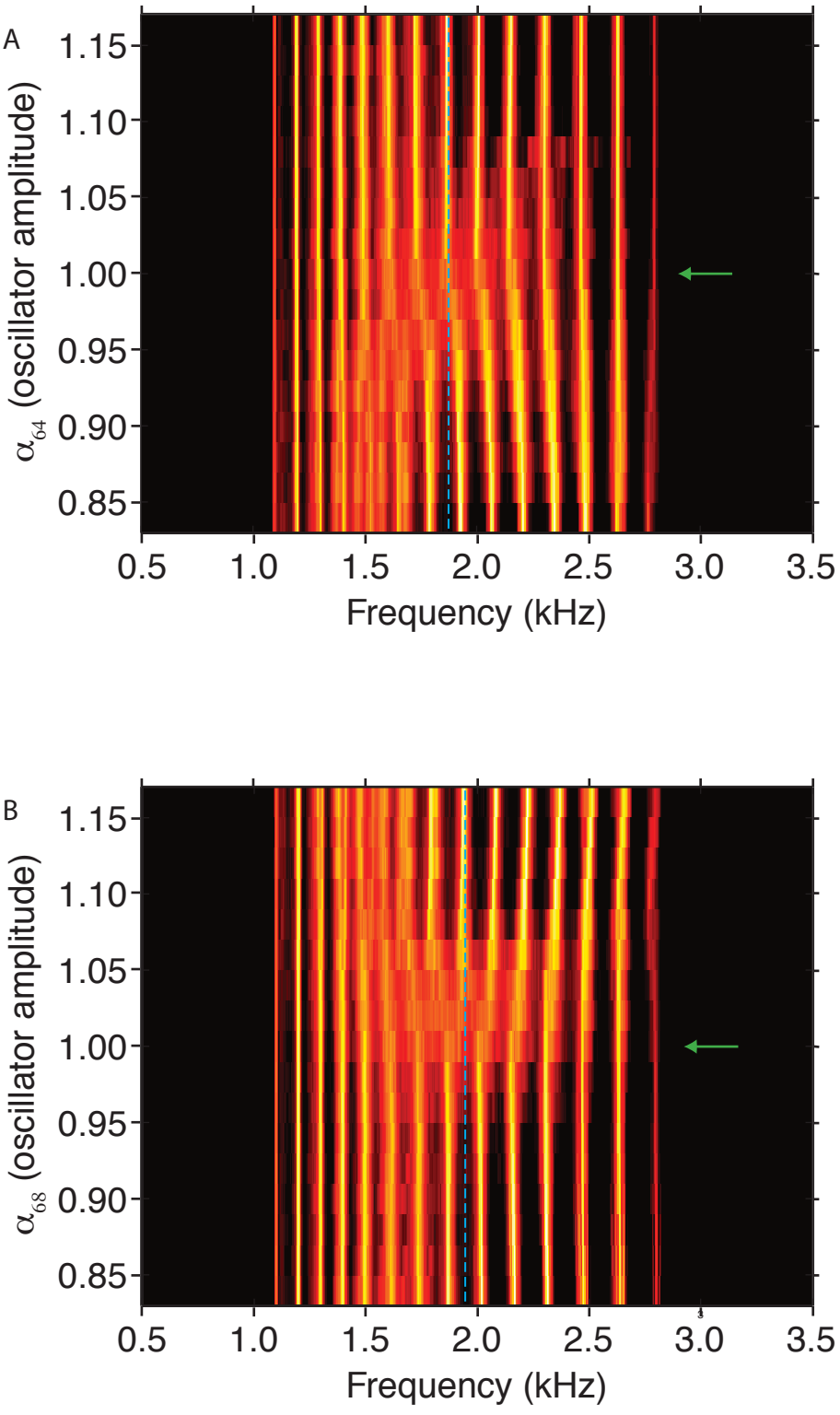
A
1.15
1.10
1.05
1.00
0.95
0.90
0.85
α_{64} (oscillator amplitude)
0.5
1.0
1.5
2.0
2.5
3.0
3.5
Frequency (kHz)
B
1.15
1.10
1.05
1.00
0.95
0.90
0.85
α_{68} (oscillator amplitude)
0.5
1.0
1.5
2.0
2.5
3.0
3.5
Frequency (kHz)

Figure 11

Figure 12. The effects of roughness and noise. A. When all the oscillators are identical, the central peaks of the power spectrum are poorly defined (blue trace). Introduction of quenched roughness in the value of the free-running amplitude α locks the oscillators into particular groups and thereby sharpens the power-spectral peaks (red trace). In this instance, the value of α over the central 74 oscillators follows a normal distribution with a mean of unity and a standard deviation of 0.03. B. When a control simulation (blue trace) is altered by the addition of white noise, the initially well-defined spectral peaks are effaced (red trace). The noise is approximated by forcing that is normally distributed around 0 with a standard deviation of 0.1 and varies every 16 ms. C. Simultaneous incorporation of noise and roughness shows the reappearance of distinct peaks (red trace).

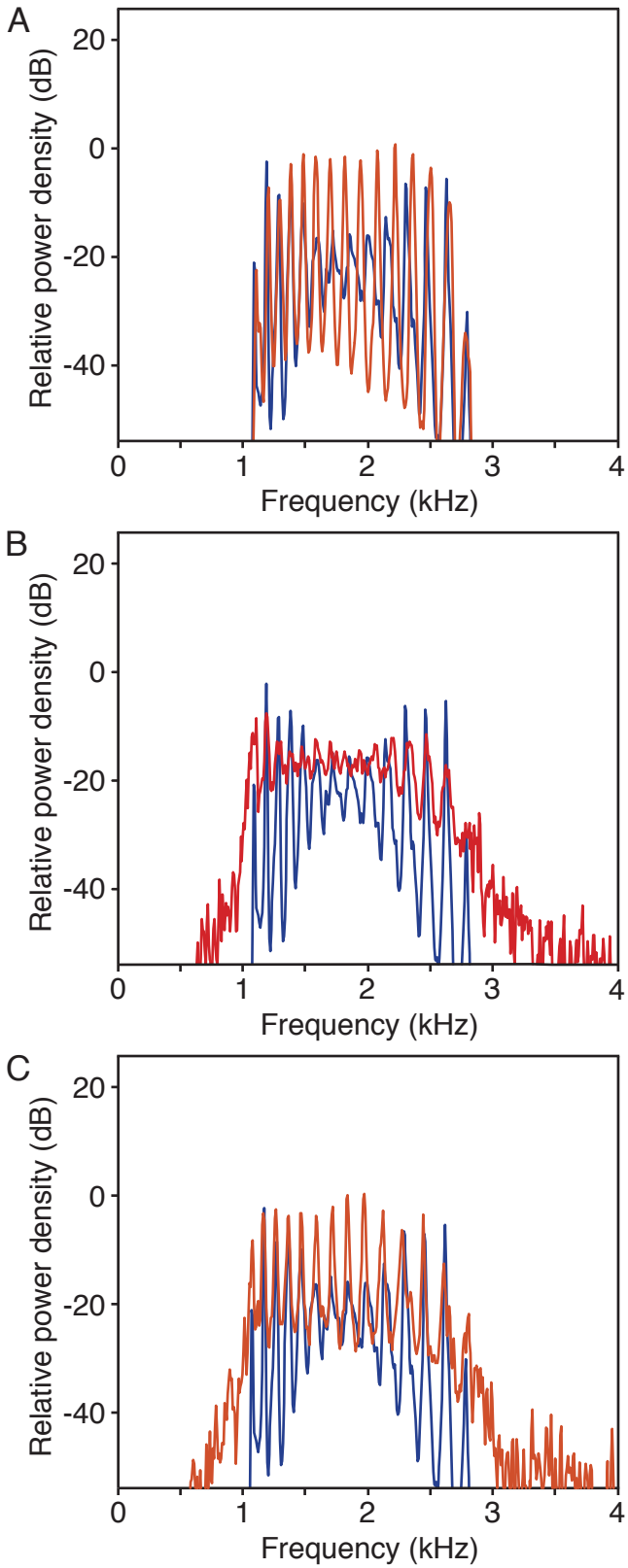
A
20
0
-20
-40
Relative power density (dB)
0
1
2
3
4
Frequency (kHz)
B
20
0
-20
-40
Relative power density (dB)
0
1
2
3
4
Frequency (kHz)
C
20
0
-20
-40
Relative power density (dB)
0
1
2
3
4
Frequency (kHz)

Figure 12

The effect of noise

Noise of either the thermal or acoustic variety could lead to variations in the frequencies of individual oscillators and thus to a more rapid shift in the pattern of synchronized groups that are formed. We simulated the effect of white noise on spontaneous otoacoustic emissions by adding an additional term to the right side of Equation 4. This term was randomly drawn anew from a normal distribution every 16 μs. In addition to introducing a noise floor in power spectra, this alteration weakened synchronized groups along the chain and dispersed the most prominent spectral peaks (Figure 12B). This effect opposed that introduced by structural roughness: when noise and roughness were simultaneously present, well-defined spectral peaks reappeared (Figure 12C). We do not know how the amount of noise required to destabilize synchronized groups in our simulations compares to that present in a gecko's natural environment.

Response to an external tone

The spectrum of spontaneous otoacoustic emissions changes in characteristic ways when the ear receives an external stimulus tone. Most notably, spectral peaks with frequencies near that of the tone usually decline in amplitude and shift away in frequency from the stimulus (Long et al., 1991; Köppl and Manley, 1994). To test the ability of our model to replicate these effects, we

introduced a sinusoidal force acting on all the oscillators. We altered Equation 3.8 for each oscillator to

$$\dot{x} = \mu\left(y - \frac{x^3}{3} + \alpha x\right) + \gamma\left(x_{n-1} - 2x_n + x_{n+1}\right) + \delta \cdot \sin(2\pi F t), \qquad \textbf{[3.9]}$$

in which δ represents magnitude and *F* the frequency of an acoustic stimulus. In the presence of a stimulus, oscillators with natural frequencies near that of the external input became synchronized with it (Figure 13). The frequency interval between an oscillator and the stimulating tone determined the magnitude of force needed to entrain that oscillator. This entrainment additionally suppressed the baseline power at frequencies near the stimulus. Like the boundary conditions examined earlier, the external force broke the symmetry of the chain by differentially affecting oscillators at different frequencies. Spectral peaks at frequencies near that of stimulation became more pronounced. Because a group of oscillators was synchronized exactly with the external input, stimulation effectively divided the chain of oscillators into two segments with negligible communication. The power spectra for individual oscillators showed a strong, narrow peak at the stimulus frequency (Figure 13B). Adjacent peaks also became better localized owing to their proximity to this imposed boundary. Some peaks were repelled by the tone, with frequencies shifting away from that of the stimulus.

The frequency range over which oscillators became synchronized increased with the strength of the external stimulus (Figure 14). Thus, the

Figure 13. The effect of external stimulation. A. A simulated power spectrum in the absence of stimulation displays relatively weak peaks in its central region (black trace). The introduction of sinusoidal forcing at a frequency of 2.0 kHz (dashed blue line) accentuates the central peaks and shifts their frequencies away from that of the stimulus (red trace). The baseline power density immediately surrounding the stimulus frequency is also suppressed; in this instance, the power falls by an average of 12 dB within the 30-Hz-wide band immediately adjacent to the stimulus. B. In the presence of stimulation at 2.0 kHz (dashed yellow line), the power spectra for individual oscillators display sharply defined groups near the frequency of forcing.

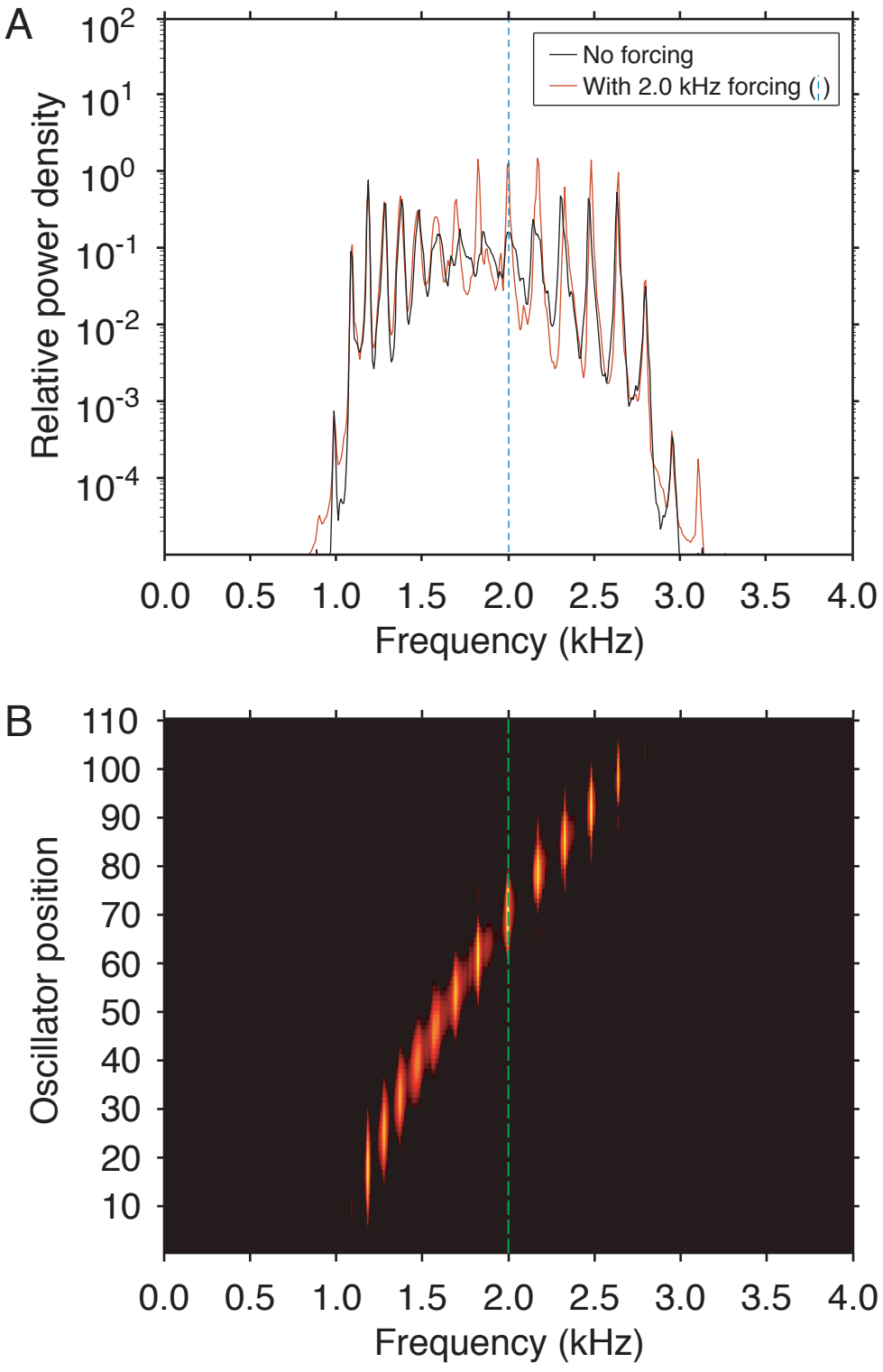
A
Relative power density
10^{2}
10^{1}
10^{0}
10^{-1}
10^{-2}
10^{-3}
10^{-4}
No forcing
With 2.0 kHz forcing (¡)
0.0 0.5 1.0 1.5 2.0 2.5 3.0 3.5 4.0
Frequency (kHz)
B
Oscillator position
110 100 90 80 70 60 50 40 30 20 10
0.0 0.5 1.0 1.5 2.0 2.5 3.0 3.5 4.0
Frequency (kHz)

Figure 13

Figure 14. External stimulation varied in amplitude or frequency A. As the forcing amplitude δ increases from the bottom of the figure toward the top, vertically layered power spectra reveal the systematic migration of the oscillation frequencies of other groups away from that of the stimulus of 1.8 kHz. B. As the external stimulus frequency is varied over a wide range, as denoted by the line running diagonally from the lower left to the upper right, vertically layered power spectra demonstrate the reorganization of successive groups of oscillators. As the stimulus frequency shifts toward higher values, oscillating groups of higher frequency abruptly disappear one by one, whereas additional lower-frequency groups appear.

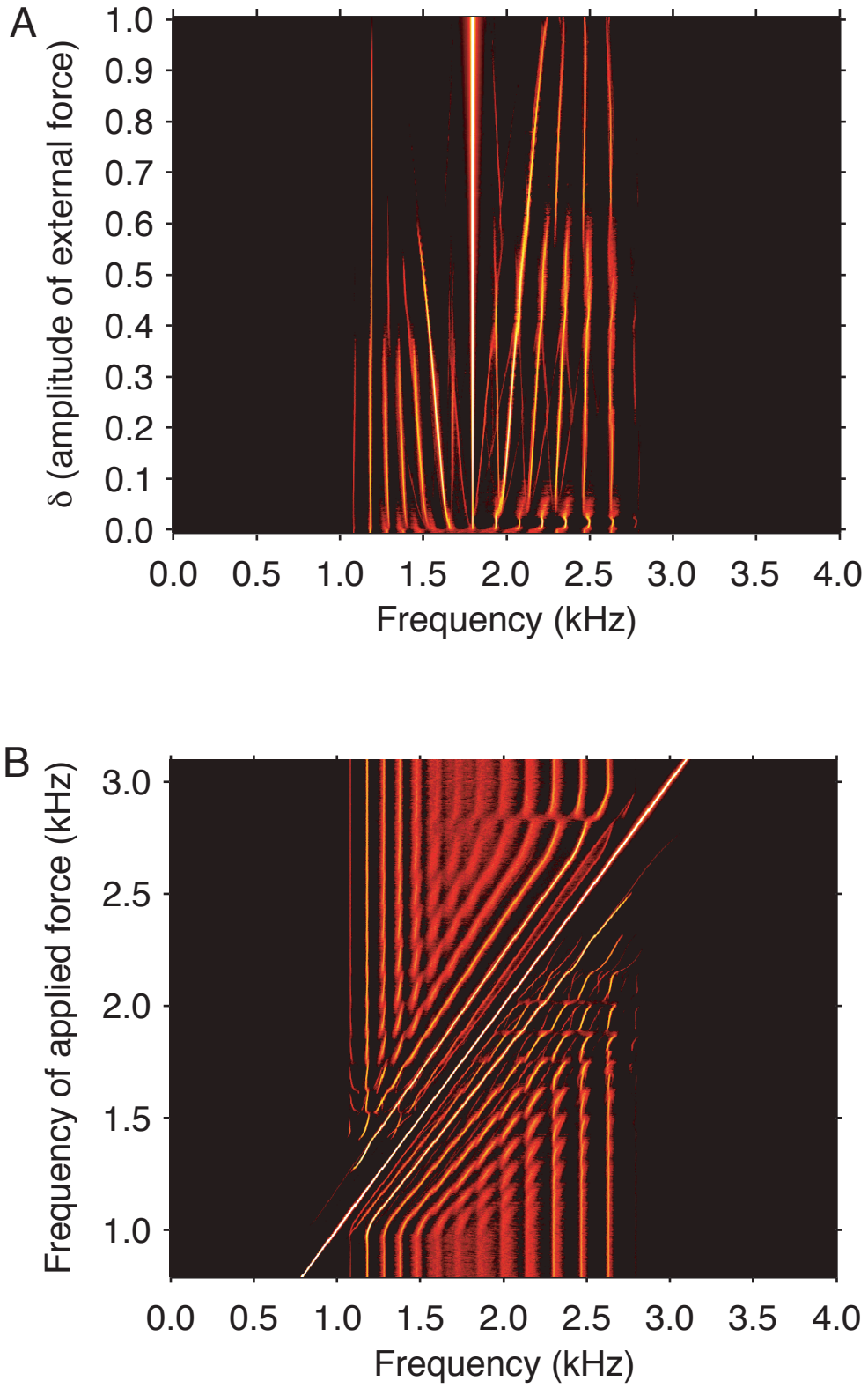
A
δ (amplitude of external force)
1.0
0.9
0.8
0.7
0.6
0.5
0.4
0.3
0.2
0.1
0.0
0.0 0.5 1.0 1.5 2.0 2.5 3.0 3.5 4.0
Frequency (kHz)
B
Frequency of applied force (kHz)
3.0
2.5
2.0
1.5
1.0
0.0 0.5 1.0 1.5 2.0 2.5 3.0 3.5 4.0
Frequency (kHz)

Figure 14

closest large peak, formed by the contributions of oscillators *not* entrained to the stimulus, moved gradually away from the frequency of stimulation. At the same time, the power spectrum of the summed oscillators progressed through several regimes with variation of the stimulus strength. A weak external force induced a rearrangement of the frequencies of spectral peaks; this likely reflected a shift in the relative stabilities of two qualitatively different patterns of synchronization. In the absence of stimulation, these patterns had similar stabilities, and both contributed to the final power spectrum. Even a weak stimulus, however, was sufficient to bias the system towards adopting a single configuration, leading to the observed frequency shifts. Further increases in stimulation then caused a repulsion of peaks with frequencies near that of the external force. This counterintuitive behavior results from the fact that, despite the apparently continuous existence of peaks across different magnitudes of stimulus, the population of oscillators that contributed to the repulsed spectral peaks in fact changed with changes in the stimulus. Increasing the amplitude of the external force synchronized oscillators with natural frequencies at ever greater distances. As a result, those oscillators desynchronized from their original groups. The frequency of the median oscillator within each of those deprived groups thus moved slightly away from that of the external force. Entrainment by these groups of new oscillators at the groups' more distant ends magnified this effect, and led to the propagation of this repulsion along the chain. Peaks at a greater remove from the stimulus frequency thus move away from it with increasing magnitudes

of stimulus. The amount of repulsion decayed at greater distances as the boundary effects of the ends of the array began to dominate. The distance between synchronized peaks thus decreased continuously with increasing stimulus, until eventually falling below a limit set by the elastic coupling coefficient. At this point a rearrangement occurred, decreasing by one the number of coupled groups. Similar to the rearrangements seen in Figure 10B, this change occurred due to positive feedback that quickly stabilized the new pattern at the expense of the original arrangement.

Varying the frequency of external stimulation provided further insight into the system's behavior (Figure 14B). For a fixed magnitude of the external stimulus, the frequency range of the oscillators that became synchronized remained nearly constant as the stimulus frequency changed. The spectral peaks adjacent to that of the external force therefore stayed separated from it by a fixed frequency interval, even as every individual oscillator that contributed to them was replaced by another. Forcing at frequencies below that of all oscillators had no effect until oscillators at the low-frequency end of the array begin to synchronize to the force. For further increases in the frequency of the external force, synchronized groups were repelled toward the chain's higher-frequency end, with those closest to the tone's frequency moving most rapidly. As in the case of an external force with varying amplitude, synchronized groups at frequencies between that of the forcing and that of the chain's high-frequency end were compressed in frequency. When the frequency interval between

adjacent groups dropped below a critical value, the entire segment of the chain undergoes a rearrangement, resulting in one fewer synchronized groups. A complementary pattern emerged at frequencies below that of the external forcing. After each rearrangement, the remaining synchronized groups recurred at the same locations as groups in the previous arrangement, providing further evidence that the size of a stably-synchronized group is tightly bounded both above and below by the strength of elastic coupling.

Previous experiments measuring the effects of external single-frequency tones on SOAEs have primarily examined the impact of tones on individual emission peaks, rather than on the entire pattern. Although the results simulated here replicated the experimentally-observed ability of external tones to repel emission peaks, the frequency range over which this effect is seen is greater in simulations than in experiments. In our model, the repulsive effect decayed gradually with frequency distance from the tone, and could be seen as far away as 1.5 kHz. We examined whether this discrepancy could also be explained by the presence of roughness in the array of oscillators. Just as roughness stabilized peaks in the perturbed spectrum, it also rendered them resistant to the effects of external forcing. In particular, roughness limited the range of oscillators that were substantially affected by forcing of a fixed amplitude and frequency. Thus, variation of an external stimulation in amplitude or frequency resulted in fewer rearrangements of the pattern of spectral peaks; instead, it more narrowly affected those peaks that fell nearby.

When the frequency of an external tone with fixed amplitude was swept across the array of oscillators in the presence of slight roughness (α = 1 ± .03), the range of effects was limited to a maximum range of 1 kHz. Surprisingly, for certain frequencies of the external tone, insignificant power was found at the tone's frequency, suggesting that no oscillators had synchronized to the frequency of the tone. Despite this, the pattern of peaks shifted in these simulations, suggesting that the forcing had nevertheless altered the synchronizations that oscillators *do* undergo. (Figure 15)

A further increase in roughness (α = 1 ± .1), limited to 500 Hz the range at which the effects of the external forcing were felt. However, a similar pattern of rearrangements to that seen in the uniform system was still seen, in addition to a new behavior. When a peak was maximally repelled by the approach of an external force, further advances of the tone did not suppress the adjacent peak, as they had in previous simulations. Instead, the repelled peak gradually approached the frequency of stimulation, until the two converged. The peak then remained synchronized to the forcing across a limited range, before the same behavior happened in reverse (Figure 16).

Use of a stronger external force (δ = .2, compared to .025 in Figures 15 and 16) could synchronize oscillators to the frequency of stimulation for all frequencies. However, the distance to the closest adjacent peak varied irregularly with frequency, unlike in the uniform system, where this distance remained constant. This discrepancy again suggests that roughness causes

Figure 15: Weak external stimulation in the presence of slight roughness

In the presence of a small amount of roughness, the effects of an external stimulus (diagonal line) persist over slightly shorter frequency intervals. The weak stimulus used here is not always able entrain large number of oscillators, as seen by the dashed nature of the diagonal line above 2 kHz.

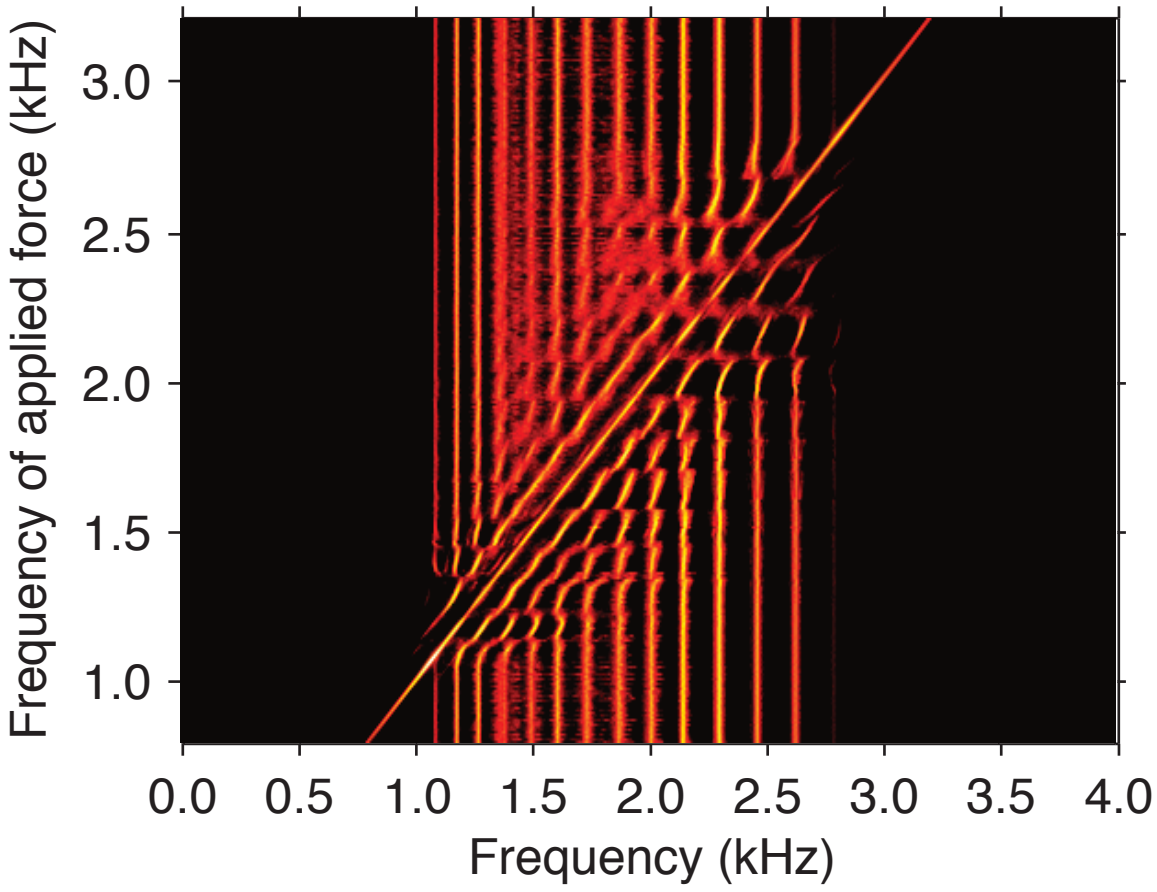
Frequency of applied force (kHz)
3.0
2.5
2.0
1.5
1.0
0.0
0.5
1.0
1.5
2.0
2.5
3.0
3.5
4.0
Frequency (kHz)

Figure 15

Figure 16: Weak external stimulation in the presence of substantial roughness

With greater amounts of roughness, the frequency intervals over which stimulation has an effect greatly decrease. The stimulus is now only able to substantially entrain oscillators near the frequencies of unperturbed peaks; thus, the diagonal line is everywhere dashed.

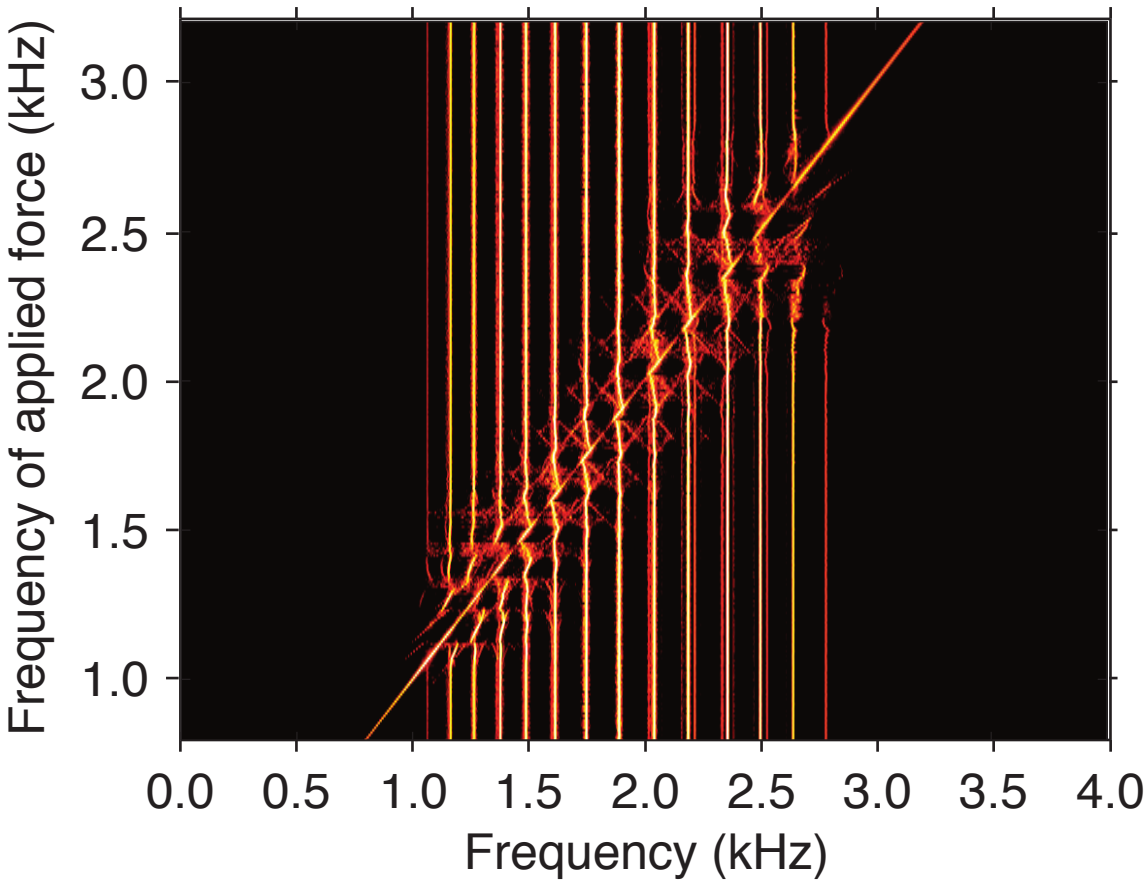
Frequency of applied force (kHz)
3.0
2.5
2.0
1.5
1.0
0.0
0.5
1.0
1.5
2.0
2.5
3.0
3.5
4.0
Frequency (kHz)

Figure 16

certain positions to be favored for the formation of synchronized peaks (Figure 17). Similarly, when the amplitude of an external force was gradually increased in the absence of roughness, the width of the area cleared of other peaks due to oscillators synchronizing to the force grew smoothly with the force's amplitude, suggesting that all positions were approximately equally favored for the formation of synchronized groups. However, in the presence of roughness, this range expanded unevenly. At certain amplitudes the range barely increased, while at others it grew rapidly as new groups of oscillators were synchronized to the forcing frequency (Figure 18).

Figure 17: Strong external stimulation in the presence of substantial roughness

With high levels of roughness, a stronger external stimulus (δ=.2) is able to entrain oscillators to all frequencies. Its effects do not propagate far in frequency, though. Two peaks with frequencies at slightly varying intervals from that of the stimulus are now nearly continuous as the stimulus is swept across frequencies (green arrows).

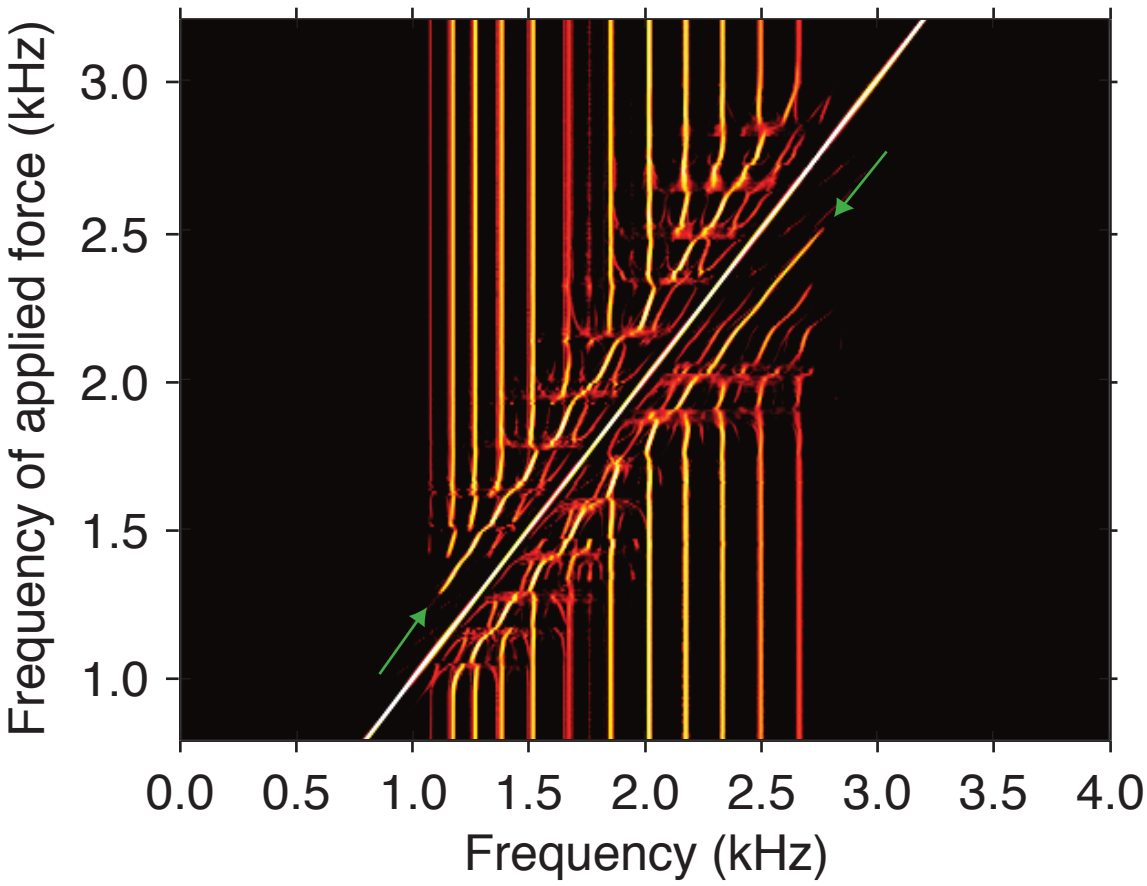
Frequency of applied force (kHz)
3.0
2.5
2.0
1.5
1.0
0.0
0.5
1.0
1.5
2.0
2.5
3.0
3.5
4.0
Frequency (kHz)

Figure 17

Figure 18: Varying the amplitude of external stimulation in the presence of roughness

In the presence of roughness, increases in the forcing amplitude δ induce uneven migration of the oscillation frequencies of other groups away from that of the stimulus, 1.8 kHz.

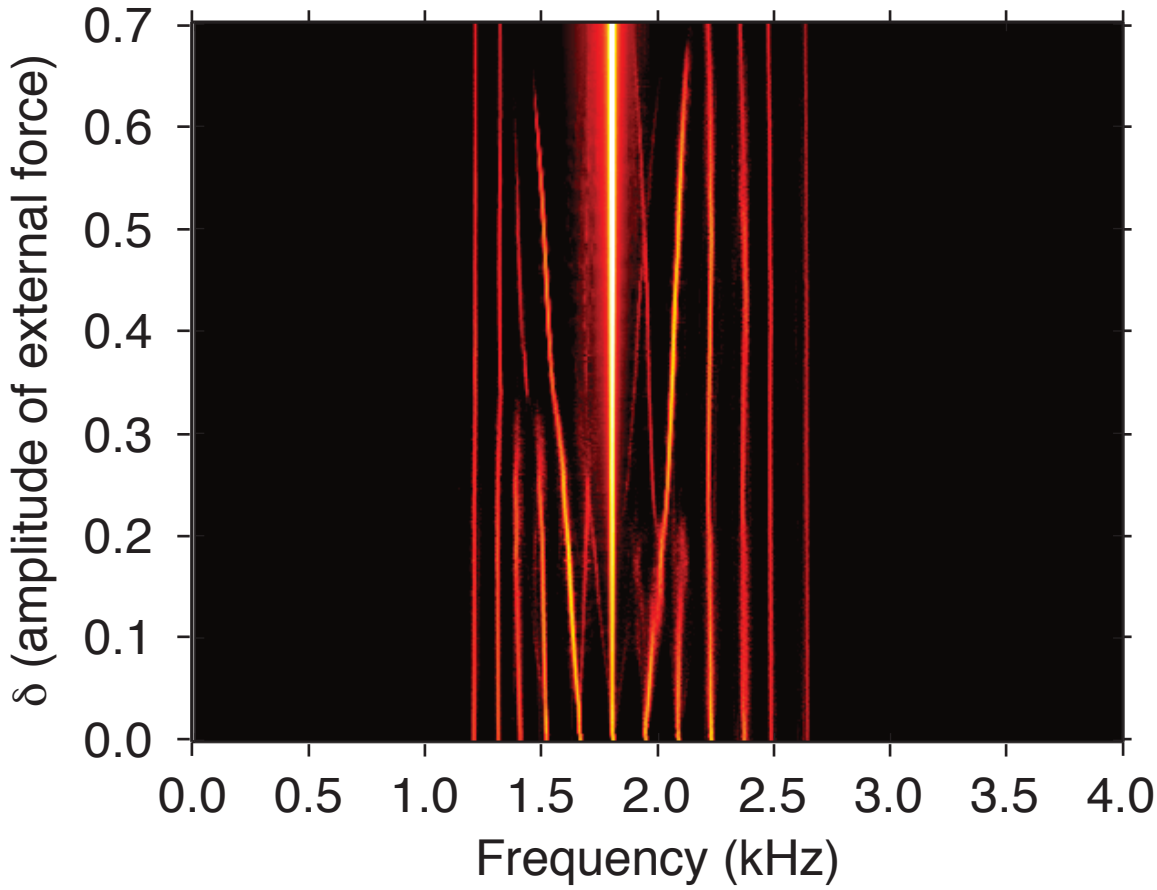
δ (amplitude of external force)
0.7
0.6
0.5
0.4
0.3
0.2
0.1
0.0
0.0
0.5
1.0
1.5
2.0
2.5
3.0
3.5
4.0
Frequency (kHz)

Figure 18

CHAPTER 4

Recording of spontaneous otoacoustic emissions from the ears of the tokay gecko

Measurement of SOAEs

Geckos anesthesized with 25 mg/kg Nembutal produced measurable otoacoustic emissions approximately 75% of the time. The spectrum of otoacoustic emissions changed only slightly over the three to five hours that a gecko remained unconscious, suggesting that emissions were largely insensitive to slight variations in anesthetic concentration. However, an excessive dose of anesthetic was frequently seen to eliminate otoacoustic emissions, even at sublethal concentrations. This finding suggests that many of the geckos that failed to produce emissions were less healthy than those that did, and thus more susceptible to the ototoxic effects of the anesthesia.

Of those geckos producing emissions, approximately 30% could not immediately be used for recordings due to the presence of a loud, periodic sound saturating the microphone's sensitivity and thus eliminating relevant information at all frequencies. This click occurred with a period varying from 1 s to as much as 10 s, and is believed to have resulted from persistent heartbeats in under-anesthetized geckos. Frequencies around 0.5 Hz are consistent with the normal range of lizard heart rates (Seebacher and Franklin, 2001) and slower heart rates

could be due to anesthesia. Administration of an additional 5-10 mg/kg Nembutal often eliminated this signal, allowing useful records to be taken from approximately 60% of all geckos.

Generic features of recorded spectra

Below approximately 800 Hz, the frequency spectrum was dominated by sources of noise outside the gecko, as determined by recording following the administration of an overdose of pentobarbital. Notable components of this noise included a broad spectral peak reaching as high as 40 dB SPL at approximately 50 Hz, as well two or three sharper peaks reaching up to 15 dB SPL, which occurred at varying positions between 500 and 800 Hz. The former likely represented a resonant mode of the room containing the experimental apparatus; although the frequencies involved were greatly removed from those being studied, this noise lowered the maximum sensitivity of the microphone and amplifier system that could be used without saturating the amplifier's response. The higher-frequency peaks were produced by a fan inside the computer used to run experiments. Their power was comparable to the largest otoacoustic emissions, and set a lower bound on the frequencies that could be studied. A large amount of power of unknown origin also appeared in the form of many other peaks at frequencies below 800 Hz.

At frequencies between 800 Hz and 5 kHz, the maximal frequency at which emissions were seen, the remaining background noise was approximately

5 dB SPL at 1 kHz and dropped off by 6.4 dB SPL, an approximate halving of sound pressure, for each doubling of frequency. This lower baseline could be seen during recording of emissions from live geckos when emissions were maximally suppressed by an external tone.

Finally, ambient noise at odd multiples of 60 Hz was sometimes observed in recorded spectra. This last source of noise, most likely introduced through the electrical wires running to the speakers used to provide external sounds into the gecko's ear, was rarely seen in the presence of spontaneous emissions, but was often 1-2 dB SPL above other background noise and thus could be seen when emissions were absent or suppressed. There is no evidence that this last artifact interfered in any way with the production or recording of spontaneous emissions.

Overall description of SOAEs

The spontaneous otoacoustic emissions of the tokay gecko are striking in their ubiquity and spectral pattern. When a sensitive microphone was used to record the sound pressure at the externally situated eardrum of a lightly anesthetized gecko, the power spectrum of the ensuing record showed the principal features of these emissions (Figure 1). Emissions could first be distinguished from background power at frequencies between 800 Hz and 1 kHz. A broad, undifferentiated peak of power extended from this range to between 4.5 kHz and 5 kHz, above which frequency emissions cannot be distinguished from background. This broad hump typically reached maximal sound levels of

approximately 5 dB SPL. Above this background sat approximately a dozen discrete spectral peaks. These could rise as little as 2 dB SPL or as many as 12 dB SPL above the broad underlying peak; the largest reached up to 15 dB SPL. The distribution of peak frequencies also varied; in some animals, the peaks were spaced regularly, by 250-300 Hz, while in others distances between peaks varied from below 100 Hz to above 400 Hz. The amplitudes of peaks within a single recording showed no clear pattern, except that those with frequencies near or above 4 kHz were characteristically lower in intensity. Because the gecko basilar papilla is known to respond to frequencies as high as 7 kHz, this may represent an inability to convey oscillations at higher frequencies toward the recording microphone, rather than the absence of oscillations above 4.5 kHz *per se*.

Recovery from damage by a prolonged pure tone

Prolonged exposure to a loud, single-frequency tone temporarily inhibits spontaneous oscillations near that frequency, an effect that persists beyond the end of the tone (Vazquez, 2001). This suppression likely correlates with the attenuation of firing of the VIIIth nerve neurons responding to that frequency.

Emissions at frequencies near an applied tone were seen to recover from suppression over a period of 30 s up to 600 s following the cessation of the tone (Figure 19). This recovery was seen in peaks as far as 450 Hz from the stimulus, and occurred over timescales that increase with greater proximity to the stimulus.

Figure 19: Recovery from noise damage

Following prolonged exposure to a stimulus tone at 3 kHz (dashed blue line), gecko SOAEs recover over 10 minutes. Recovery is slowest at frequencies near 3 kHz. Spikes seen most prominently between 3.1 and 3.6 kHz are artifactual harmonics of 60 Hz.

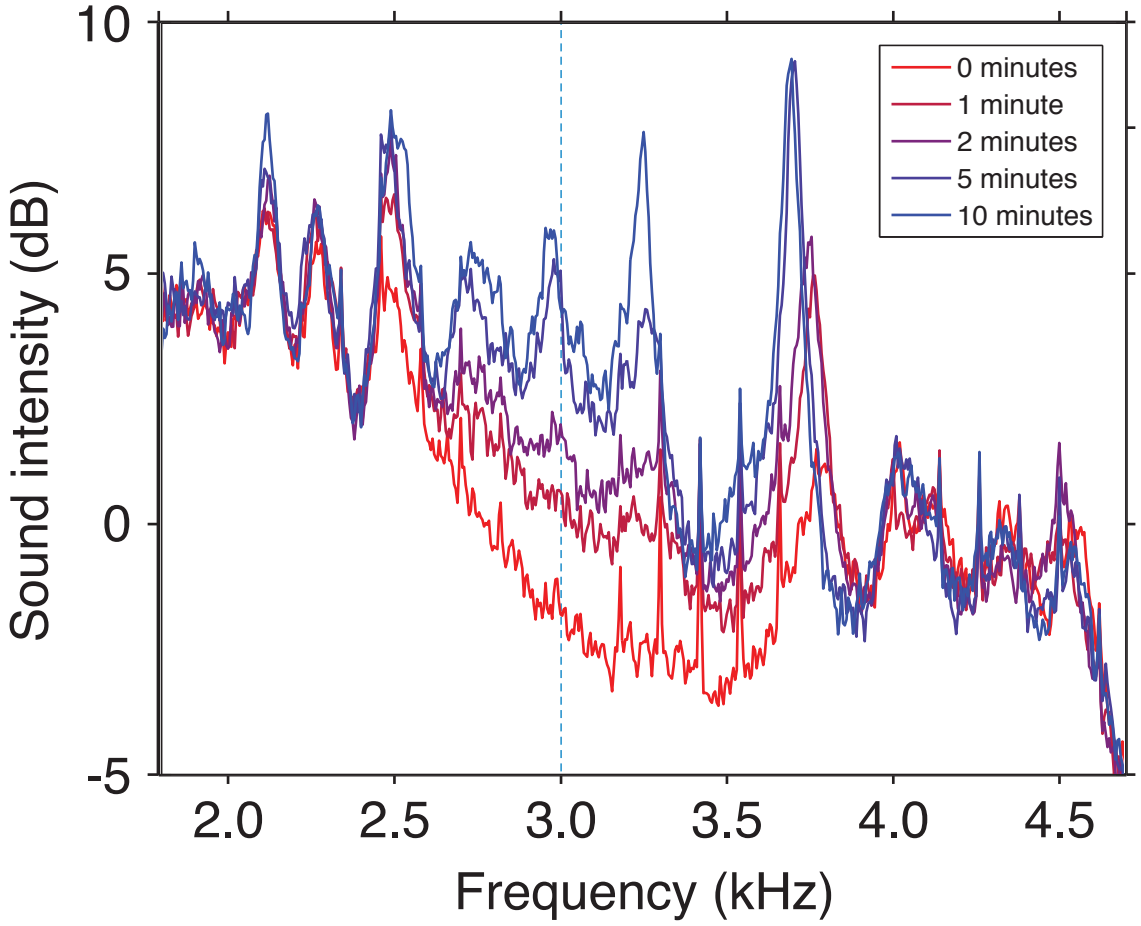
10
5
0
-5
Sound intensity (dB)
2.0
2.5
3.0
3.5
4.0
4.5
Frequency (kHz)
0 minutes
1 minute
2 minutes
5 minutes
10 minutes

Figure 19

Because experiments were not designed to examine recovery with timescales of 15 s or less, it is also possible that more distant emission peaks recovered within this period, or that nearby peaks underwent an initial, more rapid phase of recovery before that described here.

Peaks recovering from suppression usually moved towards the frequency of the tone with which they were suppressed, shifting by as much as 50 Hz. In addition, peaks sufficiently close in frequency to the external tone did not undergo frequency shifts. This pattern of movement is consistent with suppression of hair cell activity by the stimulus, with those hair cells closest in frequency to the tone being suppressed the most and thus taking the most time to recover. Thus, peaks that recover following suppression are initially formed by oscillators with frequencies that are relatively far from the tone and only later receive contributions from more proximal oscillators, leading to the shifts seen here.

Effect of a pure tone stimulus at different amplitudes

A speaker was used to introduce a single-frequency tone into the inner ear at a range of intensities, linearly distributed and randomized in order, while simultaneously recording the emissions that were produced. Several patterns were observed in the responses to this type of stimulation. Peaks in the unperturbed spectrum that fell sufficiently close to the frequency of the stimulus were eliminated for relatively low stimulus intensities, consistent with the hair

bundles producing those oscillations becoming entrained to the stimulus. More outlying peaks were suppressed and at times repelled, and the baseline was suppressed in a region surrounding the tone. The range over which these effects occurred increased with the intensity of the stimulus. On average, the baseline was suppressed over a greater frequency range at frequencies higher than the stimulus than at lower frequencies. Examples of these behaviors can be seen in Figure 20.

In addition to this overall pattern of behavior, phenomena involving small numbers of peaks were repeatedly seen and may have reflected interactions between the oscillators comprising adjacent peaks. These patterns, suggest a transfer of energy either between oscillators within existing peaks or from one or more existing peaks to a newly formed set of peaks.

In the simplest observed case, two nearby spectral peaks that were present in the absence of stimulation disappeared for stimuli greater than 45 dB SPL; at this same level an intermediate-frequency peak began to appear (Figure 21A). This behavior, similar to that seen in simulations, may have occurred as a subset of the oscillators within the peak initially found at 2.8 kHz became entrained to the stimulus frequency. The remaining oscillators from that peak could then combine with those in the peak initially found at 2.54 kHz to form a single, more powerful peak at an intermediate frequency. This pattern was also seen in a separate recording, when two peaks present in the absence of any stimulus or at low stimulus levels disappeared starting at approximately the same

Figure 20: Recorded response to a pure stimulus tone

Suppression of emissions by a 3 kHz tone applied at two different amplitudes. Suppression by a 62 dB SPL tone suppresses emissions at more frequencies and by a greater amount than suppression by a 48 dB SPL tone. For the former tone, the range of suppression extends by approximately 800 Hz toward higher frequencies, vs. only 500 Hz toward lower frequencies. A peak initially at 3.4 kHz is repelled by high stimulus intensities. The high intensity stimulus also induces a slight enhancement of emission at 2.4 kHz.

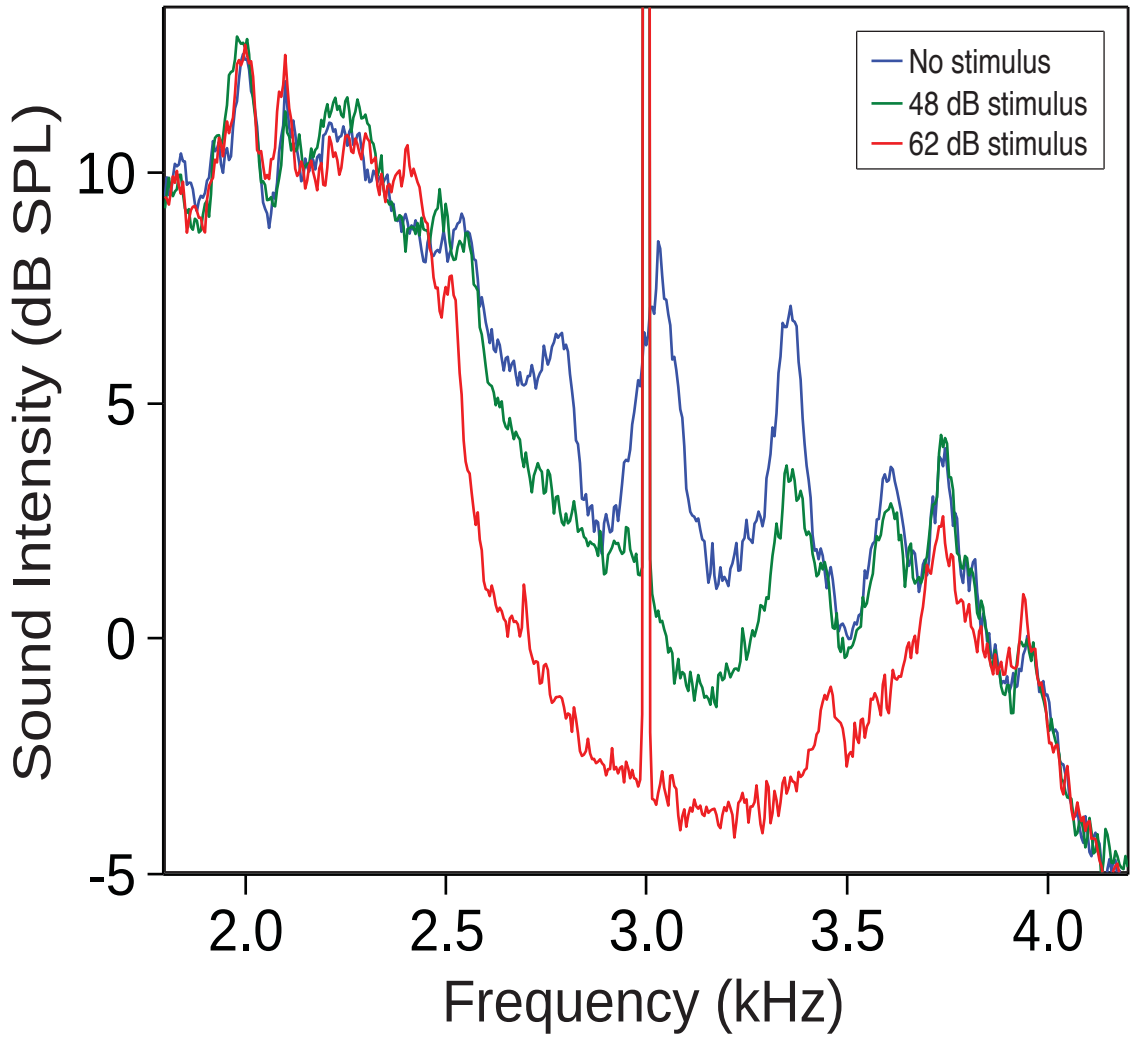
No stimulus
48 dB stimulus
62 dB stimulus
Sound Intensity (dB SPL)
10
5
0
-5
2.0
2.5
3.0
3.5
4.0
Frequency (kHz)

Figure 20

Figure 21: Response to a stimulus tone of varying amplitude: two peaks replaced by one peak

A. SOAEs recorded from a gecko vary with the magnitude of a stimulus tone at 3.1 kHz. Recordings were performed in immediate succession and with the order of stimulus intensity randomized. As in figures representing simulations, each horizontal row represents a segment of a power spectrum. Colors encode the power-spectral density at each frequency, with brighter areas indicating an increase in density; the mapping of spectral density to color varies from figure to figure to best represent emission spectra at different sound pressure levels. Two peaks present at low stimulus intensities (open arrows) merge into a single peak at higher intensities (closed arrow). In this and all similar experiments, a vertical line at the stimulus frequency is falsely colored to indicate the varying intensity of the tone. Horizontal lines and dashes, here and in all similar figures, indicate loud external noises interfering with individual recordings. B. Two nearby peaks present at low stimulus intensities (open arrows) gradually disappear with increasing stimulus, as a third peak at an intermediate frequency gradually appears (closed arrow).

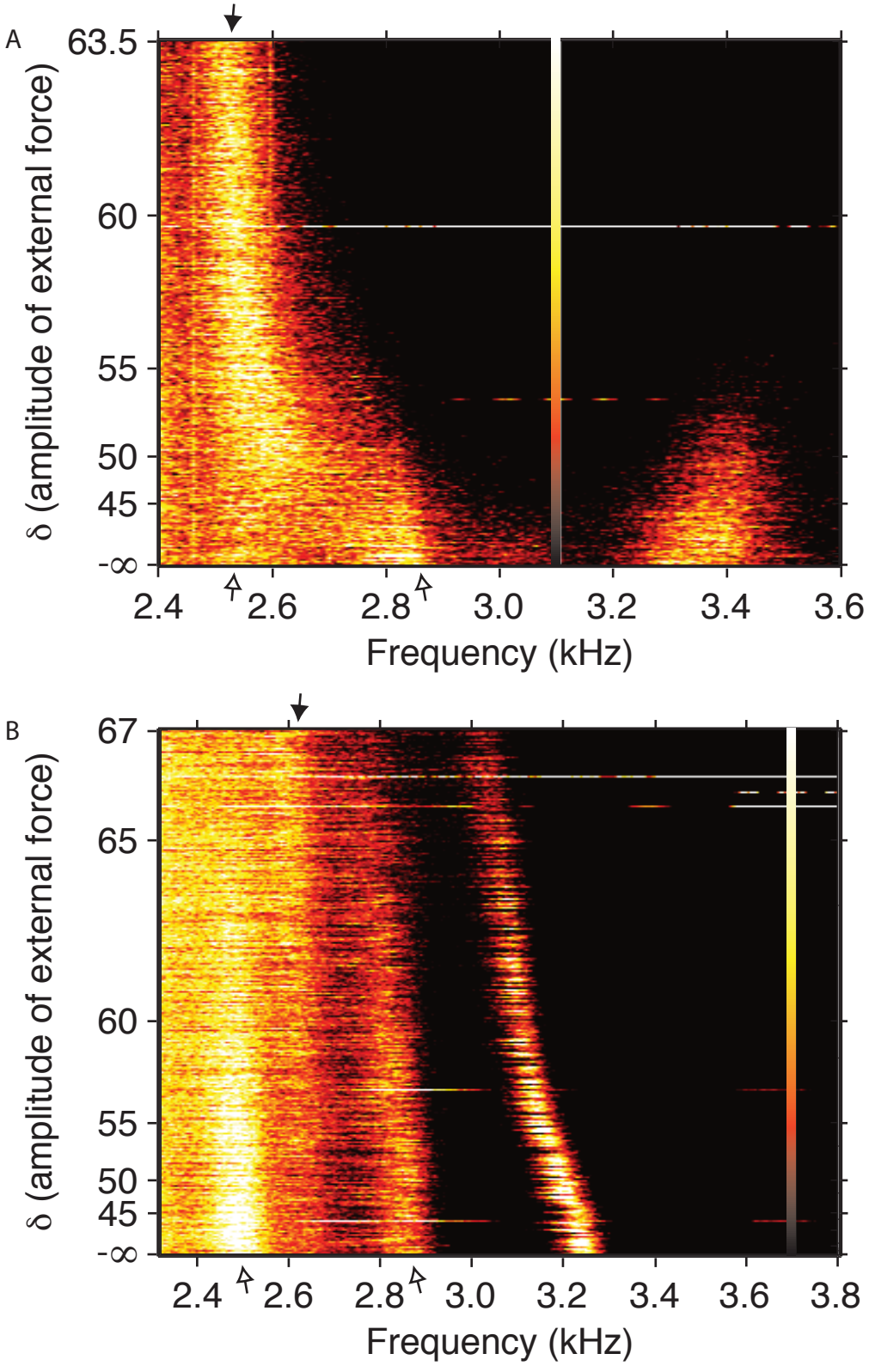
A
63.5
60
55
50
45
-∞
δ (amplitude of external force)
2.4
2.6
2.8
3.0
3.2
3.4
3.6
Frequency (kHz)
B
67
65
60
55
50
45
-∞
δ (amplitude of external force)
2.4
2.6
2.8
3.0
3.2
3.4
3.6
3.8
Frequency (kHz)

Figure 21

level of stimulus and were replaced by a novel peak at an intermediate frequency (Figure 21B).

A similar behavior was also seen in two different peaks from the same recording (Figure 22A). In this case, the lower-frequency peak was repelled from the stimulus toward a higher-frequency peak and the two eventually intersected. The resulting peak briefly has an increased intensity relative to its precursors. In another recording, two peaks were both repelled by the strengthening stimulus tone. The larger of these peaks was repelled more rapidly, though, and the two intersected and merged, forming a single peak that was further repelled for higher stimulus intensities (Figure 22B).

Two examples of related behaviors could be seen in the changing pattern of emission peaks between 2.5 kHz and 3.0 kHz in a single recording as stimulation intensity increased (Figure 23A). In both cases, rather than two peaks apparently forming a new peak, the loss of power by one peak was accompanied by either an increase in power for a nearby peak, or the appearance of a new peak. For a stimulus at 3.3 kHz with stimulus intensity below 45 dB SPL this region included three emission peaks, found at frequencies of approximately 2.6, 2.82, and 2.96 kHz. Increasing stimulus intensities slightly repelled these peaks to lower frequencies until the highest frequency peak abruptly disappeared. At the same stimulus level, the adjacent peak originally found at 2.82 kHz gained power, suggesting that a fraction of the oscillators initially found within one peak had joined the group generating the other peak. A

similar pattern was seen again with slightly higher stimulus levels. When the stimulus surpassed 56 dB SPL, the peak at 2.6 kHz gradually began to fade, as a peak at 2.7 kHz appeared. Although the cause of this rearrangement is unclear, a transfer of power from one frequency to another again seems to have occurred.

A final example of this phenomenon contained an additional twist (Figure 23B). Two peaks initially separated in frequency by approximately 300 Hz began to converge in frequency as a stimulus tone at a higher frequency gained in intensity. When the two peaks were separated by only 170 Hz, the higher-frequency one abruptly disappeared, whereas the other increased dramatically in amplitude, from an average intensity of 3 dB SPL to one of 8 dB SPL. For further increases in stimulus intensity, the strengthened peak then changed direction and moved *away* from the stimulus frequency.

Effect of a pure-tone stimulus at different frequencies

In a related experiment, an external tone of constant amplitude was introduced into the gecko's ear at a variety of discrete frequencies applied in a random order. This was repeated for several different amplitudes. For a sweep of tones 42 dB SPL in magnitude, each peak in the emission spectra was suppressed when the external tone was sufficiently close in frequency to the peak (Figure 24A). The frequency range over which this suppression occurred increased with an increase in stimulus amplitude to 57 dB SPL (Figure 24B). At this greater amplitude, it also became clear that the range over which peaks were

Figure 22: Response to a stimulus tone of varying amplitude: two peaks merge

A. One of a pair of adjacent spectral peaks (open arrows) moves away from the frequency of a stimulus as that stimulus increases in strength. When the two peaks are sufficiently close, they merge to form a single peak (closed arrow). A series of faint vertical lines visible here are artifactual harmonics of 60 Hz. B. The stronger of a pair of adjacent spectral peaks (open arrows) moves away from a stimulus frequency and the two peaks merge into a single peak, which continues to be repelled (closed arrow).

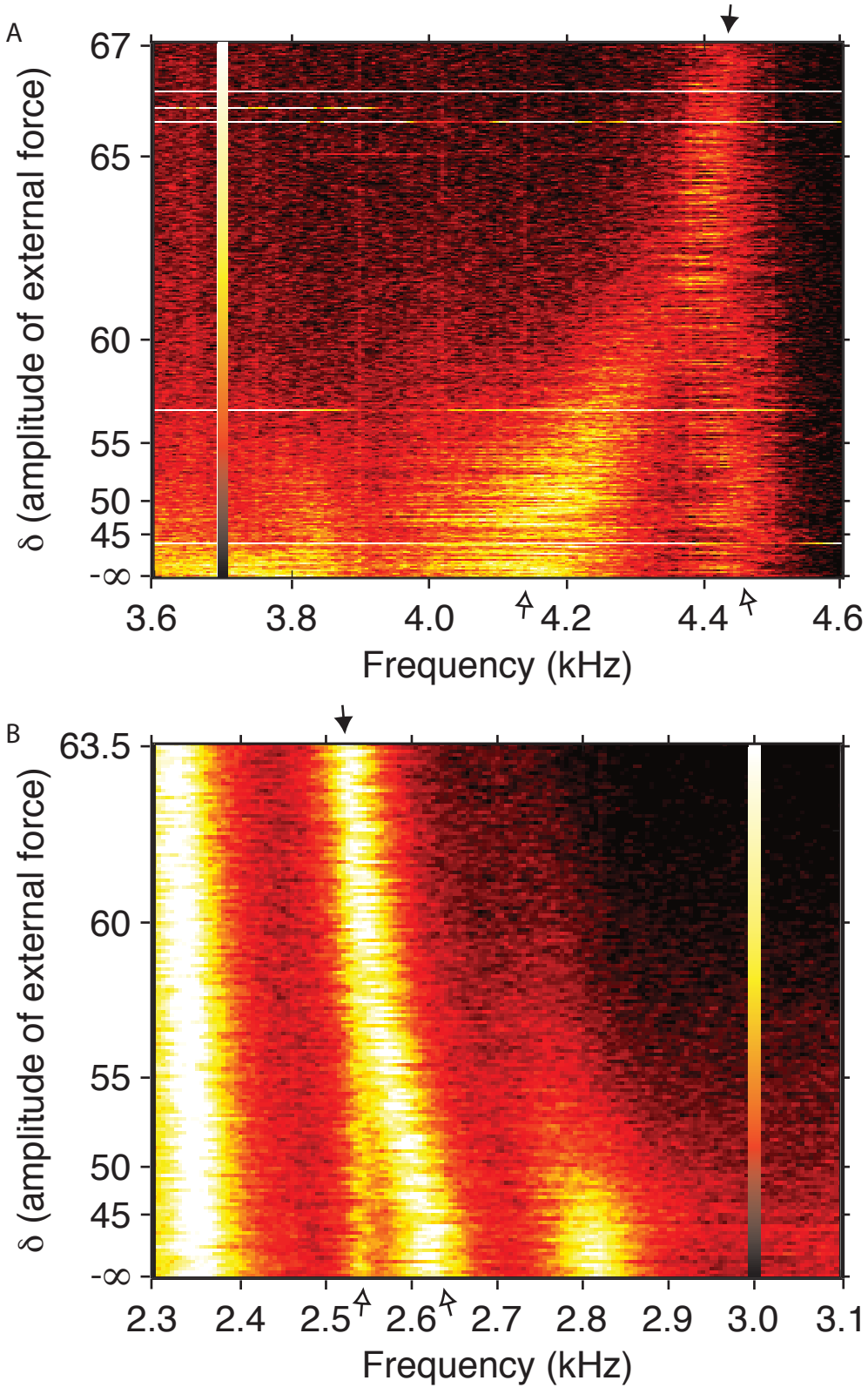
A
67
65
60
55
50
45
-∞
δ (amplitude of external force)
3.6
3.8
4.0
4.2
4.4
4.6
Frequency (kHz)
B
63.5
60
55
50
45
-∞
δ (amplitude of external force)
2.3
2.4
2.5
2.6
2.7
2.8
2.9
3.0
3.1
Frequency (kHz)

Figure 22

Figure 23: Response to a stimulus tone of varying amplitude: covariation of adjacent peaks

A. Two peaks present at low stimulus intensity (open arrows) both change abruptly for stimuli greater than 50 dB SPL: one peak disappears, whereas the other simultaneously increases in intensity (closed arrow). Independently, a third peak present at low stimulus intensities (open arrowhead) gradually weakens and is replaced by a different peak for higher intensity stimuli (closed arrowhead). B. Two adjacent emission peaks again appear to change concertedly in response to changes in the intensity of a stimulus tone. The two peaks are both present at low stimulus intensities (open arrows). They move in opposite directions in response to increasing stimulus intensities, until at a stimulus level of 52 dB SPL, one disappears. The remaining peak greatly increases in strength at that same level, and subsequently reverses direction for further increases in stimulus intensity (closed arrow).

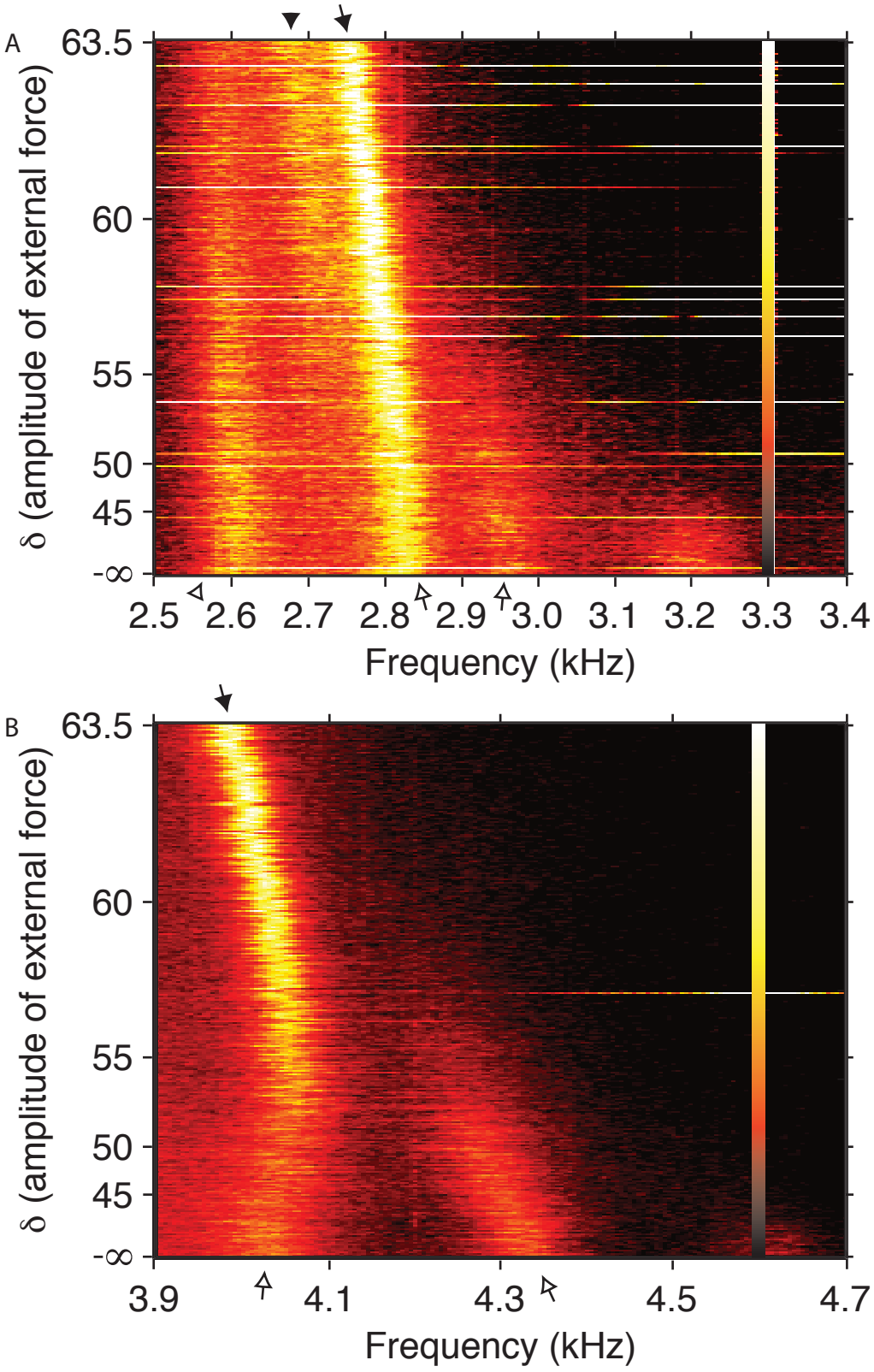
A
63.5
60
55
50
45
-∞
δ (amplitude of external force)
2.5
2.6
2.7
2.8
2.9
3.0
3.1
3.2
3.3
3.4
Frequency (kHz)
B
63.5
60
55
50
45
-∞
δ (amplitude of external force)
3.9
4.1
4.3
4.5
4.7
Frequency (kHz)

Figure 23

Figure 24: Response to a stimulus tone of varying frequency: general characteristics

A. SOAEs recorded from a gecko vary with the frequency of a stimulus tone with an intensity of 42 dB SPL (diagonal white line). Recordings were performed in immediate succession and the order of stimulus frequencies was randomized. At least seven separate emission peaks (visible as noise vertical band with intensity greater than nearby background), with frequencies between 2.4 kHz and 4.8 kHz, are visibly suppressed by the stimulus when its frequency is near that of the peak. B. A stimulus tone with an intensity of 57 dB SPL suppresses emission peaks across a broader range of frequencies. The distance from stimulus to suppressed tone increases with increasing frequency of the tone. The approaching stimulus tone repels several of the emission peaks, such as the peaks at 2.5 kHz. Suppression of the baseline emissions that lie between peaks is also present, for example at 3.4 kHz.

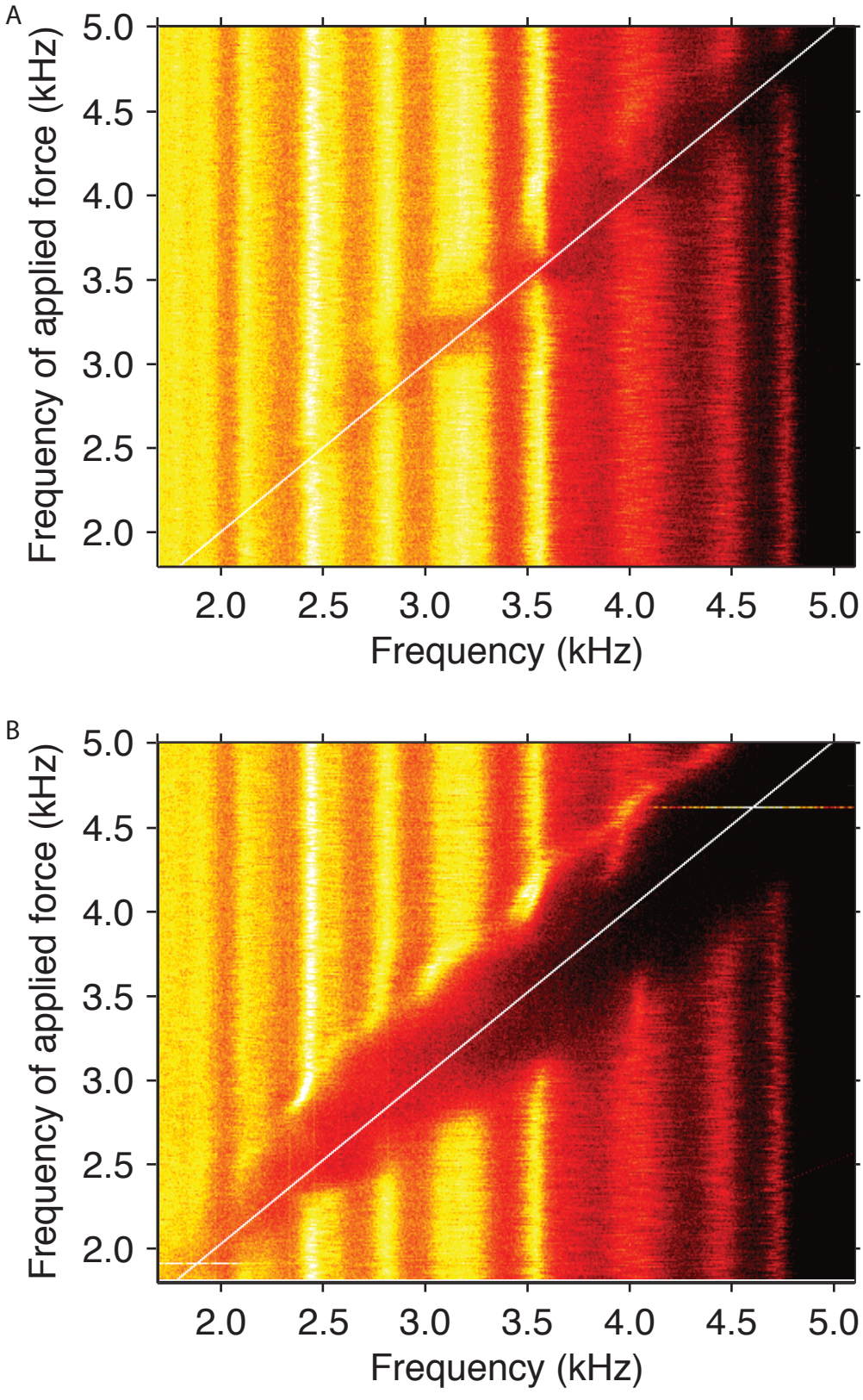
A
Frequency of applied force (kHz)
5.0
4.5
4.0
3.5
3.0
2.5
2.0
2.0
2.5
3.0
3.5
4.0
4.5
5.0
Frequency (kHz)
B
Frequency of applied force (kHz)
5.0
4.5
4.0
3.5
3.0
2.5
2.0
2.0
2.5
3.0
3.5
4.0
4.5
5.0
Frequency (kHz)

Figure 24

suppressed also increased with frequency. The power found between spectral peaks was also suppressed, and followed the same patterns.

As the stimulus tone's frequency approached that of a peak, the peak was repelled, as seen in previous experiments. Peaks thus briefly traced the outer edge of the region of suppression, usually traveling less then 100 Hz before becoming suppressed. Peaks generally showed more movement toward lower frequencies than toward higher frequencies prior to disappearing. In addition, the power present in a peak was often greater during the period of movement (Figure 25).

An unusual pattern was seen in the behavior of two spectral peaks with natural frequencies of 3.53 kHz and 4.0 kHz (Figure 26A). In both cases, after disappearing when the stimulus tone was nearby, the emission peak reappeared when the stimulus moved to higher frequencies. However, in each case it appeared as a pair of peaks which moved separately as the stimulus tone was further withdrawn, before recombining into the original peak when the stimulus was sufficiently removed in frequency. This pattern was repeated for the same peaks across a variety of stimulus levels (Figure 26B-D), suggesting that it may occur robustly for certain peaks, rather than for all peaks given the correct stimulus parameters.

A frequency sweep at a lower intensity (42 dB SPL) (seen in Figure 24A), although creating the same basic pattern, induced a different unusual behavior in one peak as the stimulus tone passes. The peak, initially at 3.55 kHz, shifted

slightly towards higher frequencies when the stimulus exceeded a frequency of 3 kHz (Figure 27). However, the peak then reversed direction twice, first moving back towards lower frequencies and then beginning to move higher before disappearing as the stimulus frequency moved through it. Upon reappearing, it underwent a similar pattern of shifts before stabilizing at the original frequency.

At the highest stimulus level (Figure 28), the edge of the area cleared by the swept stimulus tone began to show a rim: an area of slightly elevated power traveling at an approximately constant frequency interval from the tone. When this rim passed through an emission peak, it temporarily increased in power as the repelled peak moved along with it. Whereas peaks moved short distances parallel to the migrating stimulus frequency even for low stimulus levels, they began to join the continuous traveling peak only for stimuli of sufficient strength.

Figure 25: Response to a stimulus tone of varying frequency: asymmetry between high and low frequencies

Detail of Figure 24A. Three emission peaks are repelled by higher-frequency stimuli, but not by lower-frequency stimuli. Two of the peaks increase in intensity during the same recordings in which they are repelled.

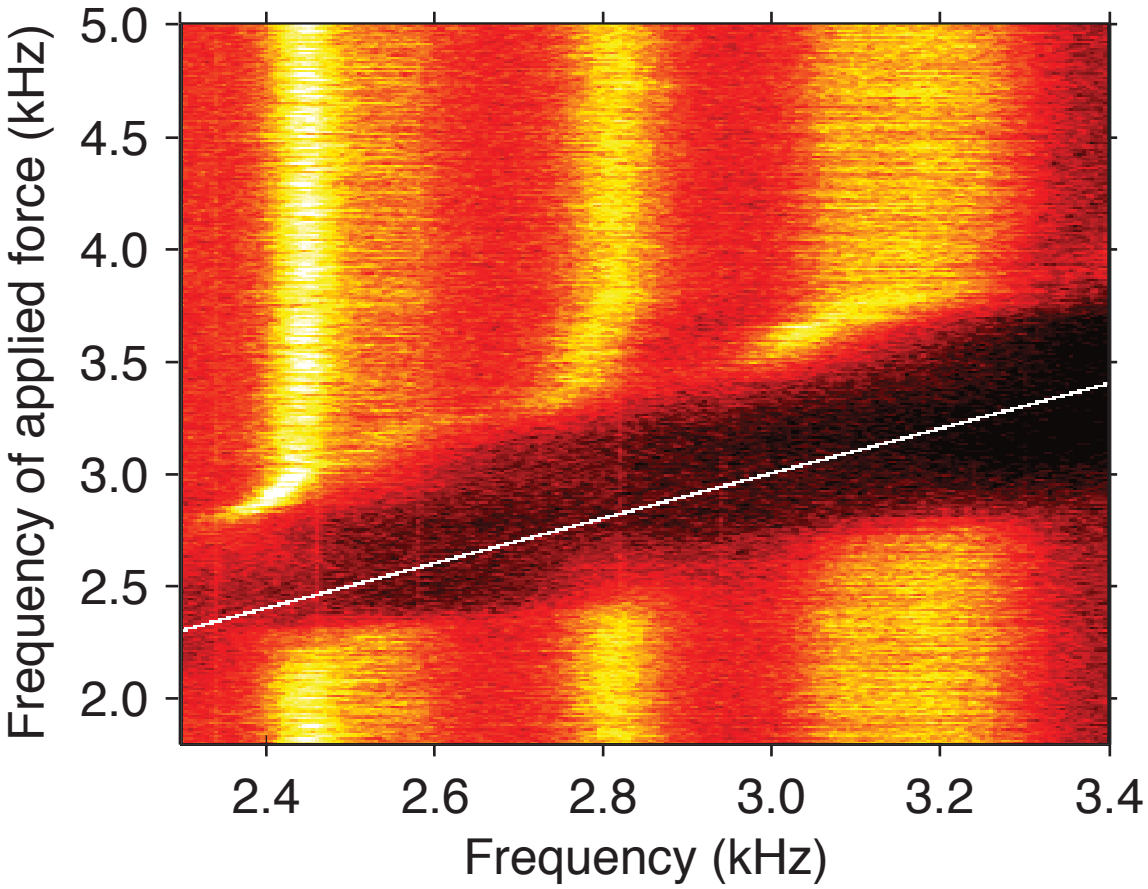
Frequency of applied force (kHz)
5.0
4.5
4.0
3.5
3.0
2.5
2.0
2.4
2.6
2.8
3.0
3.2
3.4
Frequency (kHz)

Figure 25

Figure 26: Response to a stimulus tone of varying frequency: peak splitting

A. Detail of Figure 24B. Two emission peaks are repelled slightly by lower-frequency stimuli. Both are repelled by stimuli of higher-frequencies, which cause them each to split into two separate peaks. B. The same emission peaks as seen in A, as affected by stimuli of 48 dB SPL. The splitting of the peak near 3.6 kHz for stimulus frequencies near 3.8 kHz is clearly seen.

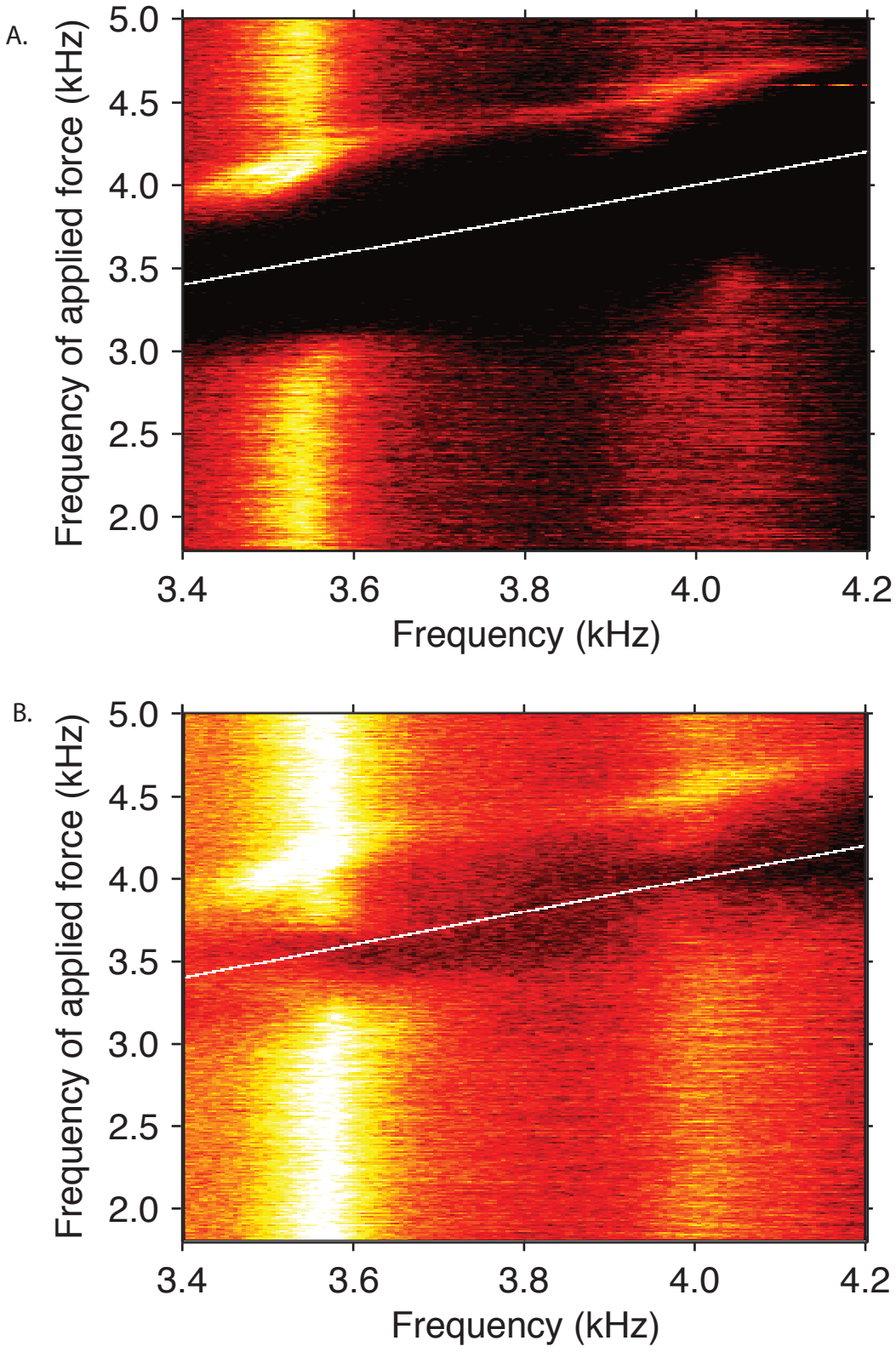
A.
Frequency of applied force (kHz)
5.0
4.5
4.0
3.5
3.0
2.5
2.0
3.4
3.6
3.8
4.0
4.2
Frequency (kHz)
B.
Frequency of applied force (kHz)
5.0
4.5
4.0
3.5
3.0
2.5
2.0
3.4
3.6
3.8
4.0
4.2
Frequency (kHz)

Figure 26

Figure 26 (continued)

C. The same emission peaks, but with stimuli of 54 dB SPL. The splitting of peaks is seen again. The peak near 4 kHz is markedly strengthened by stimuli with frequencies near 4.6 kHz. D. Detail of figure 28. The same emission peaks, but with stimuli now of 60 dB SPL. The splitting of peaks is seen again.

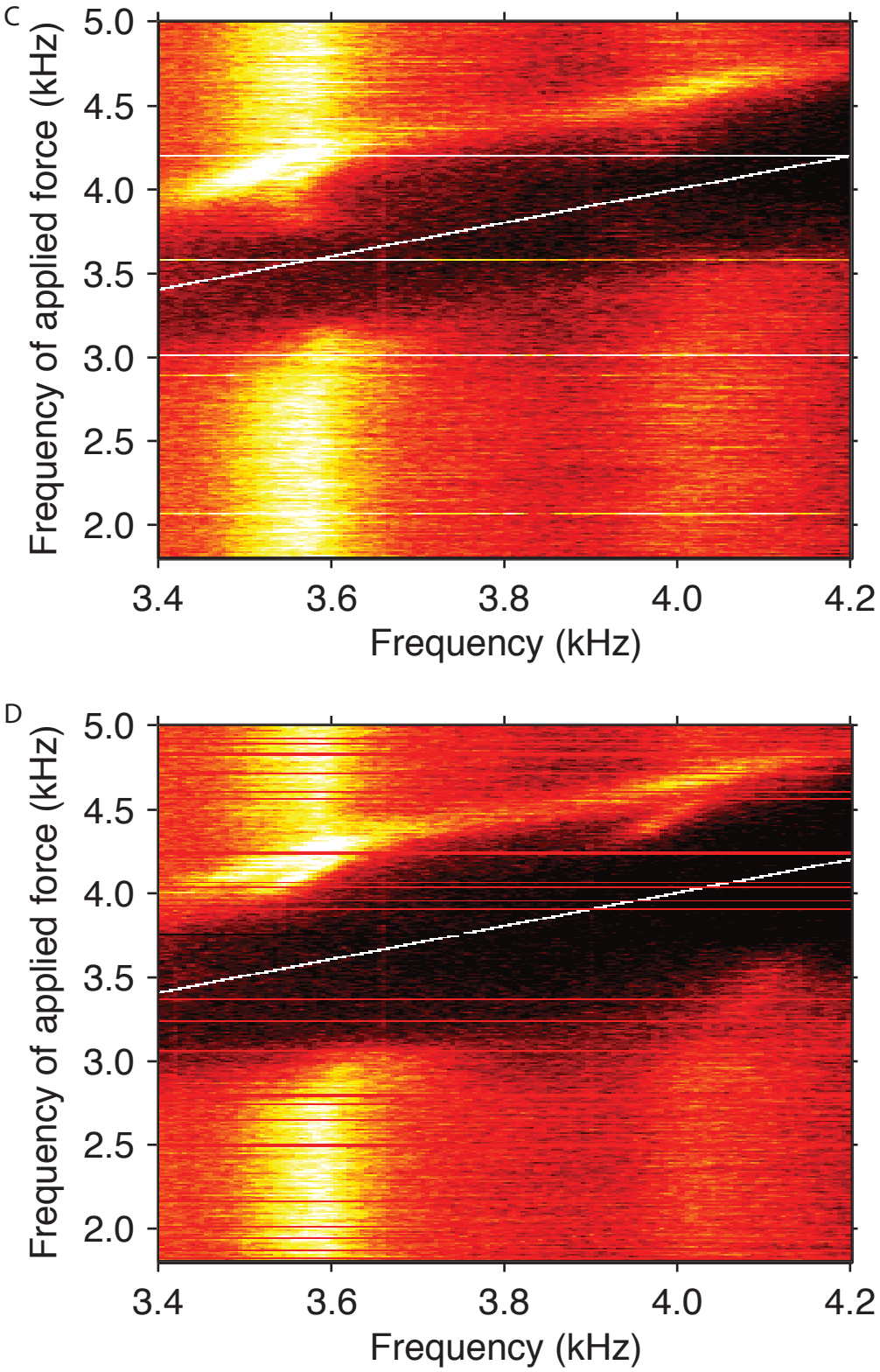

Figure 26 (cont.)

Figure 27: Response to a stimulus tone of varying frequency: double reverse. Detail of Figure 24A. The peak at 3.55 kHz is repelled, then attracted, then repelled by stimuli at lower, but increasing, frequencies. Compare to a single spectral peak in simulated Figure 16.

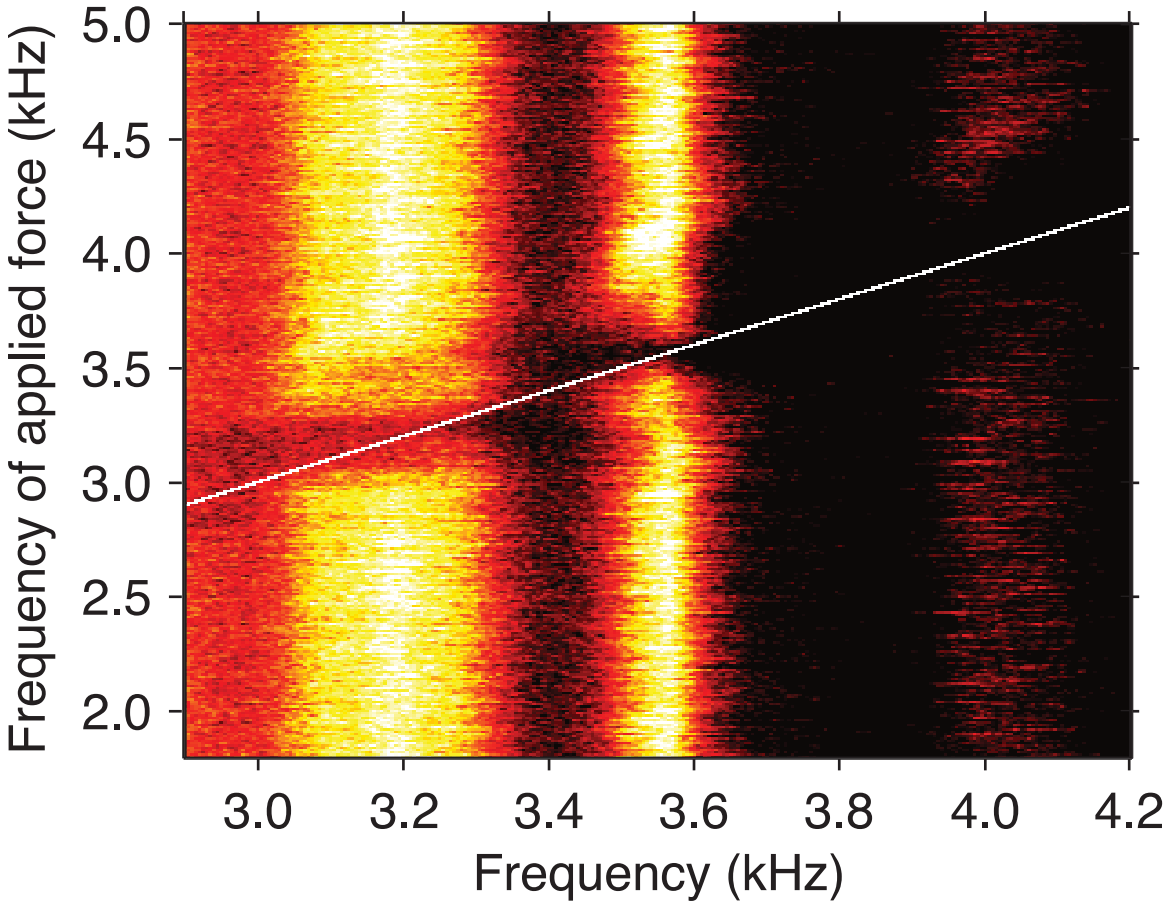
Frequency of applied force (kHz)
5.0
4.5
4.0
3.5
3.0
2.5
2.0
3.0
3.2
3.4
3.6
3.8
4.0
4.2
Frequency (kHz)

Figure 27

Figure 28: Response to a stimulus tone of varying frequency: peak moving in parallel with stimulus frequency

Stimulus with intensity of 60 dB SPL. A peak 'traveling' at a constant distance from the stimulus frequency can be seen, even at frequencies where no peak is normally found. The peak is now continuous between, for example, 2.4 kHz (when the stimulus frequency is 2.8 kHz) and 3.3 kHz (when the stimulus frequency is 3.7 kHz). Compare to the peaks indicated by arrows in Figure 17.

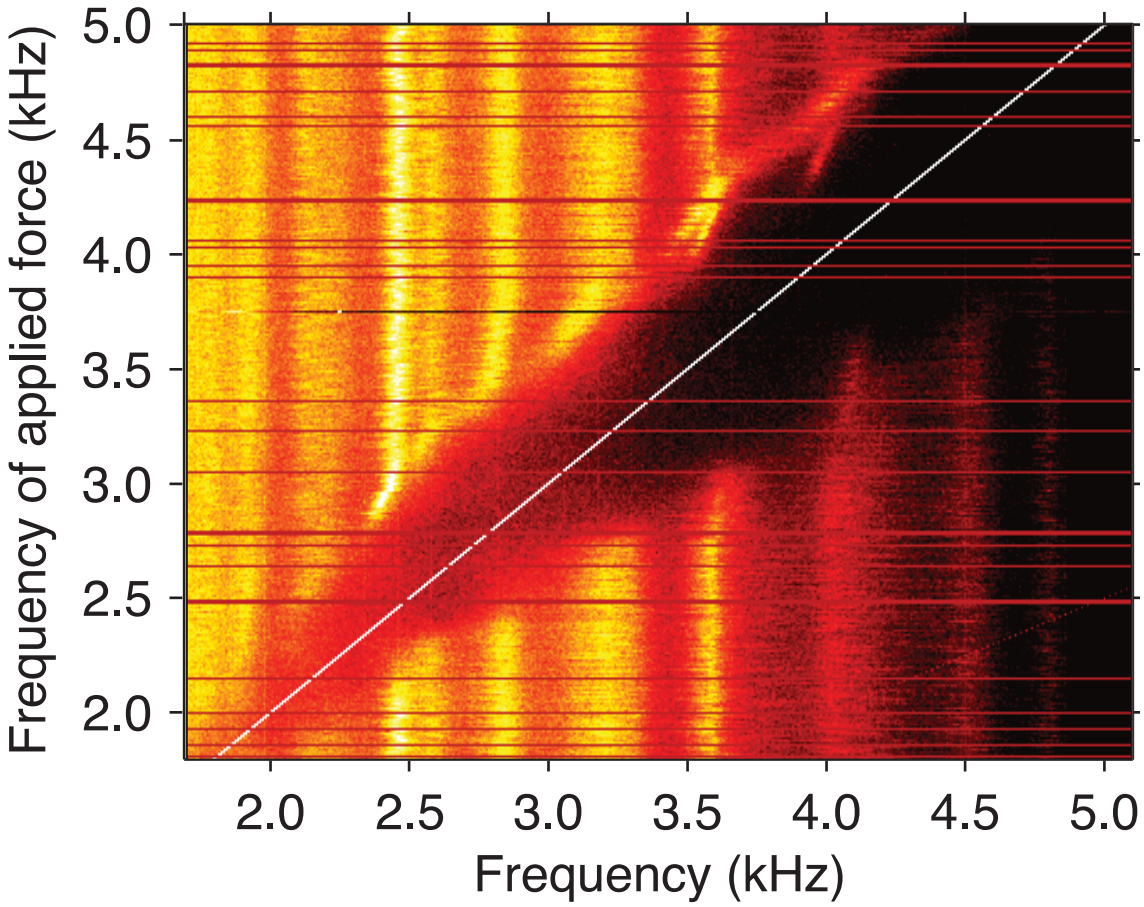
Frequency of applied force (kHz)
5.0
4.5
4.0
3.5
3.0
2.5
2.0
2.0
2.5
3.0
3.5
4.0
4.5
5.0
Frequency (kHz)

Figure 28

CHAPTER 5

Discussion

Model of hair cells as nonlinear oscillators

The two variables in our model, denoted by 'x' and 'y', were chosen to facilitate the incorporation of coupling between adjacent oscillators into the model. We required that one of the variables, 'x', represented the amount of deflection of bundle tips. The other variable then necessarily incorporated a description of all other processes in an oscillator; in the case of a hair bundle, this includes all of the system's internal mechanics.

As a highly schematized version of an array of nonlinear oscillators, our model omitted several elements that have previously been described in the gecko basilar papilla. Despite the absence of these elements, the model explains several distinctive aspects of SOAEs in the geckos, supporting our assumption that the critical component for the production of emissions lies not within the individual oscillators, but instead in the nature of the coupling that links them. Nevertheless, it is instructive to note some key aspects of hair cells and papillar structures that would need to be included in a more complete model.

Most notable among these absences are the complexities that lie within a single cross section of the basilar papilla. In our model, each cross section was represented by a single oscillator with a natural frequency primarily determined

by *f*. The reality is rather more complex. Ignoring longitudinal interactions, each cross section through the papilla contains approximately 12 hair cells as well as the tectorial structures that link them. Each of these hair cells has its own natural frequency, with at least some amount of dispersion among them. They are also not identical: as described previously, those located along the neural side of the papilla are covered by a longitudinally continuous tectorial membrane that hangs from an overarching limbic lip, whereas those along the papilla's abneural side are covered by discrete sallets. While the longitudinal interactions mediated by the tectorial membrane are a prime candidate for the source of the elastic coupling we treat here, connections perpendicular to the papilla are not present in our model. A more complete model would treat each cross-section as two clusters of six oscillators each, with tight coupling within each cluster and perhaps a looser coupling between them. It could also incorporate variability in the intrinsic frequency and other parameters of individual units within a cross section. Such a system reduces to ours in the limiting case of identical oscillators with coupling within a row greatly exceeding that between rows.

An additional complication arises from the plane of mirror symmetry within the hair cells underlying either a sallet or an equivalent section of tectorial membrane. Because of the hair cells' bidirectional orientation, a deflection in either direction promotes opening of transduction channels in half of the hair cells while promoting channel closure in the remainder. Although rotation of a single

oscillator in space by 180° would not change its behavior, the coupling of oscillators with opposite orientations must introduce new behaviors.

Finally, our model grossly simplified the mechanisms inside hair cells that power active oscillations, i.e., active hair bundle motility. A complete description of individual oscillators would more closely resemble earlier models (e.g., Nadrowski et al., 2004), incorporating the dynamics of myosin motors, Ca^{2+} binding and feedback, and other internal components.

Longitudinal coupling through drag forces

The spontaneous otoacoustic emissions of the tokay gecko are distinctive in the large number and relatively even spacing of their spectral peaks. We initially thought that this pattern might relate to the unusual anatomy of the apical portion of the basilar papilla, in which hair cells along half of the organ are covered by a large number of discrete sallets, rather than by a continuous tectorial sheet. Because these sallets provide more of an opportunity for viscous forces to play a role than does a continuous tectorial membrane, we examined a model in which adjacent oscillators interact through drag forces. Surprisingly, this approach failed to reproduce the pattern seen in experimental emission spectra. In this configuration, the oscillators did not organize into well-delineated, synchronized coalitions. Two distinct factors disfavor the formation of such groups. First, although the model incorporated explicitly only the interactions between each oscillator and its immediate neighbors, it instantiated an effectively

global coupling linking each oscillator to every other. This global coupling, at first glance, seems a probable cause for the absence of discrete synchronized groups. The inverse of the tridiagonal matrix **B** has positive values at all positions, suggesting that the intrinsic frequency of each oscillator contributes to the forces on every other oscillator. However, these contributions decay exponentially with distance along the array of oscillators, rapidly falling to negligible values. For example, for β equal to 0.2, the value that resulted in the roughness spectrum seen in Figure 3B, these contributions decay by approximately 85% for each successive oscillator, falling below 0.1% after just four increments. The distances over which oscillators can affect their neighbors were thus less than the size of synchronized groups seen elsewhere. Although the possibility remains that more complex nonlinear effects prevented the formation of these discrete groups, global coupling is unlikely to be the primary cause of the observed behavior.

A more subtle effect may instead provide the true explanation. Although elastic coupling (see below) favors the in-phase synchronization of adjacent oscillators, viscous coupling can promote synchronization either in phase or in antiphase. For example, consider a pair of linked oscillators of the identical frequency, and let both oscillators begin from rest, with one oscillator maximally displaced while the other remains at the origin. The return of the displaced oscillator towards the origin then pushes the other in the opposite direction; the opposing force then retards the return of the displaced oscillator. Thus, the

phase gap between the two oscillators has fixed points not just near 0°, but also near 180°. This anti-diffusive behavior, combined with the tonotopic variations in frequency present in our model, could have facilitated unlimited dephasing within any transiently existing synchronized chains. Thus, any such groups eventually dissolved as their extreme members formed more stable interactions with the adjacent groups. There were thus no favored locations for the formation of synchronized groups, resulting in a nearly uniform spectrum lacking well-defined peaks.

Longitudinal coupling through elastic forces

We also investigated models in which adjacent oscillators along the basilar papilla were interconnected elastically. In the gecko, such a coupling could be mediated either along the continuous tectorial membrane overlying the hair cells on the neural side of the basilar papilla or through the thin strand linking successive sallets on the papilla's abneural side. As measured by comparison of power spectra computed from simulations to those obtained from recordings in sedated animals, a model with elastic coupling satisfactorily reproduced the essential features of the gecko's spontaneous otoacoustic emissions. In particular, the use of an appropriate value for the elastic coupling constant yielded simulated power spectra with about a dozen emission peaks, a value in accord with experimental observations (Manley et al., 1996; Stewart and Hudspeth, 2000). This behavior arises from the opposition between elastic

interactions and the chain's tonotopy. In contrast to the result for viscous coupling, the spatially local and position-diffusive nature of elastic coupling favors uniformly in-phase synchronization of neighbors. At the same time, however, tonotopy limits synchronization to finite spatial ranges owing to the increasingly divergent frequencies of more distant oscillators. In our model, the result was a fragmentation of the chain into self-synchronized segments oscillating at different frequencies.

Mixed viscoelastic coupling

Coupling in the papilla is unlikely to be purely elastic. An array of oscillators incorporating high levels of both elastic and viscous coupling resembled those with solely viscous coupling, lacking organization in the form of stable groups of coupled oscillators. Surprisingly, simulations with strong viscous coupling and weak elastic coupling formed a small number of very stable groups of coupled oscillators. In such a system, the symmetry between in-phase and antiphase coupling, which prevented the formation of stable groups by purely viscous coupling, was broken by the incremental addition of elastic coupling, allowing stably coupled groups to form. The frequencies of these groups are highly sensitive to the relative strengths of the two types of coupling, and such a system matched experimental emissions relatively poorly: the number of spectral peaks was lower than that from recorded emissions, and they were too finely tuned in frequency. The addition of small amounts of viscous coupling to an

elastically coupled system, in contrast, had only small effects on the resulting emission spectrum. We therefore conclude that coupling is most likely predominately elastic, with any viscous component very weak by comparison.

The significance of longitudinal coupling

Elastic interactions between hair bundles can clearly occur across many species with wide variations in the anatomy of tectorial and other structures. Thus, the mere presence of elastic interactions is not sufficient to explain the unusual features of the spontaneous otoacoustic emissions in geckos. It is possible that the elastic interactions in the gecko are mediated by only the thin strand connecting the sallets, and are therefore weaker than interactions mediated by a continuous tectorial sheet. The weakness of these interactions might then result in the unusually large number of spectral peaks in the gecko's emissions. This hypothesis is supported by the data presented in Figure 10B, in which elevated values of the coupling constant γ led to fewer spectral peaks, which additionally had less power.

An alternate possibility is that tectorial hair cells are coupled through pressure changes in the liquid-filled space behind the tectorial curtain, a feature described only in geckos. The ability of a model with tapered ends to replicate experimental emission spectra suggests that the oscillatory activity of hair bundles along the basilar papilla decreases near the organ’s ends. This pattern accords with the fact that the tectorial curtain is interrupted at both extremes of

the basilar papilla. The liquid in the space behind this curtain is freer to shift in response to movements of the papilla near its ends than in its middle. The tectorial membrane near the ends might therefore provide less opposition to the movement of hair bundles, thus limiting the activity of those bundles relative to those farther from the edges. The ability of the tectorial curtain, rather than direct linkages between sallets or along a continuous tectorial membrane, to mediate elastic interactions could explain the unusual emission spectra produced by geckos.

The absence of inertia

The sallets of the tokay gecko are about 50 mm wide and are expected to oscillate through about ±50 nm during strong stimulation. For the stimulus frequencies represented in the apical portion of the basilar papilla, 1-7 kHz, this motion corresponds to maximal velocities of 0.2-1.3 $mm \cdot s^{-1}$. The Reynolds number, in fluid mechanics, describes the ratio between the inertial forces and viscous forces acting on a system. The behavior of systems operating at high Reynolds numbers is dominated by inertia, and is thus qualitatively different from the behavior of systems at low Reynolds numbers. The values presented above suggest that the sallets operate at Reynolds numbers of less than 0.1 and are accordingly overdamped. Our formulation therefore excluded the effect of mass. Appendix 1 reconciles the absence of significant mass in this system with the observation that salletal units appear to behave as powered harmonic oscillators.

The spontaneous otoacoustic emissions in another lizard, the bobtail skink, have been modeled as the product of a chain of coupled oscillators (Vilfan and Duke, 2008). In contrast to the model that we present here, the authors treat physical, as distinct from phenomological, inertia as a significant component of the oscillatory unit. The models incorporating viscous and elastic coupling that they present therefore do not correspond to our similarly conceived models. In fact, elastic coupling in a system that includes mass corresponds in a massless system to a coupling that unrealistically depends on the antiderivative of position. Viscous coupling in a mass-containing system, on the other hand, is mathematically equivalent to elastic coupling in a massless system. Indeed, the simulated results presented for a viscously coupled system (Vilfan and Duke, 2008) resemble the present results with elastic coupling. Our argument that the presence of significant mass is neither likely nor necessary in an actively powered salletal unit leads to the conclusion that only elastic coupling can explain spontaneous otoacoustic emissions in the gecko's papilla.

The role of roughness

Our model suggests that variations between the spontaneous otoacoustic emissions of individual geckos result from slight irregularities in the properties of the oscillatory units. Variations of only a few percent in the amplitudes of free-running oscillators sufficed to break the symmetry along the chain of oscillators and to localize the frequencies of synchronized groups. These groups coalesced

around oscillators with slightly enhanced amplitudes, whereas the discontinuities between groups nucleated near weaker oscillators. The ensuing pattern persisted over thousands of cycles of spontaneous oscillation.

Roughness of the magnitude represented in our simulations is almost certainly present in actual basilar papillae, in which the number and arrangement of hair cells varies from row to row (Miller, 1974; Köppl and Authier, 1995). Because the median number of hair cells per row is only six, any deviation from uniformity could equate to a 17% difference in oscillatory power. Although this does not necessarily translate to an equivalent deviation in oscillatory amplitude, this irregularity is of a magnitude easily able to explain much of the observed divergence between the emissions of individual geckos. We have varied α, the amplitude of oscillations; equivalent roughness in the system's other parameters, including nonlinearity, frequency, or coupling strength, could have similar effects. Whether this variation plays any physiological role remains uncertain. The model suggests that minor variations in α also cause significant variations in the responses of individual oscillators to external tones by adjusting the sizes and boundaries of synchronized groups of oscillators. Although we have examined this variation in the response to pure tones in an otherwise noiseless environment, equally large variations between individuals may occur in response to more complex and realistic auditory stimuli.

Peak repulsion by pure tones

Perhaps the most distinctive feature of the power spectra for spontaneous otoacoustic emissions, from geckos as well as other species, is the pattern of changes they undergo in the presence of sinusoidal stimuli. Externally applied tones both suppress and usually repel nearby emission peaks (Long et al., 1991; Köppl and Manley, 1994), an effect opposite to that expected naively for the application of a sinusoidal force to a single oscillator. In agreement with modeling of the skink's cochlea (Vilfan and Duke, 2008), our results suggest that the suppression results from synchronization of nearby oscillators to the tone, decreasing the power of emission at their original frequencies. The models further explain the repulsive behavior as a shift in the affiliation of individual oscillators with synchronized groups. An external tone synchronizes the oscillations in a strip of hair cells, but also leaves the outlying cells to oscillate at frequencies further from that of the applied tone. This same behavior can also account under certain conditions for the frequency attraction that is less commonly seen (Manley et al., 1996). For example, if most but not all of the oscillators constituting a synchronized groups are later entrained to an external tone, the remaining oscillators could join the adjacent group. That group's median member, and thus frequency, would thereby shift towards the frequency of the external tone. By increasing the scope of responses to external tones, these types of rearrangement might increase the amount of information conveyed centrally and thereby improve frequency discrimination. This function depends

on interactions between nonlinear oscillators, which can be entrained to different frequencies under different conditions, and thus can participate in groups that rearrange in response to faint stimuli. The potential contribution of this phenomenon to frequency selectivity, in particular, depends on the fact that the pattern of synchronization can undergo abrupt transitions, and thus produce qualitatively different responses to very similar stimuli.

The apparent repulsion of SOAE peaks by tones of nearby frequency bears some similarity to the frequency repulsion observed in some applications of mode coupling theory (Frank and von Brentano, 1994). This theory analyzes the behavior of an oscillatory system (such as light in a laser) in terms of variations in the oscillatory modes of the unperturbed system. For example, when two oscillators are coupled, their natural frequencies will interact to form two new eigenfrequencies. Under appropriate conditions, these eigenfrequencies will diverge as the coupling strength increases; the frequencies are effectively repelling each other (Breinig, 2008). An example of this phenomenon has been demonstrated experimentally using a pair of simple RLC circuits, coupled inductively (Gamarra et al., 2007). Although we have not used this theory in the analysis of our system, it is likely that a behavior similar to that described by mode-mode coupling pertains here.

Significance of model's deviations from reality

Our model, intended to represent a simplified version of the gecko basilar papilla, reproduced some aspects of the spontaneous otoacoustic emissions produced by the gecko inner ear; other features have so far not been captured by the model. Most prominently, the model we present in which adjacent oscillators were coupled elastically was, with appropriate adjustments of parameters, able to produce spectra that resembled experimental emissions in the number and spacing of spectral peaks. These features were determined primarily by the value of the elastic coupling coefficient γ, and by the distribution of the natural frequencies *f* of the collection of oscillators. A recent paper confirms this result, and suggests that in a similar system, the number of oscillators per synchronized group is approximately proportional to $(\gamma/\Delta f)^{1/2}$ (Vilfan and Duke, 2008). This value then determines the number of synchronized groups, while the groups' frequencies are observed to match those of their respective median oscillators. Adjustment of these parameters can thus replicate not only the emission patterns seen in geckos, but in principle can match those across a wide range of species.

The model also suggested that edge effects, roughness, and noise all play roles in determining the emission spectra produced by geckos, and presumably other species as well. The sharpening effect that abrupt transitions had on nearby spectral peaks suggests that any such transitions along the basilar papilla must be smoothed. Alternately, the presence of roughness may effectively create sharp boundaries everywhere, and thus provide an alternate explanation

for the fact that experimentally-recorded peaks near the high and low ends of the papilla's frequency range are not systematically different from those in the middle. Roughness also can largely explain the varying magnitudes of peaks in an individual spectrum, as well as the differences that make the spectra for different animals of the same species unique. Noise, which can broaden spectral peaks, likely accounts for the disparity between the narrower peaks observed in simulated spectra and peaks recorded experimentally, which generally cover a larger frequency range.

Merging of emission peaks in recorded spectra

Simulations correctly predicted several features of the response of otoacoustic emissions to an external tone. Experimental recordings repeatedly showed two spectral peaks being replaced by a single peak as an external tone of a nearby frequency increased in intensity (Figures 21 and 22). In some cases the two initial peaks met to form the final peak; in others the two peaks faded out as a third peak of intermediate frequency gradually appeared. In still other cases, the disappearance of one peak coincided with an increase in the intensity of an adjacent peak (Figure 23). Although these patterns take disparate forms, they could each be explained as the transition of oscillators from one synchronized group to another. Such processes were also seen in an analogous simulated experiment (Figure 18). Two peaks were replaced by a peak of intermediate frequency in one instance. In another, one peak disappeared as an

adjacent peaks gained in strength. Although the simulations and recordings did not match in every detail, the overall pattern of behavior was similar.

The movement of small numbers of oscillators between synchronized groups may also explain the response of SOAEs to changes in temperature, as described in a previous study of tokay gecko SOAEs (Manley *et al.*, 1996) and also seen in similar experiments we have performed. Temperature changes were observed to shift the power ratio between two adjacent spectral peaks, consistent with the transition of a number of individual oscillators from one synchronized group to its neighbor. The mechanism by which temperature affects the individual oscillators is not explicitly incorporated in our model, however. Temperature changes were also observed to induce the replacement of a single large spectral peak by a series of smaller peaks separated by small frequency intervals. This behavior is again consistent with temperature-induced changes in the properties of individual oscillators changing the stability of an existing synchronized groups of oscillators.

Change of SOAE spectrum in response to a frequency sweep

Some observations from experiments involving frequency sweeps matched results predicted by simulations. An external tone generally suppressed emissions that fall within a range around its frequency. This range increased with an increase in the frequency of the tone. As the tone approached the frequency of an emission peak, it most commonly first repelled the peak, then suppressed

it. In several experiments, the repelled emission peaks travelled approximately in parallel with the migrating tone; consecutive repelled peaks then connected to form a continuous peak at a near-constant frequency interval from the tone (Figure 28). This effect, not previously described in experimental recordings of SOAEs was also seen in our simulations (Figure 17), where it represents the closest cluster of synchronized oscillators that are *not* entrained to the external stimulus. One peak in an experimental spectrum, upon the approach of the external tone from either side, underwent a complex sequence of frequency shifts, moving first away, then towards, then again away from the external tone before finally succumbing to suppression (Figure 27). This pattern, seen only once, closely resembled the results of a simulation (Figure 16) in which nearly every spectral peak underwent a similar pattern of movements. The cause of this behavior, even in the model, is unclear, but its appearance in both simulations and experiments strongly supports the hypothesis that elastic interactions between adjacent oscillators are key elements in determining the pattern of SOAEs.

Roughness reconciles differences between model and experiment

In our model, boundaries enhanced nearby spectral peaks and limited their dispersion. This effect emerged from the tendency of many types of boundaries to favor formation of synchronized groups at certain positions along

the array of oscillators and to disfavor formation at other positions. Although this feature contributes to our understanding of how differences between SOAEs can arise, it also suggests that external tones should dramatically enhance emission peaks of nearby frequencies. Instead, experimental results suggest that these tones can enhance nearby peaks only slightly, and often have the opposite effect. This seeming conflict arises from the interplay between external tones and effective boundaries already present in the system due to roughness. Because this roughness already favors formation of spectral peaks at certain frequencies and disfavors formation elsewhere, the additional bias introduced by the external tone is muted. Thus, the enhancement and suppression that are seen experimentally usually result from frequency shifts due to the rearrangement of synchronized groups, rather than from the focusing effect seen in simulations of systems without roughness.

Similarly, whereas simulation of a uniform system suggests that the rearrangements induced by an external force propagate a substantial distance along the chain of oscillators, experimental results show a narrower range of impact in response to external tones. This finding again results from the presence of roughness, which, by stabilizing groups, partially insulates each peak from responding to changes in adjacent peaks, and thus increases the decay of response along the papilla. If the role of the shifting pattern of synchronization is to increase the range of neural response to auditory stimuli, then roughness could substantially limit the efficacy of hearing. This conclusion

in turn suggests that a system such as the gecko basilar papilla might be optimized by minimizing roughness in its structure.

Results left unexplained

The peak splitting seen in Figure 26 is also not clearly replicated in any simulations. Since splitting occurs preferentially for certain emission peaks, it is possible that precise conditions are required to create an emission peak capable of splitting in response to an external tone, and that these conditions have not yet been adopted in a simulation. Finally, our model did not predict the observed asymmetry between the responses of SOAEs to higher-frequency versus lower-frequency stimuli. The frequency range suppressed by an external tone extended further towards higher frequencies than towards lower frequencies. In addition, although tones at frequencies lower than that of an emission usually suppressed the emission with only slight effects on its frequency, those at higher frequencies often cause emission to undergo a more complex pattern of shifts. Thus, the spectral peak present in experimental recordings at a constant frequency interval from the stimulus tone, as seen in Figure 28, is more prominent at frequencies below the stimulus. In contrast, the analogous phenomenon was seen symmetrically in simulations, and our model does not suggest how this symmetry may have been broken. The similar model proposed by Vilfan and Duke, by contrast, demonstrates more prominent asymmetries in

response to tonal stimulation. A new model incorporating elements of both may prove better able to reproduce all aspects of spontaneous emissions.

CHAPTER 6

Conclusions

We have attempted to create a model capable of recreating the most significant elements of spontaneous otoacoustic emissions produced by the tokay gecko. Two significant assumptions played a role in the development of our model. First, we assumed that longitudinal interactions along the basilar papilla, rather than the detailed mechanics of each cross-section through the papilla, are the critical factor in determining of the nature of SOAEs. This allowed us to greatly simplify the behavior of each element along the tonotopic array, treating it as a simple van der Pol oscillator, rather than as a more complex assortment of hair bundles, tectorial structures, fluid flows, and other varied components. Significantly, this simple model was nevertheless able to replicate gecko SOAEs in many details, validating our assumption.

Second, and more controversially, we assumed that oscillations along the basilar papilla are overdamped, and thus that mass does not play a significant role. Although we believe that this assumption is supported by physical measurements of the basilar papilla, other models of the basilar papillae of geckos and other lizards have incorporated mass. Acceptance of this assumption, however, predominantly affects the interpretation of model results,

rather than the validity of the models themselves. In particular, the assumption of masslessness leads us to conclude that elastic coupling dominates interactions along the papilla. If mass were present, the same model would lead to the alternate conclusion that viscous coupling dominates. However, this alternate conclusion does not interfere with the model's success in describing SOAEs in general, and the response of emission peaks to external pure-tones in particular. This assumption is thus secondary to our conclusion that longitudinal interactions are critical for the formation of otoacoustic emissions.

Experimental recordings of gecko SOAEs both confirmed several of the predictions of our model and demonstrated new behaviors for the model to explain. In the first category, recordings repeatedly showed adjacent emission peaks combining into a single peak under the influence of an external tone. Our model explains this behavior as a reordering of the affiliations of individual oscillators. The model additionally suggests that this reordering translates small changes in stimuli into substantial changes in the frequencies of oscillation of a large assemblage of hair cells. This may provide a mechanism by which longitudinal coupling can augment the frequency selectivity of hearing. Several recordings also showed a peak of emission power at an approximately constant frequency interval from a stimulus tone. This is consistent with a papilla in which interactions along the papilla are significant, and the set of hair cells constituting a particular emission peak is fluid and able to vary continuously with changing stimuli.

In future studies, it will be desirable to use the model to explain other behaviors seen in recordings. For example, the splitting of certain emission peaks into two separate peaks upon exposure to some stimulus tones might be explained by a particular pattern of roughness along the papilla that has not yet been realized within the parameter space of our model. Further exploration of this parameter space has the potential to increase our understanding of emissions in the gecko.

Finally, although our model was designed to mimic the gecko basilar papilla, the basic description of interactions among coupled, tonotopically-arranged nonlinear oscillators is not specific to that species. It is possible, for example, that the unusual pattern of SOAEs seen in geckos, which is shared by some lizard species lacking any tectorial membranes, results from the existence of unusually *weak* longitudinal interactions. Applying the model to other species may provide further insights into the formation of otoacoustic emissions and their relation to the active process.

APPENDIX 1

Phenomenological mass and its significance for the interpretation of coupling modes

(*The ideas presented in this section originated with Oreste Piro, and the explanation was primarily written by Jim Hudspeth)*

Simple calculations suggest that sallets are in fact overdamped. However, the observed behavior of salletal units resembles that of a powered harmonic oscillator, which normally requires the presence of a significant mass. Indeed, treating salletal units along the basilar papilla as harmonic oscillators provides satisfactory estimates of their natural frequencies (Authier, Manley, 1995). It is therefore worthwhile to consider why mass-like properties emerge from our equations.

We consider the general case of a cluster of hair bundles joined to a common sallet and assume that the system has a negligible mass but is endowed with an aggregate drag coefficient x and stiffness k. If the assembly is subjected to a force F_C owing to coupling between adjacent elements and a force F_A reflecting the hair bundles' active process, the equation of motion for the displacement variable x is

$$\xi \frac{dx}{dt} + \kappa x = F_C + F_A . \qquad \textbf{[A1.1]}$$

The state of the active process is represented by the variable *y*, which might represent the intracellular Ca^{2+} concentration or some other parameter that provides linear feedback through F_A:

$$\frac{dy}{dt} = -\rho x. \qquad \textbf{[A1.2]}$$

Taking the temporal derivative of the first expression, and assuming that F_A depends on both the external variable *x* and the internal variable *y* whereas F_C depends only on *x*, we obtain

$$\xi \frac{d^2x}{dt^2} + \kappa \frac{dx}{dt} = \frac{dF_C}{dt} + \frac{dF_A}{dx}\frac{dx}{dt} + \frac{dF_A}{dy}\frac{dy}{dt}. \qquad \textbf{[A1.3]}$$

Substituting the expression for the feedback process eliminates the explicit time-dependence of *y* in the equation:

$$\xi \frac{d^2x}{dt^2} + \left(\kappa - \frac{dF_A}{dx}\right)\frac{dx}{dt} + \left(\rho \frac{dF_A}{dy}\right)x = \frac{dF_C}{dt}. \qquad \textbf{[A1.4]}$$

Although actual masses have been excluded in the formulation of the model, the resultant second-order equation of motion includes a phenomenological mass. Moreover, the phenomenological drag coefficient associated with the first-order term is of a form suited to display 'negative viscosity,' a common means of representing the active process (Gold, 1948; Neely and Kim, 1983). In fact, for a reasonable choice of F_A and with simple substitutions for ξ, κ, and ρ, Equation A1.4 in the absence of coupling is equivalent to Equations 3.1 and 3.2.

It is important to observe that coupling forces enter into the equation under a derivative operator. Consider, for example, elastic coupling between adjacent

units such as that represented in Equation 3.8. In this instance $F_C = \gamma(x_{n-1} - 2x_n + x_{n+1}) = \gamma\Delta x$, in which the discrete Laplacian operator Δ acts on the positions of the n^{th} sallet and its nearest neighbors. Then

$$\xi\frac{d^2x}{dt^2} + \left(\kappa - \gamma\Delta - \frac{dF_A}{dx}\right)\frac{dx}{dt} + \left(\rho\frac{dF_A}{dy}\right)x = 0. \qquad \textbf{[A1.4]}$$

Although the coupling is implemented through a purely elastic element, it appears as a component of the phenomenological drag coefficient. In a similar fashion, coupling of successive elements through viscous drag as in Equation 3.3 may be represented as $F_C = \beta\Delta(dX/dt)$. In the resultant relation,

$$(\xi - \beta\Delta)\frac{d^2x}{dt^2} + \left(\kappa - \frac{dF_A}{dx}\right)\frac{dx}{dt} + \left(\rho\frac{dF_A}{dy}\right)x = 0, \qquad \textbf{[A1.5]}$$

so viscous coupling has the effect of altering the phenomenological mass.

BIBLIOGRAPHY

Aranyosi AJ, Freeman DM (2005). Two modes of motion of the alligator lizard cochlea: measurements and model predictions. *J Acoust Soc Am* 118: 1585-1592.

Ashmore, J (2008). Cochlear outer hair cell motility. *Physiol Rev* 88: 173-210.

Authier S, Manley GA (1995). A model of frequency tuning in the basilar papilla of the tokay gecko, *Gekko gecko*. *Hear Res* 82: 1-13.

Bergevin C, Freeman DM, Saunders, JC, Shera CA (2008). Otoacoustic emissions in humans, birds, lizards, and frogs: evidence for multiple generation mechanisms. *J Comp Physiol A* 194:665-683.

Bialek W, Wit HP (1984). Quantum limits to oscillator stability: theory and experiments on acoustic emissions from the human ear. *Phys Lett A* 104: 173-178.

Bozovic D, Hudspeth AJ (2003). Hair-bundle movements elicited by transepithelial electrical stimulation of hair cells in the bullfrog's sacculus. *Proc Natl Acad Sci USA* 100: 958-963.

Breinig, M (2008). Coupling of modes in space. http://electron9.phys.utk.edu/optics507/modules/m6/coupling_of_modes_in_space.htm

Burns EM, Strickland EA, Tubis A, and Jones K (1984). Interactions among spontaneous emissions. I. Distortion products and linket emissions. *Hear Res.* 16: 271-8.

Camalet S, Duke T, Julicher F, Prost J (2000). Auditory Sensitivity Provided by Self-Tuned Critical Oscillations of Hair Cells. *Proc Natl Acad Sci* 97: 3183-3187.

Chan DK, Hudspeth AJ (2005a). Ca^{2+} current-driven nonlinear amplification by the mammalian cochlea *in vitro*. *Nat Neurosci* 8: 149-155.

Chan DK, Hudspeth AJ (2005b). Mechanical responses of the organ of Corti to acoustic and electrical stimulation *in vitro*. *Biophys J* 89: 4382-4395.

Chiappe ME, Kozlov AS, Hudspeth AJ (2007). The structural and functional differentiation of hair cells in a lizard's basilar papilla suggests an operational principle of amniote cochleas. *J Neurosci* 27: 11978-11985.

Corey DP, Hudspeth AJ (1983). Analysis of the microphonic potential of the bullfrog's sacculus. *Journal of Neuroscience* 3: 942-61.

Dallos P, Zheng J, Cheatham MA (2006). Prestin and the cochlear amplifier. *J Physiol* 576: 37-42.

De Vries H (1948). Brownian movement and hearing. *Physica* 14:48-60.

FitzHugh R (1961). Impuses and physiological states in theoretical models of nerve membrane. *Biophys J* 1: 445-466.

Frank W, von Brentano P (1994). Classical analogy to quantum mechanical level repulsion. *Am. J. Phys* 62: 706-709.

Freeman DM, Masaki K, McAllister AR, Wei Jesse L, Weiss TF (2003). Static material properties of the tectorial membrane: a summary. *Hear Res* 180(1-2): 11-26.

Frishkopf LS, DeRosier DJ (1983). Mechanical tuning of free-standing stereociliary bundles and frequency analysis in the alligator lizard cochlea. *Hear Res* 12: 393-404.

Gamarra DF, Josebachuili M, Zurita P, Gils S (2007). Experimental study of the frequency repulsion effect. *Am J Phys* 75: 1073-1077.

Gold T (1948). Hearing. II. The physical basis of the action of the cochlea. *Proc Roy Soc Lond B* 135: 492-498.

Holton T, Hudspeth AJ (1983). A micromechanical contribution to cochlear tuning and tonotopic organization. *Science* 222: 508-510.

Hudspeth A (1997). Mechanical amplification of stimuli by hair cells. *Curr Opin Neurobiol* 7(4):480-6.

Hudspeth AJ, Choe Y, Mehta AD, Martin P (2000). Putting ion channels to work: mechanoelectrical transduction, adaptation, and amplification by hair cells. *Proc Natl Acad Sci USA* 97: 11765-11772.

Hudspeth, AJ (1989). How the ear's works work. *Nature* 341: 397-404.

Hudspeth, AJ (2008). Making an effort to listen: mechanical amplification in the ear. *Neuron* 59(4): 530-45.

Kennedy HJ, Crawford AC, Fettiplace R (2005). Force generation by mammalian hair bundles supports a role in cochlear amplification. *Nature* 435: 880-883.

Kern A and Stoop R (2003). Essential role of couplings between hearing nonlinearities. *Phys Rev Lett* 91: 128101-1 – 128101-4.

Köppl A, Manley GA (1993). Spontaneous otoacoustic emissions in the bobtail lizard. I: General characteristics. *Hear Res* 71: 157-169.

Köppl A, Manley GA (1994). Spontaneous otoacoustic emissions in the bobtail lizard. II: Interactions with external tones. *Hear Res* 72: 159-170.

Köppl C (1995). Otoacoustic emissions as an indicator for active cochlear mechanics: a primitive property of vertebrate auditory organs. In: Manley GA et al. (Eds.), *Advances in Hearing Research*: 207-218.

Köppl C (1998). Morphology of the basilar papilla of the bobtail lizard *Tiliqua rugosa*. *Hear Res* 35: 209-228.

Köppl C, Authier S (1995). Quantitative anatomical basis for a model of micromechanical frequency tuning in the tokay gecko, *Gekko gecko*. *Hear Res* 82: 14-25.

Kroese ABA, Das A, Hudspeth AJ (1989). Blockage of the transduction channels of hair cells in the bullfrog's sacculus by aminoglycoside antibiotics. *Hear. Res.* 37(3): 203–217.

Lewis ER, Leverenz EL, Bialek WS (1985). The Vertebrate Inner Ear. CRC Press, FL.

Long G, Tubis A, Jones K (1991). Modeling synchronization and suppression of spontaneous otoacoustic emissions using Van der Pol oscillators: Effects of aspirin administration. *J Acoust Soc Am* 89: 1201-1212.

Lonsbury-Martin BL, Martin GK (1990). The clinical utility of distortion-product otoacoustic emissions. *Ear Hear*. 11(2): 144-154.

Manley GA (1997). Diversity in hearing-organ structure and the characteristics of spontaneous otoacoustic emissions in lizards. In: Lewis ER et al. (Eds.), *Diversity in Auditory Mechanics*: 32-39.

Manley GA (2000). Cochlear mechanisms from a phylogenetic viewpoint. *Proc Natl Acad Sci USA* 97: 11736-11743.

Manley GA (2001). Evidence for an active process and a cochlear amplifier in nonmammals. *J Neurophysiol* 86:541-549.

Manley GA (2002). Evolution of structure and function of the hearing organ of lizards. *J Neurobiol.* 53(2): 202-11.

Manley GA (2006). Spontaneous otoacoustic emissions from free-standing stereovillar bundles of ten species of lizard with small papillae. *Hear Res*. 212:33-47.

Manley GA, Gallo L (1997). Otoacoustic emissions, hair cells, and myosin motors. *J Acoust Soc Am* 102: 1049-1055.

Manley GA, Gallo L, Köppl C (1996). Spontaneous otoacoustic emissions in two gecko species, *Gekko gecko* and *Eublepharis macularius*. *J Acoust Soc Am* 99: 1588-1603.

Manley GA, Kirk DL, Köppl C, Yates GK (2001). *In vivo* evidence for a cochlear amplifier in the hair-cell bundle of lizards. *Proc Natl Acad Sci USA* 98: 2826-2831.

Manley GA, Köppl C (1994). Spontaneous otoacoustic emissions in the bobtail lizard. III: Temperature Effects. *Hear Res* 72: 171-180.

Manley GA, Köppl C, Sneary M (1999). Reversed tonotopic map of the basilar papilla in *Gekko gecko*. *Hear Res* 131: 107-116.

Martin GK, Lonsbury-Martin BL, Probst R, Coats, AC (1988). Spontaneous otoacoustic emissions in a nonhuman primate. I. Basic features and relations to other emissions. *Hear Res* 33(1): 49–68.

Martin GK, Probst R, Lonsbury-Martin BL (1990). Otoacoustic emissions in human ears: normative findings. *Ear Hear* 11(2): 106-20.

Martin P, Bozovic D, Choe Y, Hudspeth AJ (2003). Spontaneous oscillation by hair bundles of the bullfrog's sacculus. *J Neurosci* 23: 4533-4548.

Martin P, Hudspeth AJ (2001). Compressive nonlinearity in the hair bundle's active response to mechanical stimulation. *Proc Natl Acad Sci* USA 98 (25): 11386-91.

Martin P, Hudspeth AJ, Julicher F (2001). Comparison of a hair bundle's spontaneous oscillations with its response to mechanical stimulation reveals the underlying active process. *Proc Natl Acad Sci USA* 98(25): 14380-5.

Miller MR (1973). A scanning electron microscope study of the papilla basilaris of *Gekko gecko*. *Z Zellforsch Mikrosk Anat* 136: 307-328.

Mirollo RE, Strogatz SH (1990). Amplitude death in an array of limit-cycle oscillators. *Journal of Statistical Physics* 60 (1-2): 245-262.

Murphy W, Tubis A, Talmadge C, Long G (1995). Relaxation dynamics of spontaneous otoacoustic emissions perturbed by external tones. II. Suppression of interacting emissions. *J Acoust Soc Am* 97: 3711-3720.

Murphy W, Tubis A, Talmadge C, Long G, Krieg E (1996). Relaxation dynamics of spontaneous otoacoustic emissions perturbed by external tones. III. Response to a single tone at multiple suppression levels. *J Acoust Soc Am* 100: 3979-3982.

Nadrowski B, Martin P, Jülicher F (2004). Active hair-bundle motility harnesses noise to operate near an optimum of mechanosensitivity. *Proc Natl Acad Sci USA* 101: 12195-12200.

Nagumo J, Arimoto S, Yoshizawa S (1962). An active pulse transmission line simulating nerve axon. *Proc IRE* 50: 2061-2070.

Neely ST, Kim DO (1983). An active cochlear model showing sharp tuning and high sensitivity. *Hear Res* 9: 123-130.

Nobili R, Mammano F, Ashmore J (1998). How well do we understand the cochlea? *Trends Neurosci* 21: 159-167.

Ohmori, H (1985). Mechano-electrical transduction currents in isolated vestibular hair cells of the chick. *J Physiol* 359: 189–217.

Probst R (1990). Otoacoustic emissions: an overview. *Adv Otorhinolaryngol* 44: 1-91.

Probst R, Grevers G, Iro H (2006). *Basic Otorhinolaryngology*. 2nd ed. Thieme: 162-1633.

Probst R, Lonsbury-Martin BL, Martin GK (1991). A review of otoacoustic emissions. *J Acoust Soc Am* 89(5): 2027-67.

Rebillard G, Abbou S, Lenoir M (1987). Oto-acoustic emissions. II: Spontaneous oto-emissions: results in normal subjects or patients with tinnitus. *Ann Otolaryngol Chir*. 104(5): 363-8.

Rossi R, Maffei M, Bottinelli R, Canepari M (2005). Temperature dependence of speed of actin filaments propelled by slow and fast skeletal myosin isoforms. *J Appl Physiol* 99(6): 2239-45.

Ruggero MA, Kramek B, Rich NC (1984). Spontaneous otoacoustic emissions in a dog. *Hear Res* 13: 293-296.

Ruggero MA, Rich NC, Recio A, Narayan SS, Robles L (1997). Basilar-membrane responses to clicks at the base of the chinchilla cochlea. *J Acoust Soc Am* 101: 2151–2163.

Schloth, E (1983). Relation between spectral composition of spontaneous otoacoustic emissions and fine-structure of threshold in quiet. *Acoustica* 53: 250-6.

Seebacher F, Franklin CE (2001). Control of heart rate during thermoregulation in the heliothermic lizard *Pogona barbata*: importance of cholinergic and adrenergic mechanisms. *J Exp Biol* 204: 4361-6.

Shera CA, Guinan JJ (1999). Evoked otoacoustic emissions arise by two fundamentally different mechanism: A taxonomy for mammalian OAEs. *J Acoust Soc Am* 105: 782-798.

Shera, CA (2003). Mammalian spontaneous otoacoustic emissions are amplitude-stabilized cochlear standing waves. *J Acoust Soc Am* 114: 244-262.

Stewart CE, Hudspeth AJ (2000). Effects of salicylates and aminoglycosides on spontaneous otoacoustic emissions in the tokay gecko. *Proc Natl Acad Sci USA* 97: 454-459.

Talmadge CL, Long GR, Murphy WJ, Tubis A (1990). Quantitative evaluation of limit-cycle oscillator models of spontaneous otoacoustic emissions. In: Dallos P et al. (Eds.), *The Mechanics and Biophysics of Hearing*: 235-242.

Van der Pol B, van der Mark, J (1927). Frequency demultiplication, *Nature* 120: 363-364.

van Dijk P, Wit H (1990a). Synchronization of spontaneous otoacoustic emissions to a $2f_1$-f_2 distortion product. *J Acoust Soc Am* 88: 850-856.

van Dijk P, Wit H (1990b). Amplitude and frequency fluctuations of spontaneous otoacoustic emissions. *J Acoust Soc Am* 88: 1779-93.

van Dijk P, Wit HP, Segenhout JM (1989). Spontaneous otoacoustic emissions in the European edible frog (*Rana esculenta*): Spectral details and temperature dependence. *Hear Res* 42: 273-82.

van Hengel, P, Duifhuis H, van den Raadt P (1996). Spatial periodicity in the cochlea: The result of interaction of spontaneous emissions? *J Acoust Soc Am* 99: 3566-3571.

Vazquez AE, Luebke, Martin GK, Lonsbury-Martin BL (2001). Temporary and permanent noise-induced changes in distortion product otoacoustic emissions in CBA/CaJ mice. *Hear Res* 156(1-2): 31-43.

Veuillet E, Martin V, Suc B, Vesson JF, Morgon A, Collet L (2001). Otoacoustic emissions and medial olivocochlear suppression during auditory recovery from acoustic trauma in humans. *Acta Otolaryngol* 121(2): 279-83.

Vilfan A, Duke T (2008). Frequency clustering in spontaneous otoacoustic emisisons from a lizard's ear. *Biophys J* 95(10): 4622-30.

Zweig G, Shera CA (1995). The origin of periodicity in the spectrum of evoked otoacoustic emissions. *J Acoust Soc Am* 98: 2018-2047.